OPTIMIZATION OF FIR-TREE-TYPE TURBINE BLADE ROOTS USING PHOTOELASTICITY

By

Georg Hettasch

Thesis presented in partial fulfilment of the requirements for the degree of Master of Engineering at the University of Stellenbosch.

Study leader: Prof. W. Endres
Department of Mechanical Engineering
University of Stellenbosch
South Africa
External examiner: Dr. H. Wettstein
ASEA Brown Boveri
Baden
Switzerland

December 1992

DECLARATION

I the undersigned hereby declare that the work contained in this thesis is my own original work and has not previously in its entirety or in part been submitted at any university for a degree.

.G. Hettasch....

G. Hettasch December 1992

Vati, für was er mir war und immer sein wird.

SYNOPSIS

The large variety of turbo-machinery blade root geometries in use in industry prompted the question if a optimum geometry could be found. An optimum blade root was defined as a root with a practical geometry which, when loaded, returns the minimum fillet stress concentration factor. A literature survey on the subject provided guidelines but very little real data to work from. An initial optimization was carried out using a formula developed by Heywood to determine loaded projection fillet stresses. The method was found to produce unsatisfactory results, prompting a photoelastic investigation. This experimental optimization was conducted in two stages. A single tang defined load stage and a single tang in-rotor stage which modeled the practical situation. The defined load stage was undertaken in three phases. The first phase was a preliminary investigation, the second phase was a parameter optimization and the third phase was a geometric optimization based on a material utilization optimization. This material optimization approach produced good results. From these experiments a practical optimum geometry was defined. A mathematical model which predicts the fillet stress concentration factor for a given root geometry is presented. The effect of expanding the single tang optimum to a three tang root was examined.

OPSOMMING

Die groot verskydenheid lemwortelgeometrieë wat in turbo-masjiene gebruik word het die vraag na 'n optimum geometrie laat ontstaan. Vir hierdie ondersoek is 'n optimum geometrie gedefineer as 'n praktiese geometrie wat, as dit belas word, die mimimum vloeistukspanningskonsentrasiefaktor laat ontstaan. 'n Literatuur studie het riglyne aan die navorsing gegee maaar het wynig spesifieke en bruikbare data opgelewer. Die eerste optimeering is met die Heywood formule, wat vloeistukspannings in belaste projeksies bepaal, aangepak. Die metode het nie bevreedigende resultate opgelewer nie. 'n Fotoelastiese

ondersoek het die basis vir verdere optimeering gevorm. Hierdie eksperimentele optimeering is in twee stappe onderneem. 'n Enkelhaak gedefineerde las gedeelte en 'n enkelhaak in-rotor gedeelte het die praktiese situasie gemodeleer. Die gedefineerde las gedeelte is in drie fases opgedeel. Die eerste fase was 'n voorlopige ondersoek. Die tweede fase was 'n parameter optimeering. 'n Geometrie optimeering gebaseeer op 'n materiaal benutings minimeering het die derde fase uitgemaak. Die materiaal optimeerings benadering het goeie resultate opgelewer. Vanuit hierdie eksperimente is 'n optimum praktiese geometrie bepaal. 'n Wiskundige model is ontwikkel, wat die vloeistukspanningskonsentrasiefaktor vir 'n gegewe wortelgeometrie voorspel. Die resultaat van 'n geometriese uitbreiding van die enkelhaaklemwortel na 'n driehaaklemwortel op die spannings verdeling is ondersoek.

ACKNOWLEDGMENTS

I would like to thank the following people for their valuable and much appreciated support and assistance during the course of this project:

Prof. W. Endres for his guidance, assistance and patience.

Mr. G. Treurnicht for cutting the models and for his practical advice.

Mr. F. Zietsman for the construction of the in-rotor test rig.

All the staff of S.M.D. for their assistance and advice when I intruded on their workshop facilities.

The staff of the university libraries for their help in compiling the literature survey.

Mr. Tredoux, Rust and Buchan for the background work and test rig modifications.

Spoornet for the study leave granted to me to tackle, and complete the project.

Mr. R.F. Pönnighaus, my flatmate, for his help and support.

Miss B.K. von Bülow, my girlfriend, for her special love and encouragement throughout the project.

My brother and sister for their help in preparing the final manuscript.

My parents for their love, understanding, support, interest and guidance over the years.

TABLE OF CONTENTS

	Declaration.	ii.
	Synopsis.	iii.
	Acknowledgments.	v.
	Table of contents.	vi.
	List of figures.	x.
1	Introduction	1.
2	Problem concept	2.
2.1	Turbo machinery in general	2.
2.2	Turbine blade overview	2.
2.3	Turbine blade loads	3.
3	Literature survey	5.
3.1	General	5.
3.2	Photoelastic analysis	7.
3.3	Finite Element analysis	8.
3.4	Contact Fatigue	12.
3.5	Analytical methods	13.
3.6	Optimization	14.
3.7	Design	14.
4	The blade root / rotor attachment	16.
4.1	Root nomenclature	16.
4.2	The contact area	18.
4.3	Contact surface slip analysis	23.
5	Optimizing the blade root profile	26.
5.1	Factors influencing the performance of a blade root	26.
5.1.1	The nature of the load	26.
5.1.2	Stress distribution in the blade root	27.
5.1.3	Root operating environment	27.
5.1.4	Materials	27.
5.1.5	Operational patterns	28.
5.1.6	Manufacturing constraints	28.
5.2	Optimum definition	28.

6	Analytical blade root stress calculation	30.
6.1	The Heywood method	30.
6.2	Finite element analysis	34.
7	The experimental stress investigation	35.
7.1	Objectives	35.
7.2	Photoelasticity	35.
7.3	The experimental apparatus	38.
7.3.1	The polariscope	38.
7.3.2	The fixed friction-angle test rig	38.
7.3.3	The in-rotor test rig	39.
7.4	Model preparation	40.
8	The single tang fixed friction-angle investigation	41.
8.1	The test philosophy	41.
8.2	Implementation of the test philosophy	42.
8.2.1	The fixed friction-angle test rig	42.
8.2.2	The experimental procedure	44.
8.3	The experimental development	45.
8.3.1	Phase 1 Initial experiments (Roots 1 to 25)	45.
8.3.2	Phase 2 First optimization (Roots 28 to 39)	45.
8.3.3	Phase 3 Final optimization (Roots 43 to 66)	46.
8.4	Experimental result manipulation	50.
8.5	The experimental results	51.
8.6	Expansion of the results to the in-rotor situation	54.
9	The in-rotor experiments	73.
9.1	Experimental objectives	73.
9.2	The loading rig	73.
9.3	Experimental method	74.
9.4	Experimental results	75.
9.4.1	Centrifugal loads Alpha = 40°	76.
9.4.2	Bending loads Alpha = 40°	76.
9.4.3	Centrifugal loads Alpha = 45°	77.
9.4.4	Bending loads Alpha = 45°	78.
9.5	Cyclic centrifugal test	78.
9.6	Experimental conclusion	79.
9.7	In-rotor results	80.

10	Multiple tang tests	84.
10.1	Experimental aim	84.
10.2	The 3 tang root	84.
10.3	Experimental procedure	85.
10.4	Experimental results	85.
10.4.1	Centrifugal load	85.
10.4.2	Bending load	86.
10.5	Top fillet modification	87.
10.6	Experimental conclusions	87.
10.7	Three tang root test results	88.
11	Comparison between experimental and analytical results	89.
11.1	The Heywood formula compared to experimental results	89.
11.2	Mathematical result modeling	90.
11.3	Form0 (Formula for roots with D0=0)	90.
11.3.1	Form0 formula limitations	91.
11.4	Form1 (Formula for all roots with decreased accuracy)	91.
12	A single tang blade root design rule	97.
13	Conclusion and recommendations for further research	99.
13.1	Conclusion	99.
13.2	Recommendations for continuing the project	100.
List of references		102.

APPENDIXES

A1.1	The stress calculation program	105.
A1.2	The NC generation program for the blade root	106.
A1.3	The input information file	106.
A1.4	The NC generation program for the rotor	107.
A2	Preparation of Araldite D models	108.
A2.1	Casting Araldite D	108.
A2.1.1	The mould	109.
A2.1.2	The mixing pot	109.
A2.1.3	Casting	110.
A2.2	Machining	111.
A2.3	Storing	112.
A2.4	Final finishing	113.
A2.5	Material calibration	113.
A3	Experiment photographs	114.
A3.1	Fixed friction angle tests	114.
A3.2	In-rotor single tang tests	122.
A3.3	In-rotor three tang root tests	126.
A3.4	Fillet modification on three tang root	129.

LIST OF FIGURES

4.1	The blade root geometry	17.
4.2	Crack initiation points	20.
4.3	Force analysis pertaining to contact surface slip	23.
4.4	Ultimate slip criticality for a 10° friction angle	24.
6.1	Heywood projection test piece	30.
6.2	Heywood geometry and present geometry	31.
6.3	Force distribution patterns	33.
6.4	Some typical Heywood formula results	33.
7.1	The plain polariscope in normal (lens) mode	36.
7.2	The circular polariscope in projection mode	37.
7.3	The polariscope with the fixed friction angle test rig in place	39.
8.1	The fixed friction angle test rig	43.
8.2	S.C.F. vs Load angle for various Alpha	56.
8.3	S.C.F. vs Load angle for various Alpha	56.
8.4	S.C.F. vs Load angle for various Beta	57.
8.5	S.C.F. vs Load angle for various Beta	57.
8.6	S.C.F. vs Load angle for various R	58.
8.7	S.C.F. vs Load angle for various R	58.
8.8	S.C.F. vs Load angle for various B	59.
8.9	S.C.F. vs Load angle for various B	59.
8.10	S.C.F. vs. Load angle (Alpha = 40°)	60.
8.11	S.C.F. vs. Load angle (Alpha = 45°)	60.
8.12	S.C.F. vs geometry (Alpha = 40°)	61.
8.13	S.C.F. vs geometry (Alpha = 45°)	62.
8.14	S.C.F. vs geometry (Alpha = 40°)	63.
8.15	S.C.F. vs geometry (Alpha = 45°)	64.
8.16	S.C.F. vs geometry (Alpha = 40°)	65.
8.17	S.C.F. vs geometry (Alpha = 45°)	66.
9.1	The in-rotor test rig	73.
9.2	A blade in position showing some dimensions	77.
9.3	In-rotor centrifugal loading results for Alpha = 40°	81.
9.4	In-rotor bending load results for Alpha = 40°	81.
9.5	In-rotor centrifugal loading results for	

	Alpha = 45°	82.
9.6	In-rotor bending test results for Alpha = 45°	82.
9.7	In-rotor cyclical centrifugal tests for Alpha = 45°	83.
11.1	Comparison between Heywood and experimental results for DO > 0 roots	93.
11.2	Comparison between Heywood and experimental results for DO = 0 roots	93.
11.3	Comparison between the formula and experimental results for DO=0	94.
11.4	Comparison between the formula Form0 and the experimental results	94.
11.5	Comparison between the formula Form1 and the experimental results for all root geometries tested	95.
11.6	Comparison betweem formula Form1 and the experimental results	96.
A1.1	Root 72, used for all examples given in appendix 1	107.
A2.1	Casting in progress	111.
A2.2	Final finishing	113.

CHAPTER 1

1. Introduction

In most axial flow turbo machinery used today the blades which direct the flow of the gas are manufactured separately to the turbine disks, on which they are then mounted. The fir tree type blade attachment which is widely used, especially in turbines with high centrifugal speeds, is the subject of this thesis.

In the striving for higher power output, better efficiency, improved reliability and more stringent safety requirements it has become increasingly important to be able to quantify and thus to minimize stresses in critical areas of the turbo machine. The blade-rotor connection is a highly and complexly stressed area which if not correctly designed can fail with serious consequences.

To be able to produce a efficient and reliable design the designer needs reliable and relevant data on which to base the design. Various attempts have been made, mostly in-house by the large turbo machinery manufacturers, to develop mathematical models of the connection. Very little is publicly known of these models due to the fierce competition in the industry which precludes publication of research findings.

This thesis presents a problem definition, a literature survey of the subject together with a discussion of a mathematical model developed to solve similar problems. The main body of the report deals with a series of photoelastic experiments which were undertaken with the view to optimizing the blade-rotor connection. The data compiled from the experimental results form a base for blade root design optimization.

CHAPTER 2

2. Problem concept

2.1 Turbo machinery in general

Turbo machinery differs widely in application, size and design. Axial compressors are used in various applications from process gas compressors in chemical plant to the compression stages of gas turbine engines. Turbines are also used in a wide variety of applications from back pressure steam turbines used in combined power generation and process heating applications to gas turbines used as aircraft engines. Of these, the large gas and steam turbines used in electrical power generation plants, form the main market sector. Different applications and power ratings require a vast range of blades. To fasten these blades to the rotors a wide variety of different blade fastenings are used. One particular type of fastener, called the fir-tree type, due to its shape, is the subject of this thesis.

2.2 Turbine blade overview

Different stages of the compressor and turbine parts of turbo machinery use different blades, the properties of which are designed to meet the specific operating criteria of those stages in which they are used. The turbine stages often use blades with internal cooling while the very long blades in the final stages of large steam turbines are pretwisted so that when the centrifugal force acting on them untwist the blades the correct angular allignment with the gas flow is achieved. Often the high pressure turbine stage and the last long low pressure stage use multiple tang fir-tree type blade roots while the short and medium impulse and the low pressure stages use hammer head or single tang fir-tree type or dove-tail blade roots. Compressor blades are usually manufactured using single tang fir-tree type, dove-tail blade or hammer head roots. The designs do however differ from one machine to the other and a lot depends on the design policy followed by the specific manufacturer. For

instance, some companies use a large number of very small tangs on their roots while others prefer to use only a few tangs.

Various ways of fitting the roots into the rotor are also used. Some roots are fitted circumferentially into the rotor while others are fitted axially. The axially fitted roots can be divided into three further categories : 1. The straight axial fit in which the root forms a 90° angle with the direction of rotation, 2. The angled root which forms an angle of less than 90° with the angle of rotation and which allows better match of the airfoil to the root platform, and 3. The curved root which is generated by moving the fir-tree profile in an arc thus matching the very curved airfoils of low pressure stage blades which have to be placed close together on the rotor.

2.3 Turbine blade loads

Forces acting on the blade roots can be divided into two main categories. 1) The centrifugal forces generated by the mass of the blade and the rotation of the machine. The analysis of the strength necessary to resist these centrifugal forces is normally based on low cycle fatigue (L.C.F.) due to the number of starts and speed changes experienced by many turbines. Most constant speed turbines used for driving generators and process compressors experience less than 5000 starts in their lifetime. Aircraft engines experiencing as much as 5 speed variations per hour accumulate up to 100 000 speed variations between major (20 000 hour) overhauls. This places most turbines well within the low cycle fatigue range as far as centrifugal forces are concerned. 2) The other main load acting on the blade root is the bending force acting on the blades. This bending force has two main origins. The first is the normal nominally constant operational gas force acting on the blade. The other is a vibration force generated by high impact type gas loads in the partial impingement first stages of high pressure steam turbines and by vibrations of the blades caused by harmonics or unstable flow. The vibrations may only last a very short time but many hundreds may take place in a few seconds, thus bending loads must be subjected to high cycle fatigue (H.C.F.) analysis.

Blades are normally designed in such a way that the resultant of the centrifugal force and the nominally constant gas force acting on the blade, acts through the center of the blade root thus generating a purely radial force on the blade root. This compensation technique is only effective at one load condition. The possible bending forces generated by blade vibrations and gas forces are then superimposed on the centrifugal force. Vibrations also generate modal stresses which cannot be analysed using only simple static methods.

This investigation thus aims to study fir tree type blade roots under nominally constant radial forces with superimposed transient bending forces. Different methods of studying the stresses in the blade root were investigated. It was finally decided to use photoelasticity as the main tool in the search for an optimum blade root geometry.

CHAPTER 3

3. Literature survey

Due to the commercial importance of turbine technology coupled with the high cost of research very few research results are ever published. When papers are published the authors are vague about results. The subject of this thesis is the optimization of the profile of the blade root. A large number of publications deal with the rotor notch profile and strength rather than that of the blade root. This is due to the decreasing "desirability" of failure from the blade tip to the center of the rotor. The closer to the center of the rotor a failure takes place the greater the damage and cost attributable to the failure.

Various publications have stressed various aspects of the blade root problem. Some of the publications which were most helpful in the context of this thesis are summarized and discussed below.

3.1 General

The paper providing the most background to the problem at hand is "Stress and strength studies on turbine blade attachments" [7] by Durelli et al. In this paper Durelli stresses the importance of service conditions being accurately simulated in a laboratory instead of testing a complete turbine which is very expensive and which does not allow the isolation of any single factor. Durelli aims to grade different designs rather than to associate a particular value of stress to a design. To realize this aim Durelli divided his study into 5 parts.

1: Loading conditions are divided into radially acting centrifugal forces, and bending loads, which are divided into gas forces on the airfoil and vibrational bending forces of the blade. The loading theory was confirmed by Durelli using high temperature resistance strain gauges in a turbine in service. It was also found that the distribution of forces in the contact

region cannot be predicted due to the movement and deformations occurring there. Consequently experiments do not produce results in which the stress is a linear function of load. Variations from a linear function however are low, and do not exceed 10%.

2: Using brittle coatings Durelli determined that the force distribution along the axial length of the blade root is not uniform. Uniformity is greater in roots loaded only with centrifugal forces than in those carrying a combined load. Due to the fact that the roots have a uniform geometry along their axial length, a two dimensional analysis is justified thus creating a series of two dimensional problems with the same geometry but different loads.

3: Employing a loading rig similar to the one used for this thesis (which is fully described in section 9.2) photoelastic and brittle coating techniques were used to determine stress patterns in various blade root. Using the results obtained Durelli was able to grade the geometries according to his order of merit. The specific geometries studied and the results obtained are not presented.

4: The optimization of fillets is discussed next. No definite optimum geometries are presented but Durelli does state that the optimum fillet differs for different load conditions. A practical optimum geometry would thus be reached using a representative loading condition. Optimization is achieved by removing the material in which the highest stress occurs, thereby enlarging the fillet in the critical stress area and thus reducing the stress.

5: The influence of protuberance angle (called Alpha in this thesis) on the stress concentration factor in the fillet was also studied. Durelli found that with centrifugal loading only, the S.C.F. decreased with an increase of protuberance angle. In combination loads on 3 tang roots the S.C.F. in the top tang decreased with increasing angle and the S.C.F. in the middle and lower tangs increased with increasing angle.

Subjects that Durelli also discuses but that are not as important in the context of this thesis are: the influence of lack of simultaneity (due to manufacturing tolerances), determination of individual tang loading from photoelastic data and high temperature fatigue tests.

3.2 Photoelastic analysis

In their paper "Photoelastic and Holographic Analysis of a Turbine-engine Component", Parks and Sanford [23] combine classic photoelasticity with holography to produce a more complete stress distribution picture than is possible with photoelasticity alone. The investigation was prompted by a service life problem experienced in the compressor section of a military jet engine. A two dimensional photoelastic study was made using a conventional polariscope to determine the isochromatic and isoclinic fringe patterns and a holographic polariscope was used to obtain the isopachic fringe pattern. Isopachic fringes are lines of constant sum of principal stresses. Together, isochromatic, isoclinic and isopachic fringes can be used to give the complete stress field in two dimensions. A stress concentration factor defined as the fillet stress over the average stress in the narrowest part of the rotor, or blade, was defined (similar to the definition used in this thesis). The subsequent modifications made to the fillet geometry resulted in a S.C.F. reduction from 5.2 to 3.8. The fillet modification had the added advantage of moving the stress peak away from the contact surface, thus reducing the danger of fretting damage induced crack initiation The authors point out that although a dramatic decrease in S.C.F. can be achieved the solution (as in this case) is not always viable. The low S.C.F. is attained with a fillet of constantly varying radius which is more difficult to manufacture than a single radius fillet. A suggestion is made to use an optimization which consists of a single radius fillet. Improvements in S.C.F. may not be as dramatic but machining cost and complexity are reduced creating a true practical optimum.

The paper illustrates the possibilities available to the designer in the field of practical fillet optimization very well. The ease of effective analysis and effectiveness of the photoelastic method are well demonstrated.

3.3 Finite element analysis

The contact problem in blade attachments has also been studied using numerical methods. The authors of publications in which such methods are used always strive to present a comparison to experimental data, obtained from photoelastic or similar experiments, to prove the accuracy of the method being studied.

A recently published paper on this subject is "Contact stress distributions in a turbine disc dovetail type joint - a comparison of photoelastic and finite element results" by Kenny et al.[21]. The main aim of the paper is to look at the contact zone of the blade root in contrast to most other studies which concentrate on the fillet part of the blade root which does not carry any surface loads. The authors of the paper assume that the centrifugal forces are the only important forces and that the problem can be considered as being two dimensional. Three different loading conditions were considered, each using an aluminium (dural) loading pad at a different position in the contact region. The length of the pad was 1/3 of the contact region length. The usefulness of this procedure is questionable as in practical situations the whole contact region is loaded. Using a loading pad also does not reflect the true contact force distribution. The validity of loading the rotor section of the experiment with pins situated in the rotor notch section should also be questioned as this does not model the true situation. The shear difference method was used to determine the stress at internal points in the blade root, concentrating on the contact zone and immediate surroundings. Another weakness in the study appears in the fact that the "complex stress situation on the contact surface prevented reliable data being obtained at distances less than 2mm from the surface". As the surface is the normal origin of cracks and other failure mechanisms, and the shear stresses reach their peak just below the surface (less

than 2 mm below the surface) the usefulness of the results obtained are constrained to academic interest. For the numerical analysis a loading angle of 45° was used instead of some value related to the true friction conditions in the contact region. Possible movement of the contacting parts is also not considered although this is known to have a definite influence on stress patterns and fatigue strength of the contact zone.

The authors report that initially contact elements which necessitate the definition of a friction coefficient were used in the numerical modeling but it was found that ordinary elements simply loaded on their surfaces gave the same results. Using normal elements had the advantage of not having to define a rotor section but simply a boundary load. The boundary load was chosen as a uniformly distributed load over the 1/3 of the contact surface being investigated (similar to the dural pad loading). The direction of the load was parallel to the blade shank. The similarity in the results indicates that further development of contact elements for finite element analysis is necessary. The stresses obtained using the finite element methods were all higher than those obtained from the photoelastic experiments. For some situations the position of the peak stresses also differed. The error in fillet stress with loading nearest the fillet is most pronounced and the stress gradient is reversed. To obtain these results a very fine finite element mesh had to be used especially in the surface region.

The study highlights the problems experienced when using a normal commercially available package to model contact problems which does not make expressed use of well developed contact elements. Photoelastic and finite element analysis techniques all experience difficulties in regions were stress gradients are high and a high resolution analysis is necessary to obtain accurate results. With discrepancies between the experimental and finite element results of up to 32% the necessary accuracy to use the numerical method presented as a design tool, was not achieved.

In contrast to the previous paper Boddington, Chen, He and Ruiz [3], [26] and [15] go into considerable detail to develop a good contact element strategy. Using normal finite element analysis techniques special conditions were imposed on the contact surface elements to simulate friction. The system works on a iterative basis within the main load incrementing cycle. The nodes in the contact region are checked to determine the forces acting on them (normal and shear). From the forces the node is deemed to be 'stuck', 'free' or 'sliding' using certain friction related criteria. This cycle is continued until all nodal forces in the contact region are in equilibrium. The next load step is then taken and the process is repeated. This method, as opposed to previous methods which made use of infinite friction coefficients, can determine the amount of slip taking place between the mating surfaces. This, as will be seen later, is a very important factor for determining the fretting fatigue resistance of the joint. The method was tested and found to give good results when compared to analytic and photoelastic data. One weakness of all finite element analysis published to date, is the limited resolution. To identify narrow stress spikes, which occur in contact regions which are subjected to surface shear or sliding forces, very small elements must be chosen which increase the machine space and time required to solve the problem. In this study 20 nodal points were used in the contact region which produced a adequate resolution. Increasing the number of contact nodes causes a large increase in program running time due to the smaller load steps that can be taken to ensure accurate inter-nodal slip prediction and subsequent nodal alignment. New window calculation techniques may solve this problem in future.

The study conducted in "Slipping behavior and fretting fatigue in the disk/blade dovetail region" by Hattori et al. [13] is a very complete study of one blade root as it is implemented in a compressor described in "Development of a High-Pressure-Ratio Axial Flow Compressor for a Medium-Size Gas Turbine" by Kashiwabara et al. [20] in which a general overview of compressor design is given. Hattori uses strain gauge and displacement meter measurements taken in simulated service

conditions and compares them to finite element analysis results to validate the numerical method used. It was found that the friction forces in the contact region play an important part in the resulting stress fields and must be accurately modeled to achieve usable finite element results. This facet of the problem was neglected by Kenny et al. [21] but is well developed by Hattori. He uses experimental results to determine the friction coefficient. In the heavily (fretting) damaged lower 4 mm of the contact area a friction coefficient of 0.7 is used while for the undamaged upper 12 mm a friction coefficient of 0.15 is used. Only stresses in the rotor slot corners and the contact region were studied for this paper. The importance of vibration damping by contact region slip and the resulting fretting fatigue are also stressed in this study. A critical bending moment is defined as that bending moment which has to be applied after a certain centrifugal force for the whole contact surface to slip. Slip does occur before this critical bending moment only on a microscopic scale at various points in the contact zone while bending moments above the critical level cause macroscopic slip along the whole length of the contact region. Using finite element analysis it was found that the critical bending moment is proportional to the centrifugal force. These results were confirmed by experimental observations. Conclusions that can be drawn from this result are that vibration damping will work best at low rotational speeds (low centrifugal force) where total slip is more likely to occur than at high speeds. This is practically useful as rotational stall and resonant vibrations occur at low speeds were the vibration damping is most effective. The damping can however only be used for short durations to avoid wear damage.

The other field of interest studied by Hattori is that of the distribution of the contact surface stress. Stress hysteresis loops were generated for bending moments above and below the critical value. It was found that the stress at the lower end of the contact region (Mu = 0.7) is high and shows a high fluctuation with changes in bending moment while the hysteresis loop size and thus the movement are small. The upper end of the contact region (Mu = 0.15) shows a low stress and low stress

amplitude but has a large hyteresis loop size indicating large movements. The overall shape of the stress distribution is typical of two flat surfaces in contact with high stress values at the ends and a low stress at the middle forming a parabolic shape. A working compressor was then instrumented similarly to the experimental set up and the tests were repeated under service conditions. These experiments showed that the blade stress is proportional to the rotor notch stress under vibration conditions but the rotor stress is only about 1/4 of the blade stress. The results also show very good vibrational damping by the contact region with low stress amplitudes in the rotor notch while high stress amplitudes acted on the blade.

3.4 Contact fatigue

The fretting fatigue of the dovetail joint is the subject of two papers by Ruiz et al. [15] [26]. A simple biaxial test rig was used in which, according to Ruiz [26], the stress field of a true rotor and blade root is reproduced satisfactorily. The blade is loaded as if a centrifugal force were acting on it. The sheet, which simulates the rotor, is also loaded at right angles to the blade load to simulate the circumferential stress and elongation generated in the rotor due to its rotation. Stresses in the rotor contact area were studied with special reference to crack formation and growth. Different friction angles were specified in the finite element analysis to show the influence of friction on the stresses. The research showed that two parameters play an important role in the fretting fatigue life of the rotor. These are first mentioned in the first paper [26] and are fully defined in the second paper [15]. The fretting damage parameter (FDP) is defined as (shear stress on the contact surface * relative displacement of the surfaces). The fatigue-fretting damage parameter (FFDP) is defined as (local tangential stress in the contact area * shear stress on the contact surface * relative displacement of the surfaces). The second paper [26] takes up the theme of the first and adds high temperature tests. At elevated temperatures tangential stress is reduced by 12 % and the tensile stress is 40 % lower due to reduced friction coefficient and Youngs modulus. This

shows the relative importance of tangential stress to failure at high temperatures. It was also found that the FDP is unchanged from room temperature to elevated temperature. The FFDP is significantly lower at high temperatures due to a shift in the position of the stress peaks which is caused by the lower friction coefficient and the change in Youngs modulus.

As mentioned Hattori also devotes attention to contact surface damage caused by stresses and movement in the contact region.

3.5 Analytical methods

The only attempt to find a method of solving the fillet stress problem analytically is presented by Heywood in "Tensile Fillet Stresses In Loaded Projections" [19]. With the aim of optimizing screw thread profiles, Heywood used a range of different geometries to develop a formula with which stresses in the fillet of loaded projections can be calculated. Various fillet radii, flank angles, loading angles and loading positions were studied using photoelastic techniques. The results were correlated by a new formula. The formula has the form: Fillet stress = K * (M + L) , were K is a stress concentration factor, M is the nominal bending moment factor and L is a load proximity factor. In long cantilevers, L becomes negligible and ir situations were the load is very close to the fillet M become negligible. The good theoretical basis of the empirical formula make it a valuable analytical tool. Gear teeth were analysed with the formula and results show the formula to be more accurate than the Lewis and the Modified Lewis formulas. The analysis of screw thread profiles also produced good results. Although the turbine blade root per se is not mentioned in the paper the geometry of the tangs is similar to the geometries covered by the formula presented by Heywood. The use of the formula and the results obtained will be discussed in detail in a chapter 6.

Smith and Liu present an analysis of "Stresses due to tangential and normal loads on an elastic solid with applications to some contact stress problems" [28]. This paper could be used as part

of an analytical tool to solve the root/rotor interaction problem. The analysis has one drawback in that the force distribution and boundary geometry are prescribed and fixed. In addition to the fact that this makes the contact stress problem mathematically solvable, it also makes it useless as a practical tool to solve the problem at hand. A similar analysis is presented by Föppl in "Drang und Zwang" [11].

3.6 Optimization

In "Lighter and Stronger" by Durelli and Rajaiah [8] the optimization of blade root fillets is discussed. Here the authors make use of a coefficient of efficiency (K_{eff}) which is a measure of how efficiently the material at the fillet edge is being used. An efficiency of 1 means that the whole length of the fillet boundary is subjected to a stress which is equal to the yield stress of the material being used. In the geometry under consideration in the paper the efficiency was improved from $K_{eff} = 0.52$ to $K_{eff} = 0.76$. It is also shown that fillet stresses can be reduced by 30 % without much trouble. The paper does not however give a description of the optimized fillet profile. When discussing S.C.F. improvements it must be kept in mind that a large improvement in S.C.F. is as much a reflection on the starting geometry as on the optimization method.

3.7 Design

Most books which deal with turbine design concentrate on the fluid mechanic and thermodynamic aspects. Traupel in "Thermische Turbomaschinen" [30] covers all aspects of turbomachinery design in some detail. The blade and rotor design is discussed together with turbine control, dynamics, thermodynamics and fluid mechanics. The basic background description given is a very good aid to the inexperienced engineer who wants to study turbomachinery design. Due to the age of the book many of the technical limitations mentioned by Traupel are no longer design obstacles but the basic principals are still valid.

To give a fast reference to the subjects covered in the different papers the following matrix was set up.

Subject / Paper	Photoelastic Experiments	Contact Experiments	Strength Experiments	Finite elem. Analysis	Analytical Analysis	Design	Other comments
[1]			X	X		X	Finite element analysis in gear design
[3]				X			Mathematical theory for contact F.E. analysis
[7]	X	X	X			X	General experimental method and fillet optimisation
[8]	X					X	Fillet optimisation using photoelasticity
[13]		X	X	X		X	Design of a blade root with silp and friction analysis
[15]		X	X	X			In depth contact surface fatigue study
[19]	X				X	X	Heywood stress formula for loaded projections
[21]	X	X		X			Simple finite element analysis
[23]	X					X	Design correction of failing rotor notch
[26]		X	X	X			Friction and freting analysis of contact area
[27]				X			Simple finite element analysis
[29]	X						Elementry photoelastic analysis
[30]						X	General guide to all aspects of turbine design

CHAPTER 4

4. The blade root / rotor attachment

4.1 Root Nomenclature

An example of the fir tree type blade root profile which will be studied in this thesis is shown in figure 4.1. Roots can have one or more pairs of tangs which are normally just referred to as tangs. The simplest profile is the single tang (one pair of tangs) profile. When the design requires it, this basic single tang profile is repeated downwards at an angle to form a multiple tang root. Each tang thus has the same basic shape.

To be able to generate (draw or machine) the blade geometry at will, a set of simple easily visualizable parameters were chosen to fully and unambiguously describe the root geometry. It is important to choose the defining parameters carefully so that each different geometry can be uniquely defined. This may seem obvious and trivial but as shall be seen in chapter 6, geometric definitions have been used in some studies which do not uniquely describe one geometry. The principal parameters describing a single tang are

Alpha; the top or contact angle

Beta; the lower tang angle

R1; the tang fillet radius,

R2; the tang end radius,

B; the horizontal projection of the contact area length

When a multiple tang root is defined the parameter which determines the geometric relationship between tangs is:

D; the horizontal increment between consecutive tangs

The parameter used to define the direction of the load on the root is:

Rho; the angle between the load direction and the line perpendicular to the contact area.

Rho is simultaneously the friction angle and is thus limited to Rho_S while the contact surfaces do not slip and to Rho_D while contact surface slip takes place.

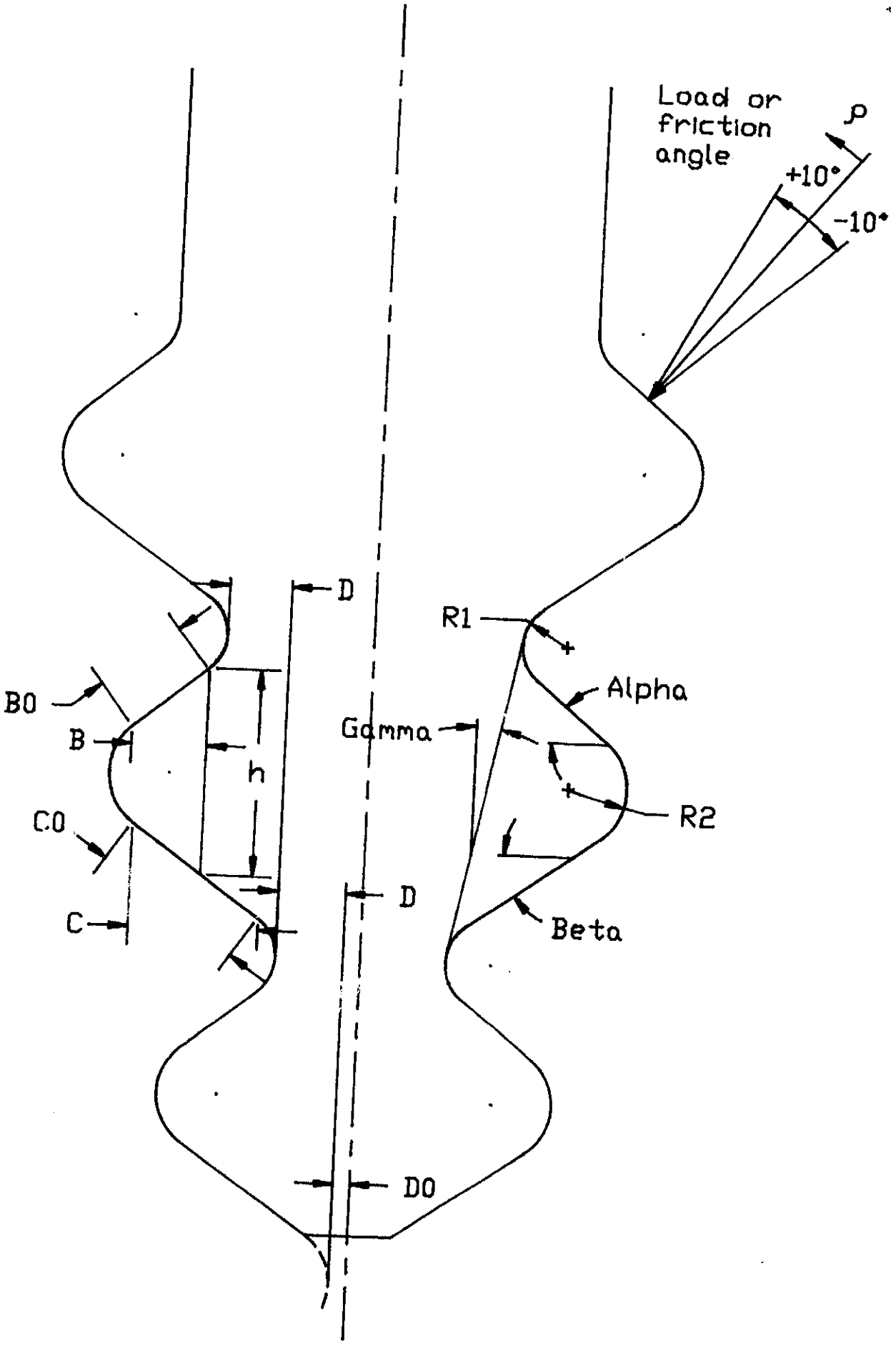

Figure 4.1 The blade root geometry.

The above parameters are all independent of each other and are thus the minimum number of parameters needed to uniquely define the geometry. A number of auxiliary parameters which are dependant on the above parameters were also used to make calculations and visualization easier. These are:

B_o; the actual length of the contact area

C; the horizontal length of the tang lower surface

C_o; the actual length of the lower surface of the tang

Gamma; the halfangle of a multiple tang root

h; the vertical shear length of a tang at its base

The last parameter D_o is independent of the rest and is the thickness added to the center of the root, normally to ease root manufacture. The parameters are all shown in figure 4.1 which should clarify any uncertainties.

In all the Pascal programs written in the course of this project the user is prompted for: Alpha, Beta, B, D_o, R1 and R2, and is given the choice of entering Gamma, D or C to complete the geometric description.

Although a difference is made here between R1 and R2, in most of the work in the thesis the values R1 = R2 and both radii are then referred to as having size R. When using a single tang root the parameters D and D_o are not normally identifiable and Gamma cannot be defined. For clarity and practicality the dimension D_o was defined as shown in the figure. The shank width of all roots is equal to: 2 * (D_o + D * number of tangs).

4.2 The contact area

As the blade root tang profile and the rotor tang profile are almost symmetric the following remarks on the contact area apply to the rotor and to the root.

The stresses in the blade root fillet (R1) are the main interest of this thesis. To be able to study them fully a good understanding of the areas adjacent to the fillet and how they interact with the fillet must be developed. The contact region

which is adjacent to the root fillet and is the region which is subjected to the severest working conditions in the blade root.

Consider what happens in the contact area during different stages of turbine operation. Before startup the whole turbine is at a uniform ambient temperature and is stationary. At this stage the blades are normally slightly loose in the rotor notches and tend to rattle if the turbine rotor is turned slowly. When the turbine is started the centrifugal force generated seats the blade roots firmly in the rotor notches. The forces generated at the contact surface are a normal compressive force and a secondary tangential force acting away from the blade shank on the root (resisting movement away from the rotor axis). The tangential force exists because the contact surface angle Alpha is bigger than zero. This tangential force causes many problems due in part to the slip which occurs when the tangential force overcomes the frictional resistance between the contact surfaces. The problem is quantified by He and Ruiz [15] as described in section 3.4. The stick-slip nature of the tangential force overcoming the frictional force can cause a reduction in the tangential force but it is very difficult, if not impossible, to determine when slip will take place and how much slip will take place and what the tangential force will be after the slipping action. As turbine operation continues the temperature of the blades and consequently that of the blade roots rises causing an expansion of the root and a consequent tangential force. This tangential force act towards the blade shank on the root thus tending to force the blade back towards the rotor axis. As the rotor warms up with continued operation the rotor expands and the tangential forces tend to act away from the blade shank on the root again.

From the preceding it can be seen that it is very difficult to determine the direction and magnitude of the tangential force in the contact area due to the changing load, thermal and frictional conditions. The uncertainty increases when the blade is subjected to cyclical bending loads as experienced during blade vibration. The movement of the contact surfaces relative to one another is the cause of scoring which in turn provide

points for crack initiation, which eventually lead to root failure.

It has been found in practice that cracks start at two distinct places on the turbine root. The first type of crack starts at the point were the stress is highest in the fillet region and propagates at an angle approximately perpendicular to the surface were it started. As the fillet stress is sometimes influenced by remnant stresses the cracks do not always originate were expected. The other type of crack is initiated at the end of the contact surface nearest the fillet and propagates perpendicular to the contact surface. In a preliminary study undertaken by Tredoux [29] it was found that the stress on the edge of the root profile reaches two peak values which correspond to the points of crack initiation. To prevent confusion when referring to these points they were called peak I and peak II respectively as shown in figure 4.2.

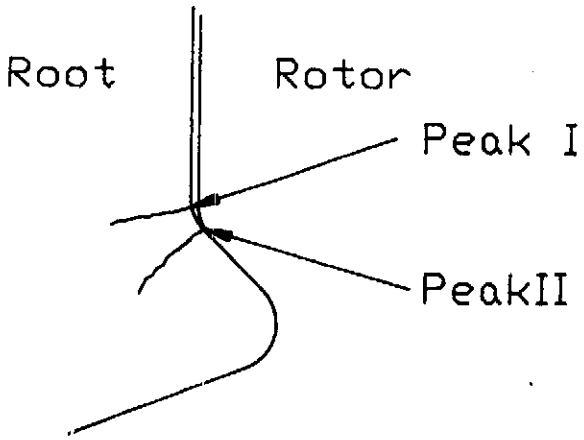

Figure 4.2 Crack initiation points.

As the contact surface is so near the fillet and because the end of the contact region is critical with regard to crack initiation a short discussion of the contact stresses is in order.

The method of determining stresses generated when two spheres are in normal contact was developed by Hertz and is described in most strength of material text books. When two finite flat surfaces are in contact the Herzian theory does not apply any

more. The problem is also very difficult to formulate because a different solution exists for each set of boundary conditions.

If the problem is simplified to a finite flat surface contacting an infinite flat surface it can be analysed. The error of the assumption is immediately apparent when one compares the boundary conditions of the two problems. However as is found in many problems the simplification does yield some useful results. In their paper, "Stresses Due to Tangential and Normal Loads on an Elastic Solid with Application to some Contact Stress Problems" Smith and Liu [28] study contact stresses when normal and tangential forces act on a flat surface. The force distribution for the normal load was assumed to be semi-eliptical and the tangential force was assumed to be a fraction of the normal force. This type of force distribution would be expected between a cylinder and a semi-infinite flat section with a constant friction coefficient. For the root/rotor contact a similar situation exists with the exception of the force distribution and uncertainty about the true friction characteristics. Smith and Liu found that the magnitude as well as the position of the maximum stresses changes as the friction coefficient changes. For a low friction coefficient the maximum shear stress is below the surface at the ends of the contact region and the maximum principal stresses are at the surface and in the middle of the contact region. As the friction coefficient rises the maximum shear stress rises to the surface and all principal stresses move away from the center of the contact region. From the results presented by Tredoux [29] it is seen that the root/rotor contact develops high stress peaks at the ends of the contact region. The results presented by Föppl [11] support this observation.

As is seen from the above, friction plays a major part in determining the stress distribution in the contact region. On the one hand a high degree of friction causes high tangential forces but it reduces movement in the contact region which leads to scoring as described by He and Ruiz [15]. The ideal situation exists when the product of the shear stress and the relative movement of the contacting parts (FDP) is minimized.

In practice some turbine manufacturers use coatings on the contact surfaces to reduce friction coefficients. High temperature lubricants which were specially developed for similar applications (such as high temperature screw thread pastes) can also be used to protect surfaces from corrosion and fretting as described by Herschel [14].

By reducing the friction coefficient the high stresses at the ends of the contact region are reduced thus minimizing the danger of crack initiation and propagation from "peak II". This shifts the critical area in the design from the contact region to the fillet area which is the other crack initiation region.

The other design possibility to turbine manufacturers is to leave the contact area unlubricated and to encourage high friction with the aim to eliminate movement of the contacting surfaces. Stress relieving fillets cut at the ends of the contact region help to isolate the contact surface from tangential forces. However nothing short of welding the root in place (which is not widely practiced in gas turbines) will eliminate movement. Lacking the ability to eliminate movement of the contact region, the designer strives to limit the damage any movement will cause by employing the best lubricants available. This together with the necessity to design the fillet with the lowest surface stresses become the prime root design objectives.

Another philosophy in the design process which is followed when designing blade roots is to minimize the stresses causing failure instead of just building in elements to withstand the higher loads. Blade shanks are made long and vibration dampers are inserted between blade platforms to protect the blade root from blade vibrations as far as possible thus partly eliminating the need for highly durable contact surfaces.

4.3 Contact surface slip analysis

From elementary force equilibrium theory it is known that in any static body the extensions of all force vectors acting on that body must meet in one point. The blade root is no exception to this rule. For the single tang case the resultants will pass through the contact regions at an angle smaller than the friction angle for that specific contact. If the reaction force assumes an angle larger than the attainable friction angle the contact will slip until a new equilibrium is reached with the reaction force angle within the friction angle. A simplification of the loading situation in which the reaction force is considered to pass through the center of the contact region is shown in figure 4.3.

Using a known (or assumed) friction coefficient for the contact surface, the angle at which the resultant combined centrifugal and bending load will cause contact surface slip can be calculated.

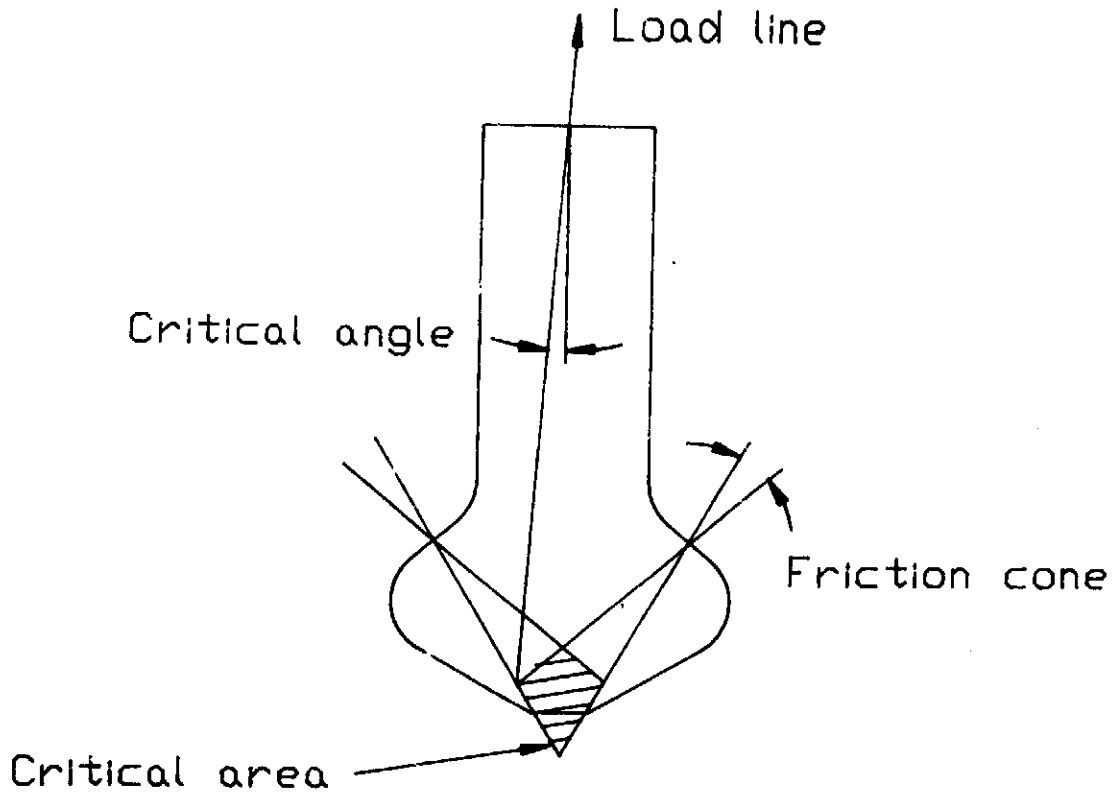

Figure 4.3 Force analysis pertaining to contact surface slip

If the load angle does not pass through the critical area as shown in figure 4.3 the first stage of slip criticality is reached. Increasing the load angle beyond this point may not cause immediate slip but will move the reaction force positions towards the ends of the contact regions. This situation is illustrated in figure 4.4. In this case the critical area is bounded by lines passing through the ends of the contact surfaces and which form an angle with the contact surface normal. This angle is the assumed or known contact surface friction angle as described above. When the extension of the loading force vector moves outside this critical zone slip will take place. It should however be noted that to reach this situation large contact force shifts must have taken place.

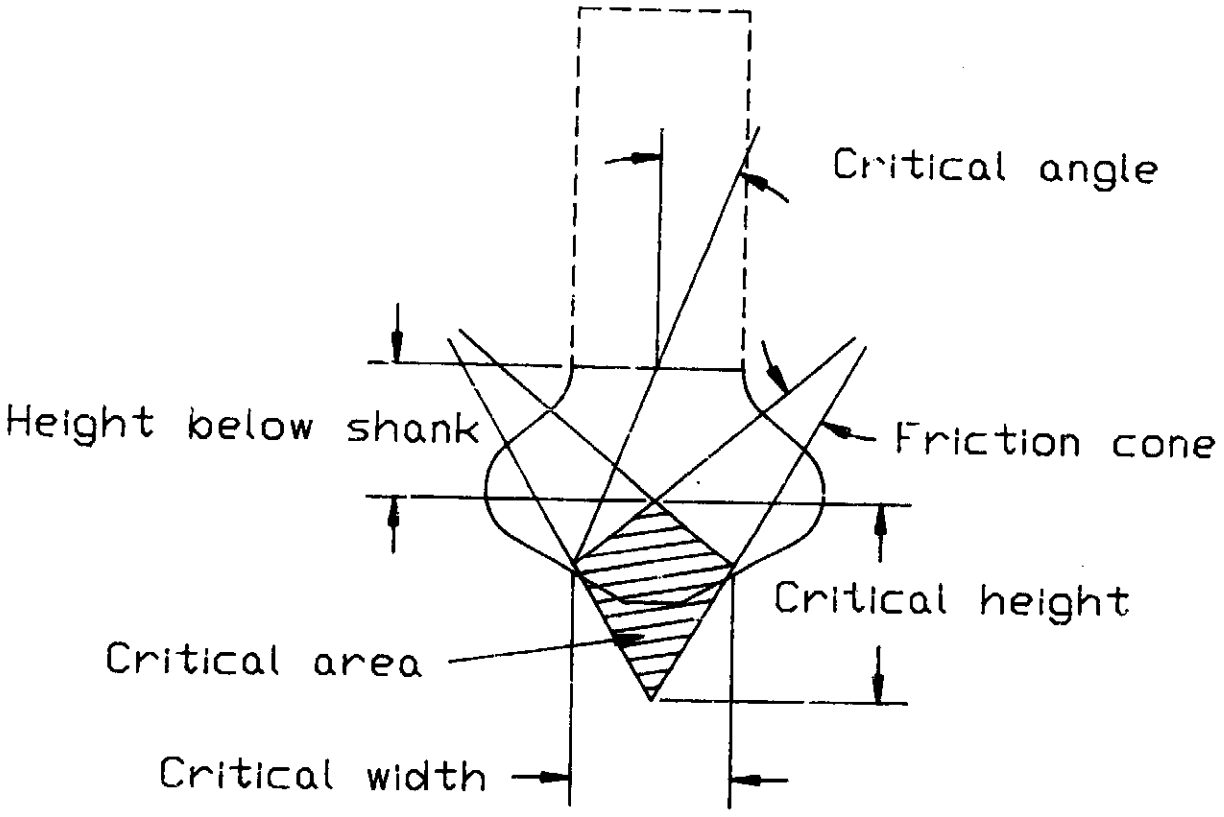

Figure 4.4 Ultimate slip criticality for a 10° friction angle.

The design of a turbine blade should be such that the resultant of the loads carried by the blade should always pass through this critical area. From the figure it can be seen that this

criterion places a limitation on the ratio of bending force to centrifugal force and on the length of the shank. The shorter the shank, the more bending force can be applied for a certain centrifugal force. Calculating the critical height, critical width, height below shank and critical angle formed part of the stress calculation program discussed in appendix 1.

The definition of the critical angle as presented in figure 4.4 allows easy comparisons to be made without involving varying shank lengths. It should however be noted that the real load angle will be much less due to the length of the shank and airfoil as illustrated in figure 4.3.

Experimental verification for this analysis can be obtained from Hattori et al. [13] who analysed the contact surface slip experimentally. It was found that a friction coefficient of 0.15 existed in the contact region close to the shank while the friction coefficient close to R2 was 0.7. As the friction coefficient close to the shank has a far greater influence on the critical angle it can be used for the whole surface. A combined centrifugal and bending load angle of 4°, measured 185 mm above the start of the shank region, produced total surface slip in Hattoris experiments. The analysis as described above yields the same result for the geometry.

The method can be used to analyze designs provided that the friction coefficient in the contact region is known. As this changes with time, number of cycles, oxidation and creep an accurate analysis is seldom possible. On the other hand the analysis could be used to determine friction coefficients from experimentally determined critical load angles.

CHAPTER 5

5. Optimizing the blade root profile

5.1 Factors influencing the performance of a blade root

5.1.1 The nature of the load

The main load (seen from a force magnitude point of view) is the centrifugal force acting radially through the center of gravity of the blade due to the rotation of the rotor. Together with the nominally constant gas force acting as a bending moment on the blade, a radial force acting through the center of the blade root is set up. The magnitude of the force is dependant on the rotational speed of the turbine and on the mass of the blade. A low cycle fatigue scenario exists here because the load cycles are determined by the number of starts and speed variations that the turbine undergoes. This number falls well into the low cycle fatigue region.

The second important force acting on the blade and consequently on the blade root is a bending force with a predominantly vibrational nature. The force is generated by high frequency variations in gas force as experienced by first stages in steam turbines with partial impingement and by vibrations of the blade. Other causes of variations in gas forces result from variations in tip losses due to misalignment of housings, variations in the circumferential gas temperature profile due to differences in burner performance. In the case of turbines using a single burner non uniform circumferential gas distribution also causes high cycle gas force fluctuations.

Due to the high frequency of these loads and in spite of their usually short duration they fall into the high cycle fatigue region.

5.1.2 Stress distribution in the blade root

The ideal mechanical design makes optimal use of all material utilized. In terms of material stress this means that all the material present in a component should be critically stressed just before total failure occurs in the component. Only ropes and cables can be designed to meet this criterion. A compromise which would make the strategy practical would be to define certain areas of the component as critical and to strive to achieve criticality in these regions simultaneously or in the sequence of magnitude of the risk or damage induced.

As cracks and other failures usually originate at the surface of a component, surface stresses are usually the subject of intense design scrutiny. The fillet region of the blade root is one such critical region. The aim of an optimization exercise would be to manipulate the root geometry in such a way as to minimize the fillet stress while making optimal use of the root material.

5.1.3 Root operating environment

Turbine blades operate in severe thermal and chemical conditions. In spite of shielding and cooling the temperatures at the blade root and the chemical composition of gases surrounding the root are not ideal. In gas turbines combustion products and in steam turbines the steam and even more condensate with selective contaminants can attack the blade and rotor materials. Thermal gradients in the root and the rotor generate forces in the contact region which can lead to slip with the consequent fretting and eventual failure.

5.1.4 Materials

High alloy steels, nickel, cobalt and titanium alloys are the principal materials used in modern turbines. These materials have various individual properties which must be taken into account. An analysis of different material properties falls outside the scope of this project. Among the most important characteristics in a blade material are high temperature

strength, fatigue characteristics, crack propagation properties and fretting tendency. The single crystal blade technology used by some companies requires a different approach to the blade design problem due to the anisotropic directional properties of the material. With the advent of ceramic technology for turbine blades, totally new design philosophies may have to be adopted.

5.1.5 Operational patterns.

As with most machines varying load conditions do not favour long turbine life. Changes in heat load and mechanical loads on components accelerate fatigue. Turbines running at constant loads with few starts can be expected to outlast their counterparts.

5.1.6 Manufacturing constraints

Almost any blade root and rotor notch could be manufactured. The challenge lies in designing a blade root which is mechanically and operationally optimized yet easy and cost effective to manufacture.

5.2 Optimum definition

From the above factors which influence the choice of an optimum it can be seen that "optimum" can mean many different things. The factors to be taken into account to achieve the optimum and those which cannot be quantified must be defined. For instance if the material from which the root will be manufactured and the working loads of the root are known the definition of an optimum would be much more specific and targeted than if these factors would have to be considered as free variables.

With all of the above in mind it is difficult (if not impossible) to develop one generic optimum blade root profile. If limitations are introduced to eliminate the factors which cannot be simulated easily and accurately and emphasis is placed on the more important aspects of blade root operation a easier and feasible optimization criterion can be generated.

For this study the optimum blade root is defined as the one with the lowest fillet stress concentration factor (S.C.F.), where the fillet is the rounded section between the blade shank and the load carrying surface. The stress concentration factor is defined as the maximum stress on the fillet surface (peak I) divided by the average shank stress. An additional and very important optimization requirement is that the blade root be practical for manufacturing, operational, maintenance and cost considerations.

To keep the optimization simple yet meaningful the root geometries were limited to constant radii fillets and protuberance angles (Alpha) of less than 45°. The constant fillet radii make manufacture and comparison between different fillets easier. Making Alpha bigger than 45° moves the root into regions were fretting and the possibility of roots "walking" out of the rotor radially become critical although some small roots with Alpha bigger than 45° are used in practice.

Various ways of reaching an optimum were tried in the course of the study. These are fully described in the relevant chapters.

CHAPTER 6

6. Analytic blade root stress calculation

If theoretical means would exist, they would be a powerful tool to optimize the blade root geometry. Existing methods which could be used to solve the blade root optimization problem are therefore reviewed here.

6.1 The Heywood method

The basis for this analysis is the paper by R.B. Heywood [17]. Heywood studied the tensile fillet stresses generated when projections are loaded with a point load. The projections, having flat upper and lower surfaces were considered to be attached to a semi-infinite plate. The crest and fillet radii were chosen to be equal. Loading was by a point force on the top face. A typical projection test piece as used by Heywood in his work is shown in figure 6.1 below.

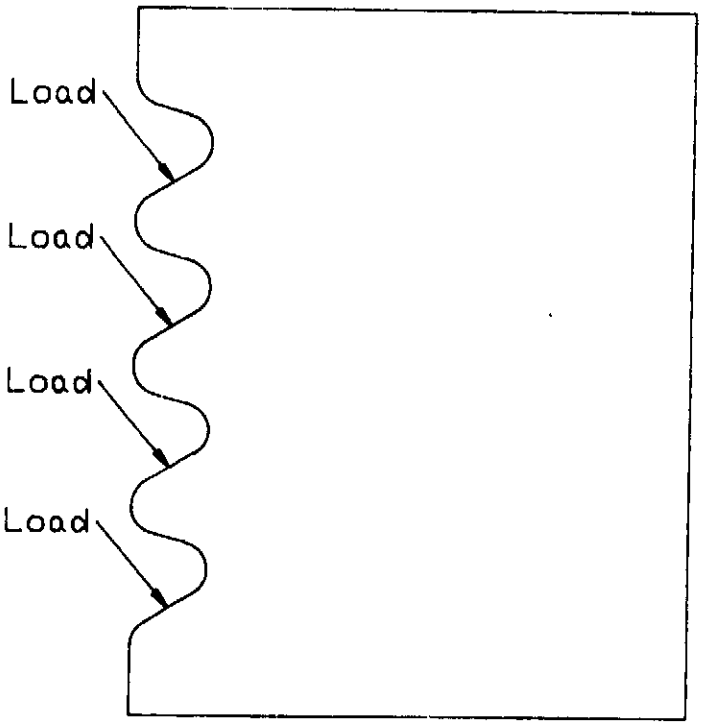

Figure 6.1 Heywood projection test piece.

Heywoods work was aimed at determining optimal shapes for screw threads. As an additional result his work could also be used to determine the fillet stresses in gear teeth more accurately that

the Lewis formula. From a series of photoelastic experiments Heywood compiled a formula to calculate the fillet stress of a loaded projection. The formula will be discussed in detail later. As can be seen from figure 6.1 the Heywood Projection is similar to a single tang of a fir tree type blade root. This similarity in geometry prompted the question if the formula developed by Heywood could be used to predict the fillet stress in a turbine blade root. For the purpose of using the Heywood formula the geometric formulation used by Heywood had to be equated to the formulation selected for this work as discussed in chapter 4. Figure 6.2 below compares the two formulations in a pair of tangs on a multiple tang root which is symmetric about its center line.

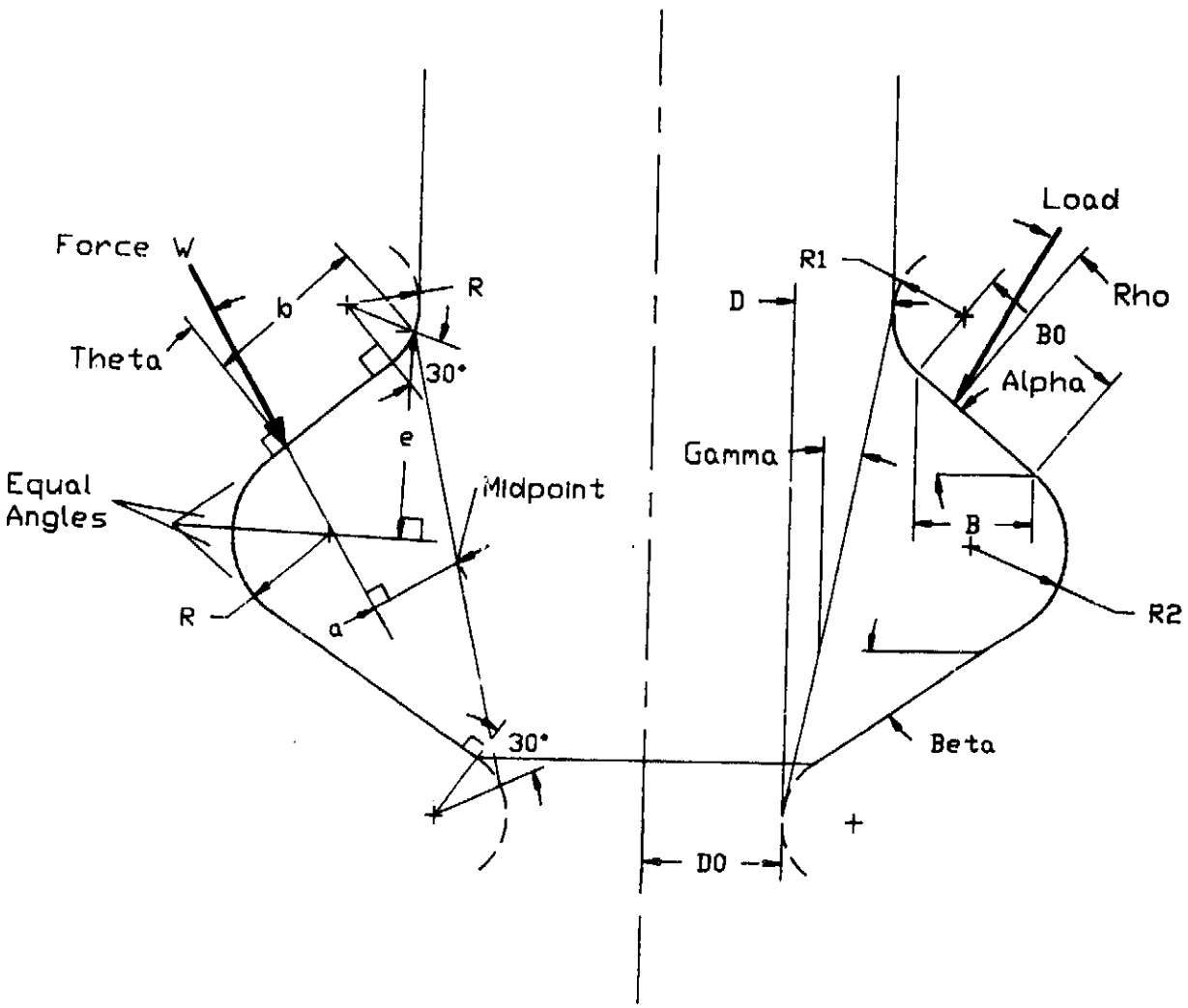

Figure 6.2 Heywood geometric parameters (left) Present geometric parameters (right).

The Heywood formula is given by:

$$\text{Fill. Stress} = \left[1+0.26\left(\frac{e}{R}\right)^{0.7}\right]\left[1.5\,\frac{a}{e^2} + \sqrt{\frac{0.36}{b\ e}}\,(1+\tfrac{1}{4}\sin\ \text{Gamma})\right]\frac{W}{t}$$

With a, b, e, R and Theta as given in figure 6.2 . W is the force of the point load and t is the thickness of the material.

The formula has its roots in elastic stress analysis as can be seen from its form: Fillet Stress = K * (M + L) where M expresses the nominal bending moment, L represents a proximity factor depending on the distance between the load and the fillet and K is a stress concentration factor. If certain limiting cases are studied the sound theoretical basis of the formula can be established. Limiting cases include the long cantilever where the proximity factor tends to be very small and the small projection case with a large fillet radius where the stress concentration factor becomes small. The formula has its limitations as was found when it was implemented with a harsh choice of blade root geometry (for which the formula was not intended but seems suitable).

As can be seen from the figure the load in the Heywood geometry is applied as a point force while in blade roots the load is applied over the whole upper surface (ie. length BO). The difficulty arising here is the lack of knowledge of the distribution of the force in the true loaded situation. A similar problem was encountered by various authors in their finite element modeling an discussed in chapter 3.

To apply the formula to the blade root a computer program was written which transforms the blade root variables chosen here (figure 4.1) into the variables used by Heywood. The program then implements the formula to calculate the fillet stress. The program also makes provision for different load distributions by superimposing the results of a series of point loads. Provision was made for the five force distribution patterns shown in figure 6.3.

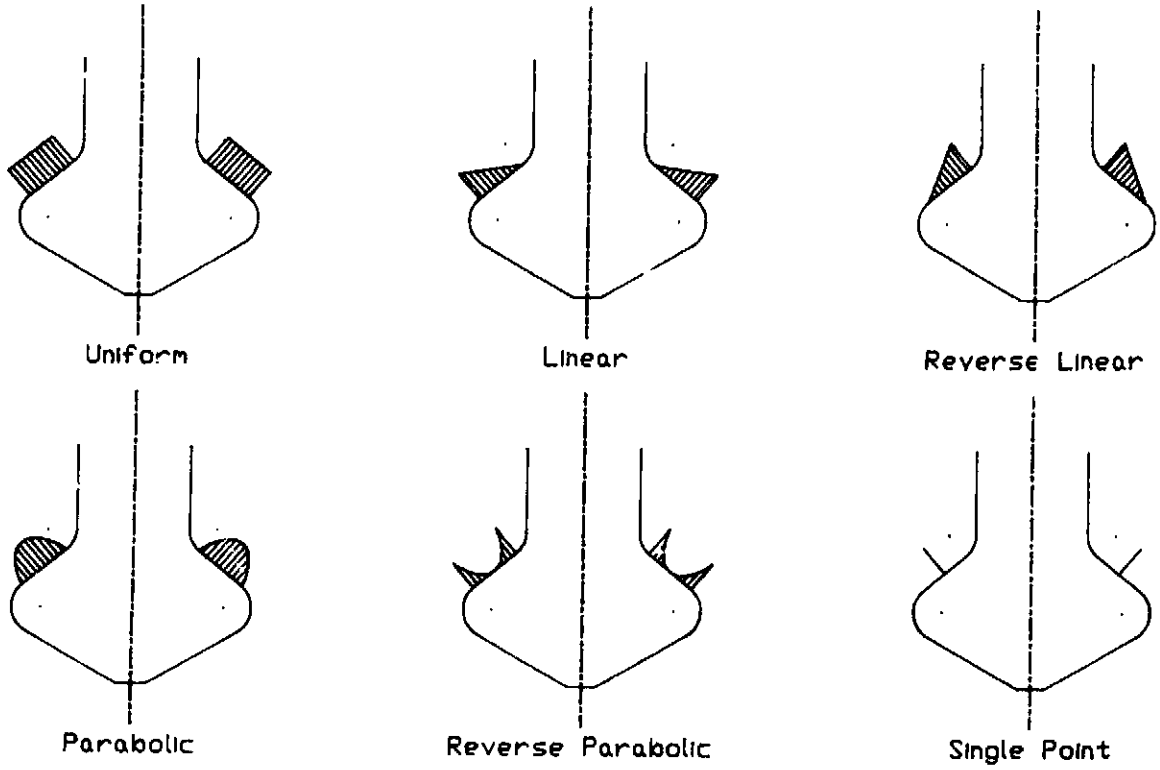

Figure 6.3 Force distribution patterns

						Peak II Stress concentration factors				
Alpha	Beta	R1	B	D	DO	Uni	Lin	Revlin	Para	Revpara
40	34	3.1	4.3	5.23	9.08	3.77	4.15	3.39	3.69	3.93
45	34	3.10	4.3	5.25	9.08	3.41	3.81	3.01	3.32	3.59
35	34	3.10	4.3	5.24	9.08	4.23	4.61	3.85	4.16	4.38
40	39	3.10	4.3	5.66	9.08	3.53	3.90	3.16	3.45	3.69
40	29	3.10	4.3	4.90	9.08	3.98	4.38	3.57	3.90	4.13
40	34	3.60	4.3	5.74	9.08	3.48	3.81	3.15	3.41	3.61
40	34	4.10	4.3	6.24	9.08	3.25	3.53	2.96	3.19	3.35
40	34	3.10	4.3	5.23	6.08	2.98	3.28	2.68	2.92	3.11
40	34	3.10	4.3	5.23	12.1	4.56	5.03	4.09	4.46	4.75
40	34	3.10	4.3	7.72	9.08	4.82	5.27	4.37	4.73	5.01
40	34	3.10	4.3	3.20	9.08	3.00	3.33	2.67	2.93	3.14
40	34	3.10	3.3	4.74	9.08	3.83	4.20	3.52	3.80	3.99
40	34	3.10	5.3	5.73	9.08	3.69	4.11	3.28	3.60	3.88
50	34	3.10	4.3	5.31	9.08	3.16	3.57	2.75	3.05	3.36
40	34	5.10	4.3	7.25	9.08	2.90	3.12	2.68	2.86	2.98
40	45	3.29	6.7	10.0	0.00	1.75	1.97	1.53	1.69	1.87
40	15	4.97	8.3	10.0	0.00	2.20	2.45	1.96	2.16	2.28
40	15	6.10	6.7	10.0	0.00	1.89	2.05	1.72	1.86	1.94
40	45	5.30	5.0	10.0	0.00	1.31	1.44	1.19	1.29	1.36
40	30	6.60	5.0	10.0	0.00	1.52	1.63	1.42	1.51	1.56
40	15	7.20	5.0	10.0	0.00	1.65	1.75	1.54	1.63	1.68
45	45	5.20	5.0	10.0	0.00	1.13	1.27	0.99	1.10	1.19
45	30	6.50	5.0	10.0	0.00	1.42	1.53	1.30	1.39	1.46
45	15	7.10	5.0	10.0	0.00	1.56	1.68	1.45	1.54	1.60

Table 6.4 Some typical Heywood formula results

A preliminary optimization process was then carried out by analyzing various geometries using the program. It was found

that the predicted stress concentration factors fell below 1.00 for some cases which is clearly not possible. At the same time the first photoelastic tests were conducted (which are described in chapter 8). On the strength of this comparison it was decided to conduct the main optimization process using photoelasticity due to the inherent accuracy of experimentation and the higher trust which can be vested in the results.

Some typical results obtained from the Heywood formula program are given in table 6.4. A comparison with the photoelastic results and a discussion of the differences is given in chapter 11.

6.2 Finite Element Analysis

As a part of the introductory work Rust [25] carried out a undergraduate thesis study into the possibility of modeling the blade root contact area and fillet region using finite element analysis. Although the work did not probe very deeply into the latest developments in finite element analysis it was found that a large amount of work is required just to get to know the finite element programs to an extent were trustworthy modeling can be done. The complex nature of the contact region of the blade root precludes any simple modeling. Rust also found that using the contact surface elements provided in the finite element package did not give satisfactory results.

It was thus decided from the onset not to include finite element analysis into this study as the primary aim was to find a optimal blade root geometry and not to develop finite element methods which are capable of modeling complex contact area stress situations. After studying the papers by Boddington, Chen, Ruiz and He [3], [13] and [24] the decision was reconsidered but it was decided to continue on the set course.

CHAPTER 7

7. The Experimental Stress Investigation

7.1 Objectives

The experimental stress investigation is aimed at determining the fillet stress concentration factor for a number of different blade root geometries. Using different loading rigs, different loading patterns could be simulated on various root geometries from which the optimal root geometry could be determined.

7.2 Photoelasticity

Photoelasticity is a very powerful experimental tool which can be used to determine stresses in geometries which are difficult to analyze analytically or numerically. For the purposes of this thesis only limited use was made of the potential power of the method. A number of excellent textbooks by Durelli [5], [6], Frocht [12], Hetenyi [16], Heywood [18] and Kuske and Robertson [22] have been published and serve as a valuable reference base on the subject of photoelasticity. Shorter articles such as the one by Post [25] give a good introduction to the subject.

The experimental method of photoelasticity is based on the phenomenon of temporary double refraction displayed by certain transparent non crystalline materials such as Araldite D. The material, which is optically isotropic in a stress free state becomes optically anisotropic when stressed mechanically. This effect persists while the loads on the material are maintained but disappear when the loads are removed. When passing polarized light through a photoelastic model in the loaded state, the light is split into two refracted components rays. Owing to a difference in refractive index, which is related to the principal stress magnitude, the refracted components have different light velocities while traveling through the material. The so called extraordinary ray has a greater velocity than the ordinary ray and therefore, on emerging from the material, there

is a phase difference, or relative retardation, between the two rays. This relative retardation is proportional to the difference in the magnitude of the principal stresses and to the length of the optical path through the material.

The tool used to study the phenomenon is called a polariscope. A simple polariscope consists of a light source, two polarizing filters and two quarter wave plates. The filters and the quarter wave plates can be rotated about the axis of the light beam. Two stress characteristics can be measured using a simple polariscope.

1) Using only the polarizing filters between the white or monochromatic light source and the model and between the model and the observer results in isoclinic fringes appearing in the model when it is loaded. Isoclinic fringes are dark (black) bands connecting points at which the direction of principal stress is parallel to the polarization plane of the light. By rotating the polarization filters and noting the position of the dark fringes in the model the direction of the principal stresses at all points in the model can be determined for a specific loading state. When using white light, bands of colour also appear in the model. These bands indicate only a partial

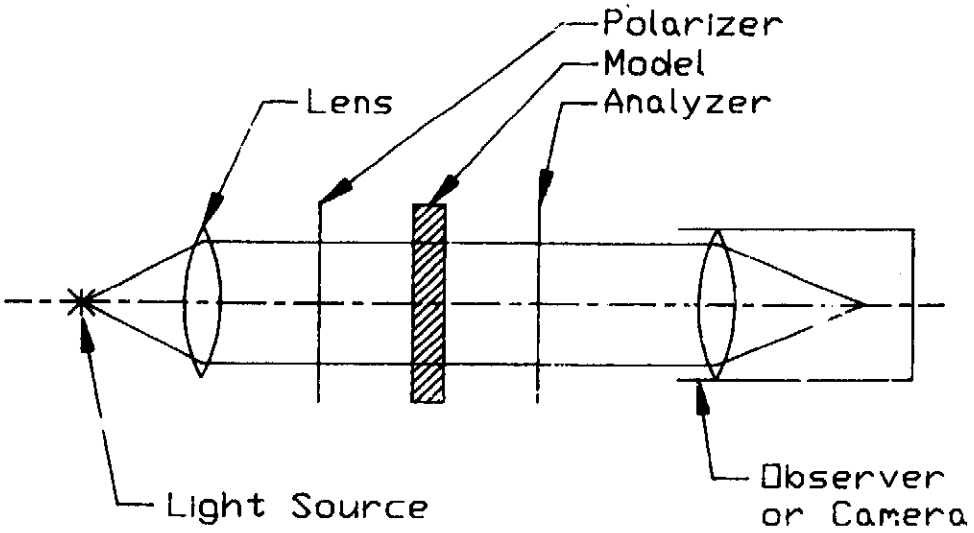

Figure 7.1 The plain polariscope in normal (lens) mode.

extinction of the light and are not isoclinics, but so called isochromatics.

2) Isochromatic fringes only, without isoclinic fringes, can be seen after inserting the quarter wave plates between the model and the polarizing filters. With monochromatic light, these fringes are dark (black) bands joining points of equal principal stress difference. The relationship between the number of fringes and the stress difference is given by the formula:

$$\sigma_1 - \sigma_2 = N f_\sigma / h$$

were σ_1 and σ_2 are the principal stresses, N is the number of fringes, h is the thickness of the model and f_σ is the material fringe value of the photoelastic material being used. As the maximum shear stress in a material is given by:

$$\tau_{max} = (\sigma_1 - \sigma_2)/2$$

the maximum shear stress for all points in the model can be directly determined from the isochromatic fringe pattern. As most critical stresses such as those in the fillet of the blade root are found on an unloaded surface, and one principal stress on such a surface is always zero, the other principal surface stress can be directly and accurately determined from the isochromatic fringe pattern.

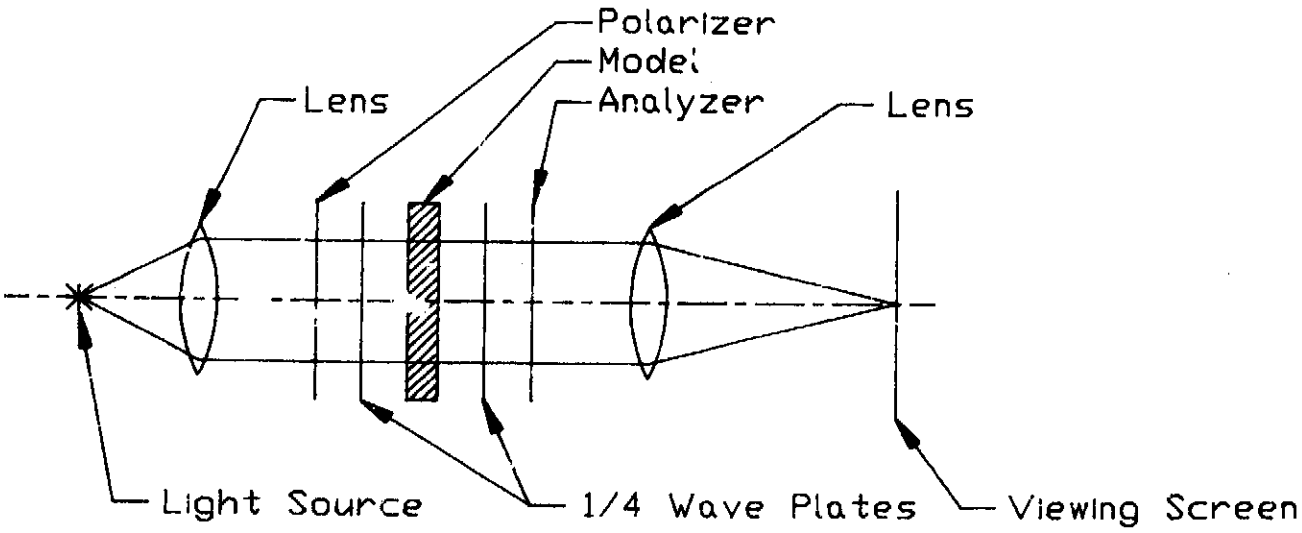

Figure 7.2 The circular polariscope in projection mode.

7.3 The experimental apparatus

The experimental apparatus used to perform the photoelastic experiments consisted of a polariscope and two loading rigs. The two loading rigs were designed and partially built by the student.

7.3.1 The Polariscope

The polariscope used in the experiments for this study could be set up in various ways. In the normal mode the model was viewed by looking through the polariscope from the analyzer side. In the projection mode the image of the model was projected onto a translucent screen placed at the analyzer end of the polariscope. To study isoclinic fringes (principal stress directions) only the polarizer and analyzer are used thus creating a plane polariscope (as shown in figure 7.1). To study isochromatic fringes the polariscope is converted to a circ lar polariscope by adding quarter wave plates between the model and the polarize and tne model and the analyzer as shown in figure 7.2.

For the experiments the polariscope was set up to be used as a circular projection polariscope as shown in figure 7.3. It was found that the best image resolution was obtained by using a mercury vapour light as the point light source in conjunction with a green filter. Photographs were taken using a SRL camera fitted with a 50mm lens. Standard ASA 100 colour film for prints was used. For some of the photographs in which fine detail was required the 50 mm lens was reversed using a standard reversing ring to give a powerful magnification.

7.3.2 The fixed friction angle test rig

The first rig was used to test single tang blade roots under controlled loading conditions. A system using two loading shoes tensioned by stainless steel cables running over "rollers" was used with which the loading direction and loading position could be adjusted to suit the experiment to be undertaken. The rig is

discussed in greater detail in section 8.2. The rig is pictured in figure 8.1.

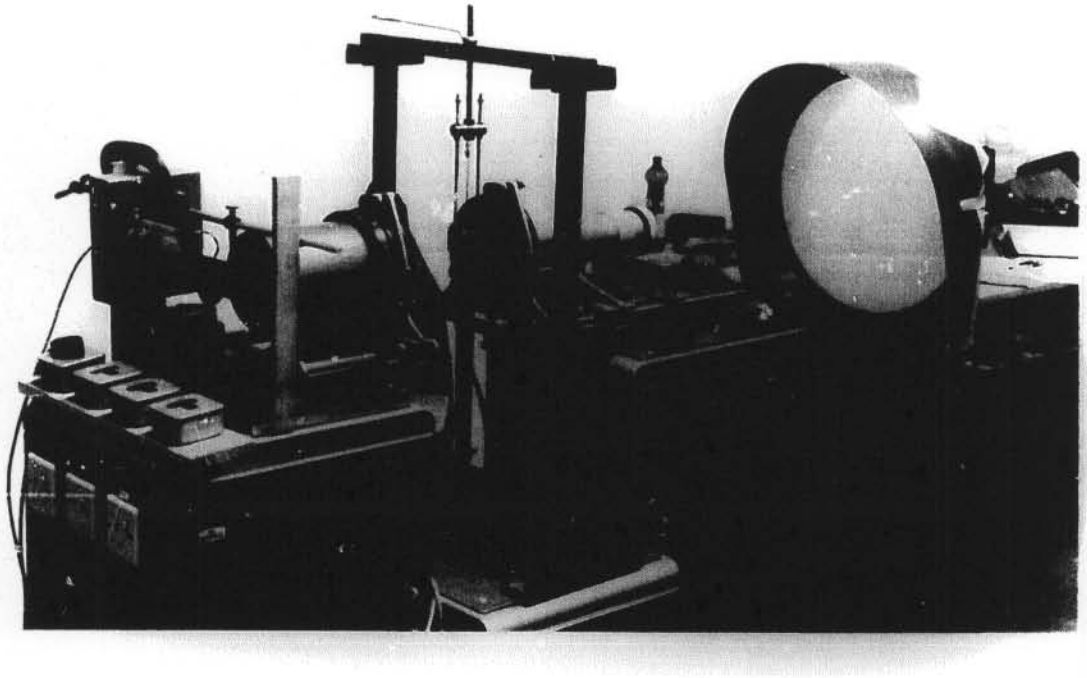

Figure 7.3 The polariscope with the fixed friction angle test rig in place.

7.3.3 The in-rotor test rig

The second loading rig was made to test blade roots in the "in-rotor" position. On the rig five identical blade roots could be fitted into a matching rotor section. The roots could then be loaded either radially, using a system of levers to balance the load between the roots, or offset radially to model a combination of centrifugal and bending forces. The rig is discussed in detail in section 9.2 and is pictured in figure 9.1.

The polariscope loading frame was used to support the in-rotor test rig. The loading frame was equipped with a set of hand wheels which enabled the rig mounted on it to be moved horizontally and vertically in the polariscope allowing different parts of the large model to be viewed.

7.4 Model preparation

The models used in the experimental investigation were all machined from Araldite D sheets which were cast by the student. The casting, machining and storing of the Araldite D require special precautions. Included air bubbles, thermal residual stresses, chipping and time edge effects have to be guarded against. A special method of casting, machining and storing was developed and is fully described in appendix 2.

CHAPTER 8

8. The single tang fixed friction angle investigation

This chapter describes the thinking behind and execution of the single tang fixed load investigation. The results and their implications are also discussed. Many references are made to results which have been included at the end of the chapter in tabulated and graphical form.

8.1 The test philosophy

To study the stresses in a blade root which is in its working position in a rotor, is a complex problem. Different turbines operate under different conditions and various critical areas can be considered, in the definition of an optimum. From practical failures it has been seen that cracks initiate from two areas on the tang of the blade root as was described in chapter 4.

To reduce the complexity of the problem, as many uncontrollable variables as possible have been eliminated from the problem in order to subject it to analysis. The load distribution and load angle, which make up the loading condition variables, are the main uncontrollable variables. When the blade is in its working condition in the turbine rotor these variables are controlled by turbine load, surface condition and thermal effects, to mention but a few. From the results of tests in which these normally uncontrollable variables are artificially controlled, a preliminary optimum geometry could be chosen. Experiments in which the artificial restraints placed on variables are removed can then be conducted to determine how the preliminary optimum geometries perform in simulated operating conditions. On the basis of these results an optimal single tang geometry can be defined. From here the optimum single tang root can be expanded to a multiple tang root. Although only one three tang geometry was tested the optimization process can be expanded but that falls outside the scope of this thesis.

Most in-house studies by major turbine manufacturers make use of normal stress concentration theories (obtained from photoelastic studies) backed up by photoelastic and finite element testing. Photoelastic testing was selected for this investigation because it does not idealize the practical situation as in finite element analysis. Frictional effects and machining inaccuracies which would be lost in a finite element analysis, clearly show up in the photoelastic tests making the results obtained realistic and practically usable.

8.2 Implementation of the test philosophy.

8.2.1 The fixed friction angle test rig.

The test rig shown in figure 8.1 was designed and built to test blade roots under controlled conditions. The load shoes on the test rig could be adjusted to set the load position and the load angle. The load position was adjusted by placing the end of the load shoe at the fillet end of the contact area thus loading the whole contact area. The loading cable was positioned so that it intersected the contact area in the middle. The load angle was set by moving the lower load cable guide roller up and down, thus changing the angle between the cable and the contact surface. The position and angle of the cable were dependant on one another and had to be adjusted together. The adjustment of the loading was checked using a ruler and a protractor on the projection screen. Using the polariscope in the projection mode, made the manual adjustment of the load angle and position very accurate due to the triple magnification produced by the projection.

Despite careful adjustment, a reproducible load distribution could only be achieved within certain limits. Microscopic, or near field, modeling in the contact region is difficult due to the large effect which small geometric variations have on the load distribution. In practice turbine rotors are spun to overspeeds to plastically deform contact asperities thus creating the desired flat, well matched contact surface.

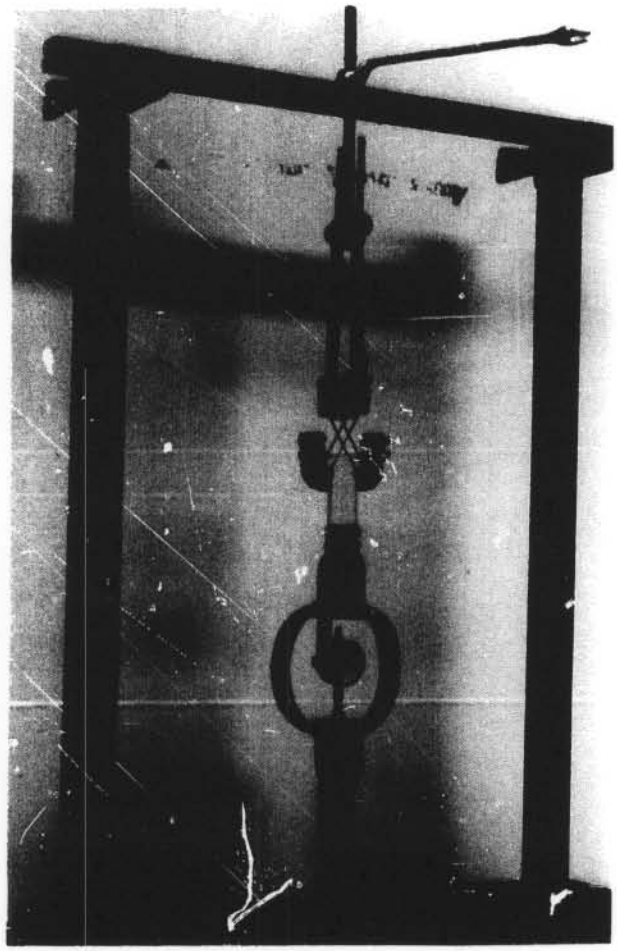

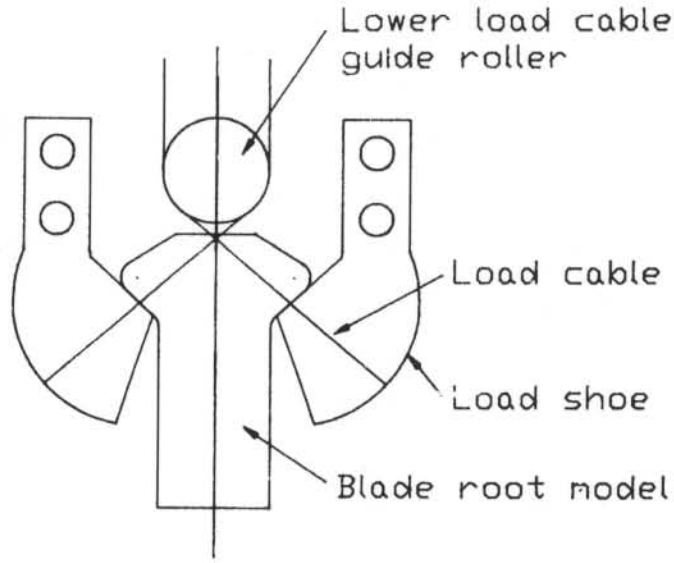

Figure 8.1 The fixed friction angle test rig.

To achieve this situation with the Araldite D used in the photoelastic experiments, the contact surfaces were smoothed by hand as described in appendix 2. The results achieved using this method were satisfactory. To achieve proper contact conditions the load shoes were made by clamping a piece of Araldite D with the contour corresponding to the rotor tang between two pieces of steel. Using like surfaces and rigid clamping produced experimental conditions as close to practical conditions as possible. Combining this with accurate loading, produced good reproducible results.

8.2.2 The experimental procedure

After smoothing the contact surfaces the roots were clamped and fixed into the test rig as shown in figure 8.1. The load angle was set at -10°, -5°, 0°, 5° and 10° respectively and the root was loaded to a shank fringe order of 4. A full load release followed each test to make adjustments to the load angle possible. The fringe order was kept to 4 in the shank to prevent plastic deformations in the contact and fillet regions. The test rig was also close to its load limit and would have had to be strengthened to withstand higher loads. Fringe orders of 4 in the shank gave maximum accuracy of +/- 0.125 on the stress concentration factor due to the limitation of maximum readable accuracy of the fillet stress being 0.5 fringes. As can be seen from the results however, the experimental scatter exceeded 0.125 in some cases. Because each root was represented by 5 data points (one for each load angle) the overall repeatability (accuracy) could be maintained. Using lower fringe orders in the shank would have compromised the accuracy and generated more scatter. No special tools (like compensators) were used to determine the fillet stresses, because the polariscope setup and the model size did not make it practical. Accuracies which are theoretically attainable with compensators and other accuracy enhancing tools could not be reliably obtained due to loading inaccuracies, edge effects, steep stress gradients in critical areas and focus difficulties due to the model thickness. The higher accuracy would thus have been artificial and not practically repeatable. The results presented in this report have proven to be repeatable to the accuracies mentioned above.

Photographs were taken of the different loaded conditions and a record was kept of the fillet fringe value. The fillet fringe value can be counted relatively easily from the projection on the polariscope screen even in areas of high stress gradient i.e. high fringe density. Although the fringes could be counted from the photographs, it is far more difficult and can become unreliable in high stress gradient zones . Thus the photographs simply served as a means of reporting results and of backing up experimental data.

8.3 The experimental development

The single tang fixed friction angle experiments can be divided into three phases: Phase 1. An initial set of exploratory experiments. Phase 2. An initial optimization. Phase 3. A rigidly structured, practicality orientated final optimization.

8.3.1 Phase 1. Initial experiments. (Roots 1 to 25)

The first part of the investigation consisted of a rather random approach to the optimization problem and was performed essentially to get a feeling for the experimental procedures. Casting model machining, model preparation, load positioning and photography techniques were all very crude at this stage and development of these skills was undertaken in this phase of experimentation. The test rig was also modified in certain areas to enable easier and more accurate adjustment and to make provision for testing a wider variety of geometries so that the rig produced suitable and reproducible results and was easy to use. Although the results of the experiments were not as useful as the results of subsequent experiments, the experimental skill gained and the result processing experience justified the work involved. Techniques which received special attention in this phase and which were much improved by the experience gained were: Plate casting methods, machining of roots, photographing skills and testing procedures. (Note: Roots 26 and 27 were not tested)

8.3.2 Phase 2. First optimization (Roots 28 to 39)

The lessons learnt in the first experimentation phase were implemented in the second phase. The second phase aimed to obtain an optimum by varying the key geometric parameters of a reference root, one at a time, to produce an optimum for each parameter. Using the principle of parameter independence, the combination of the independent optimums should in theory produce the total optimum. The reference geometry was chosen on the basis of the results of part one. Two factors motivated further experimentation: 1. The experimental data indicated the need for

further extensive experimentation and 2. the extrapolated optimum would not have been a practically viable geometry. At this point it was decided to try a different approach to the problem which would stand on a firmer theoretical footing and would be more goal orientated. This approach is described in phase 3.

Problems with photography, loading accuracy and data scatter resulted in a low level of trust being ascribed to this set of experiments which, although, useful as a step to further work, could not be used as final results.

8.3.3 Phase 3. Final Optimization (Roots 43 to 66)

In the optimization process up to this point very little cognizance was taken of the practicality of the geometry. Three components constitute the practicality of the geometry:

1. The ease of manufacture. Most rotors are made by milling or broaching slots for the roots into a disc. In order to transfer sufficient cutting torque to the milling cutter the "shank" section of the lowest tang must be sufficiently wide to accommodate an adequate cutter shaft. For broaching the limitations are not as harsh but long broaches must be used. The parameter D_o in the root geometry would therefore be zero to make optimal use of the available material but is normally larger than zero to accommodate the afore mentioned manufacturing limitations. Some manufacturers use a large D_o to achieve a large radius at the bottom of the root to reduce the S.C.F. in the bottom of the rotor groove for turbines which have large and frequent speed variations and are therefore susceptible to high cycle fatigue. The last argument for increasing D_o above the absolute minimum is less applicable to constant speed turbines with a low number of startup-shutdown cycles (5-10000). The roots used in this phase of experimentation all used D_o=0. This simulates the ideal condition and the compromise to be made by enlarging D_o to facilitate manufacture would have to be made by the manufacturer to accommodate his needs. D_o can be enlarged by widening the

whole blade root or by only widening the lower part of the root which in effect is similar to reducing Gamma (see chapter 2). To complete the analysis of all probable (as opposed to possible) root geometries, a further study would have to be undertaken to cover variations in D_o but such a substantial investigation fell beyond the scope of this thesis.

Most optimized fillets (not only blade root fillets) use constantly varying radii (similar to a spiral) to achieve low S.C.F.. Manufacturing such a fillet may however present problems mainly from a cost viewpoint. The fillets used in this investigation only use a single radius, but small improvements may be possible by using varying fillet radii.

2. The practicality of the root. The larger the contact angle Alpha and the larger the circumferential dimension of the blade root, the higher the tendency of the root to "walk" out of the notch in a radial direction. Blades "walk" out of rotor grooves by a stick-slip action produced by variations in centrifugal forces and temperature changes causing lateral expansion in the course of turbine operation. The smaller the contact angle, Alpha (α) is, the less the possibility is of the root "walking". Conversely it is not difficult to intuitively see that an increase in Alpha would decrease the stress concentration factor in the fillet. From the result of phase 2 it can be seen that this does happen in practice.

The other factor which is very important in root design is the amount of fretting which takes place in the contact region. The amount of fretting damage is directly proportional to the magnitude of the contact surface movement as presented by He and Ruiz [15]. Limiting or eliminating the movement would result in much improved fretting characteristics. The fretting damage is also proportional to the shear stress in the contact zone and to reduce this stress high temperature lubricants are used in the contact region thus increasing the possibility of movement. The lubrication also helps to prevent the root from walking as the resulting low friction coefficient does not allow the root to stick. The magnitude of the movement is proportional to Alpha.

The size of Alpha must now be chosen as high as possible (for the best fillet S.C.F) without compromising practicality with regard to "walking" and fretting.

For the purpose of this study Alpha was restricted to 40° and 45° with the idea of using the 45° roots for small blade roots where the movement in the contact region is restricted by virtue of the size of the root. Large roots would be restricted to Alpha = 40° due to the larger possible movement in the contact region. The choice of angles is based on practical industrial experience passed on to the student by Prof. Endres. Some turbines have been built with Alpha higher than 45° and in at least one case (Alpha = 60°) the roots walked out of the rotor after a few months of operation. The extreme case of small contact surface angle (Alpha = 0°) is the hammer head root which is still widely used for moderate centrifugal forces.

<u>3. Optimization from an average stress or maximum material utilization point of view.</u> Up to now and in much of the work that is to follow, the optimum root geometry was defined as the geometry which resulted in the lowest fillet stress concentration factor. A different approach to optimization can also be followed which is based on the philosophy of maximum material utilization. In other words, arranging the available material in such a way that the stress criticality in every point in the stress field is equal and that when failure occurs, all the material in the stressed member fails simultaneously. The ideal is impossible to achieve in practice, the theory can, however, be used as a tool if a few simplifying assumptions are made.

<u>Assumption 1.</u> Three critical areas can be defined in the root geometry: The shank cross section, the contact surface and the tang shear section. Each of these critical areas are characterized by a different kind of stress. The shank cross section is in tensile normal stress, the contact surface is in compressive normal stress and the tang shear area is subject to a shear stress. Other possible critical areas such as "peak II"

are not studied in this section but should form an important part of a future study.

<u>Assumption 2.</u> The stresses in the critical areas are uniformly distributed. This assumption is rather radical as the whole study is aimed at achieving a shank stress as uniformly distributed as possible (S.C.F. = 1) and now it is being assumed as a starting point. Also the friction in the contact region distorts a uniform stress distribution even more than is the case between normally loaded flat contacting planes. The bending moment in the tang, as well as the non-uniformity of the shear stress distribution are disregarded.

In practice the above assumptions are implemented by limiting the combinations of parameters to geometries which obey certain rules. In order to achieve failure in the three critical regions at the same time, the relationship between the areas must be based on some failure theory. The von Misses failure criterion was chosen for the relationship between the shank cross section and the shear section due to its easy form and proven practical accuracy. For the relationship between the shank cross section and the contact surface area a variation was allowed. For most steels it is assumed that the tensile and compressive yield stresses are equal. It is however possible to allow much higher compressive yield stresses if the practical situation is taken into account. The contact surface allows some plastic deformation to take place. This is indeed encouraged by overspeed spinning of the rotor before the turbine is commissioned and serves to equalize the stress distribution in the contact region. It must also be remembered that the shank cross section can never be fully utilized because of the fillet stress concentration factor. Ratios of tensile stress to compressive stress were taken as 1:1.0, 1:1.2, 1:1.5 and 1:2.0

To summarize, the limitations imposed on the final single tang tests were:

1.	$D_o=0$	Material efficiency
2.	Alpha = 40° and 45°	Prevents root walking
3.	$h/D = \sigma/\tau = 1.732$	von Misses failure
4.	B/D = 1, 0.83, 0.66, 0.5	Contact region area

8.4 Experimental result manipulation.

As with all experiments, some results can be seen to be incorrect, and this study is no exception. Each root yielded 5 experimental data points, one for each loading (friction) angle. These results, taken directly from the experiments, are listed and discussed on the following pages together with some judiciously modified data which was obtained as follows:

1 Smoothed: Using a simple least squares fit, a parabola was fitted through the 5 experimental points. The values of the parabolic fit were then listed as "Smoothed".

2. Modified: The weakness inherent in simply smoothing experimental data lies in the fact that experimental errors are not removed but simply spread more evenly. Inspecting the experimental data, erroneous values can often be easily spotted. Modifying the data involved removing data point which did not look correct and fitting a curve through the remaining points. The point on the graph corresponding to the removed point was then substituted as the correct value. This procedure yielded the "Modified" data. In some cases where compliance of experimental data was very unsatisfactory, a duplicate root was cut from new material and the test was redone.

3. Modified smoothed: Having removed the "wrong" data the resultant data could be smoothed with a parabolic least squares fit as in 1 above. These results were listed as "Modified Smoothed". The product of these data manipulations provided the best data for optimization analysis purposes because it was reasonably free of experimental errors.

To effectively show the results graphically in a way in which the different roots could be compared, presented a problem in that each root was represented by 5 data points. The geometric variations between the roots also had to be shown on the graphs to make S.C.F. variations versus geometric variations visible. Each graph on the following pages was created to show as much useful information as possible in the context of the experiment

in which it was created. When only one data point is given per root it is the 0° load angle reading.

8.5 The experimental results.

A listing of all the results obtained for the fixed friction angle experiments is given at the end of the chapter. The most important findings will be discussed here.

Phase 1. : As mentioned previously the results obtained in this phase were not accurate enough to make a quantitative analysis. As can be seen in the result listing no clear direction was followed in the choice of geometries thus making analysis impossible. A more orderly approach to the problem was required and this was done in phase 2.

Phase 2. : Using a base geometry (Root 38, Alpha = 50°, Beta = 45°, R = 5 mm, B = 5 mm, D_o = 6 mm, Gamma = 15°), chosen as representative average from a group of industrially applied geometries, variations were made to the main parameters facilitating a orderly optimum search. Alpha, Beta, R (R1 and R2) and B were varied above and below the original values. A graphic representation of the results is given in figures 8.2 to 8.9. For each parameter a graph of the actual experimental results and a graph of the "modified smoothed" results are given. This was done to illustrate experimental scatter, which at this stage of the experimentation was still large, and to bring to the fore the clear trends of S.C.F. variations for the geometry changes using the "modified smoothed" results which cannot be seen so well in the straight experimental data. Although the experimental scatter is large when compared to differences between the curves, The results can be interpreted with reasonable accuracy due to the smoothing method employed.

Alpha: (Figures 8.2 and 8.3) As Alpha is increased from 40° to 50° the S.C.F. decreases as would intuitively be expected due to the reduction in the sharpness of the fillet. A result that is not expected is the rise in S.C.F. as Alpha is increased above 50°. From the results Alpha = 50° presents a S.C.F. optimum.

Beta: (Figures 8.4 and 8.5) Beta = 40° gives a minimum S.C.F. in the range tested. An Interesting phenomenon found in this section is that the S.C.F. for Beta = 45° shows a greater variation for different load angles than Beta = 40° and Beta = 35°. This reflects the influence of the combination of the projection's "beam" height and the load angle on the S.C.F. The higher the beam the larger the influence of the load angle will be on the S.C.F. In practice this means that a root with a large Beta, subjected to vibrational bending forces, which reverse the effective load angle, will be more susceptible to fatigue failures by virtue of the greater stress fluctuations. On a modified Goodman diagram the effect of increasing the stress fluctuation amplitude can be clearly seen to move the allowable mean stress before failure downwards. Beta should thus be kept rather too small than too large to provide an optimum.

Fillet radius R : (Figures 8.6 and 8.7) According to classical stress raiser theory the largest radius will give the smallest S.C.F. The results of the experiments only bear the theory out partially in that the medium radii return small S.C.F. for low load angles. What is disturbing about the results is the fact that an increase in radius does not always lead to a decrease in S.C.F. as would be expected. This is due to the longer bending lever produced in the geometry by a larger fillet.

Contact area length B : (Figures 8.8 and 8.9) This shows a minimum at B/D = 5 along most of the load angle axis. The smaller variation in S.C.F. between maximum and minimum load angle for B/D = 5.5 should be noted. Again the theory that the longer contact zone should give the lower stress is compromised by the fact that the center of the load moves further away from the fillet, thus creating a higher bending stress, as the contact length increases.

From the above it can be seen that even for individual parameters no single value can be considered a general optimum. Combining these optimums to form a general overall optimum would create even greater difficulties. If however, specific demands

have to be met in the design of a root the above approach to reaching an optimum may be the best. For this study however, it was decided to try the material utilization approach as well, to gauge its effectiveness.

Phase 3.

Phase 3 was divided into two sections, one consisting of roots with Alpha = 45° and the other with roots of Alpha = 40°. Both sets of roots were restricted to h/D = $\sqrt{3}$ and D_o=0. The experimentation range was B/D = 1.0, 1/1.2, 1/1.5 and 1/2.0 . The results obtained are graphically depicted on the following pages using four approaches. 1. S.C.F. vs. load angle graphs, similar to those presented in the previous section, for all the tested geometries using "modified smoothed" data.(Figures 8.10 and 8.11) 2. Three dimensional graphs of S.C.F. vs. R/D and Gamma.(Figures 8.12 and 8.13) 3. Non-dimensional graphs depicting the S.C.F. range as influenced by load angle (Figures 8.14 and 8.15) and 4. Non-dimensional graphs showing actual root geometries (Figures 8.16 and 8.17). A complete listing of all the results and geometries is given at the end of the chapter.

The results for both sections show two clear tendencies: 1. The S.C.F. decreases with a decrease in B/D, that is, a rise in average contact surface pressure (with constant Beta or R/D), and 2. Along a line of constant B/D the S.C.F. decreases with a decrease in Beta or an increase of R/D. The decrease in S C.F. with an increase in fillet radius is expected due to the stress relieving effect of large fillets in contrast to smaller fillets.

The decrease in S.C.F. with decreased contact zone length B, can be ascribed to the reduction in the length of the effective bending lever and the effective deepening of the projection beam height resulting from the prescribed constant h/D = $\sqrt{3}$. The actual influence of varying any one parameter cannot be isolated. For this reason, the apparent influence of Beta on the S.C.F. is not regarded as important (in the context of the geometric restraints placed on the choice of geometry) due to

the expected stronger influences of fillet radius and contact length. Alpha = 40° yields a lower and flatter optimum curve than Alpha = 45° as can be seen when comparing figures 8.14 to 8.17. The parameter R/D could not be included on these graphs as only a limited number of variables can be sensibly plotted on one two dimensional graph.

The average S.C.F. for the 40° roots seen as a group is also less than that of the 45° roots. This result is not expected from an intuitive point of view because a higher Alpha is associated with a lower S.C.F. due to the smaller included fillet angle.

Figures 8.16 and 8.17 are useful to get a feeling for what a optimum root should look like. The actual root geometries, as tested, are plotted on the same set of axis as the geometric variables and the S.C.F. of each root.

8.6 Expansion of experiments to the in-rotor situation.

As seen from the results of the previous section the optimization curves for both Alpha = 40° and Alpha = 45° are very flat. The maximum variations in S.C.F. for the geometries tested were 18% and 25% respectively. These relatively flat optimization curves account, to a large degree, for the variations in root geometries used in industry. The choosing of an optimum becomes difficult because the choice of geometry does not have a considerable effect on the S.C.F. while effects, such as contact surface stress, assume critical status. Thus the relatively flat optimization curve moves the optimum geometry decision away from the S.C.F. limitation to the contact surface stress limitation.

It was decided to test two geometries in the in-rotor simulation, one with Alpha = 40° and the other with Alpha = 45°. A limitation of B/D > 0.6667 was originally placed on the geometries to be tested but, due to the success that the configuration with B/D = 0.5 achieved in the S.C.F. tests, it was decided to relax the limitation. Due to the similarity in

shape of the optimization curves for the two Alpha angles, it was decided to straddle the apparent optimum and use B/D = 0.5 for one root and B/D = 0.6667 for the other. With judicious interpolation, straddling the apparent optimum also widens the data field available for analysis. The two roots are also expected to show comparable resistance to "walking" as the low contact surface angle (Alpha = 40°) root has the shorter contact surfaces (B/D = 0.5) and the steeper contact surface angle (Alpha = 45°) root has the longer (B/D = 0.6667) contact surfaces. The decision was also motivated by the fact that these root geometries are currently being used by two turbine manufacturers. The two root geometries with which it was decided to continue the study were:

1. Alpha = 40°, Beta = 30°, B/D = 0.5, h/D = √3
2. Alpha = 45°, Beta = 15°, B/D = 0.6667, h/D = √3

The experiments conducted and results obtained are described in the following chapter.

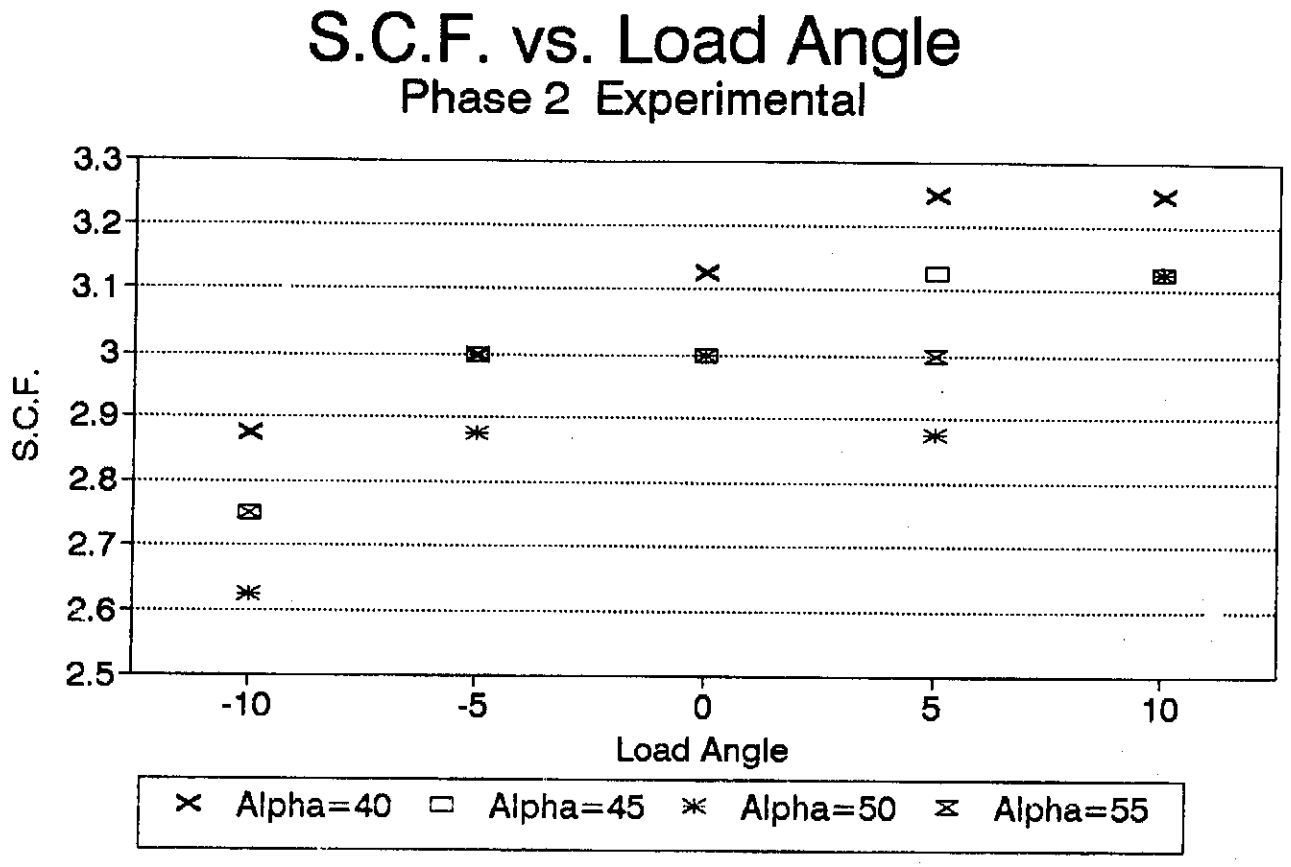

Figure 8.2

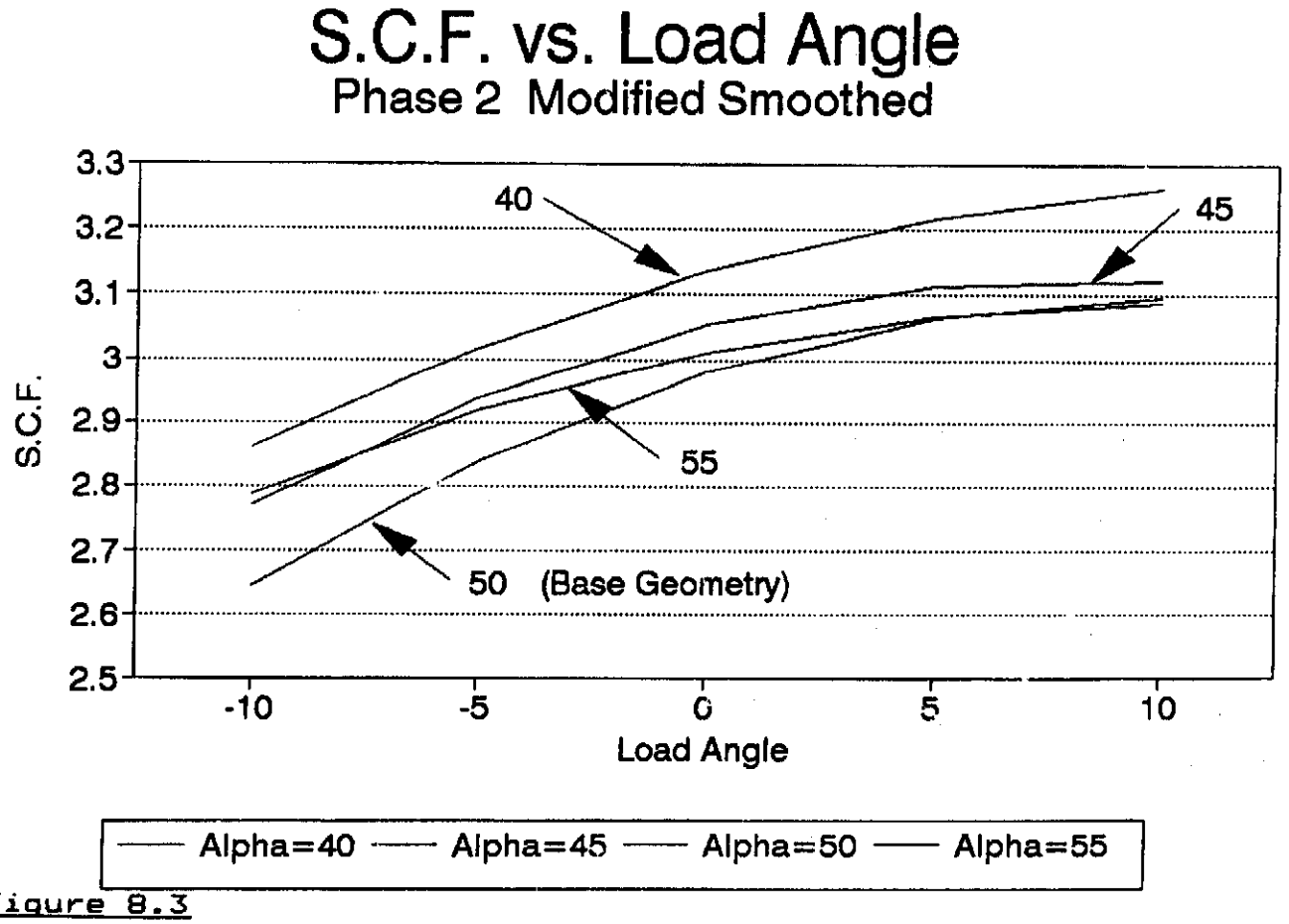

Figure 8.3

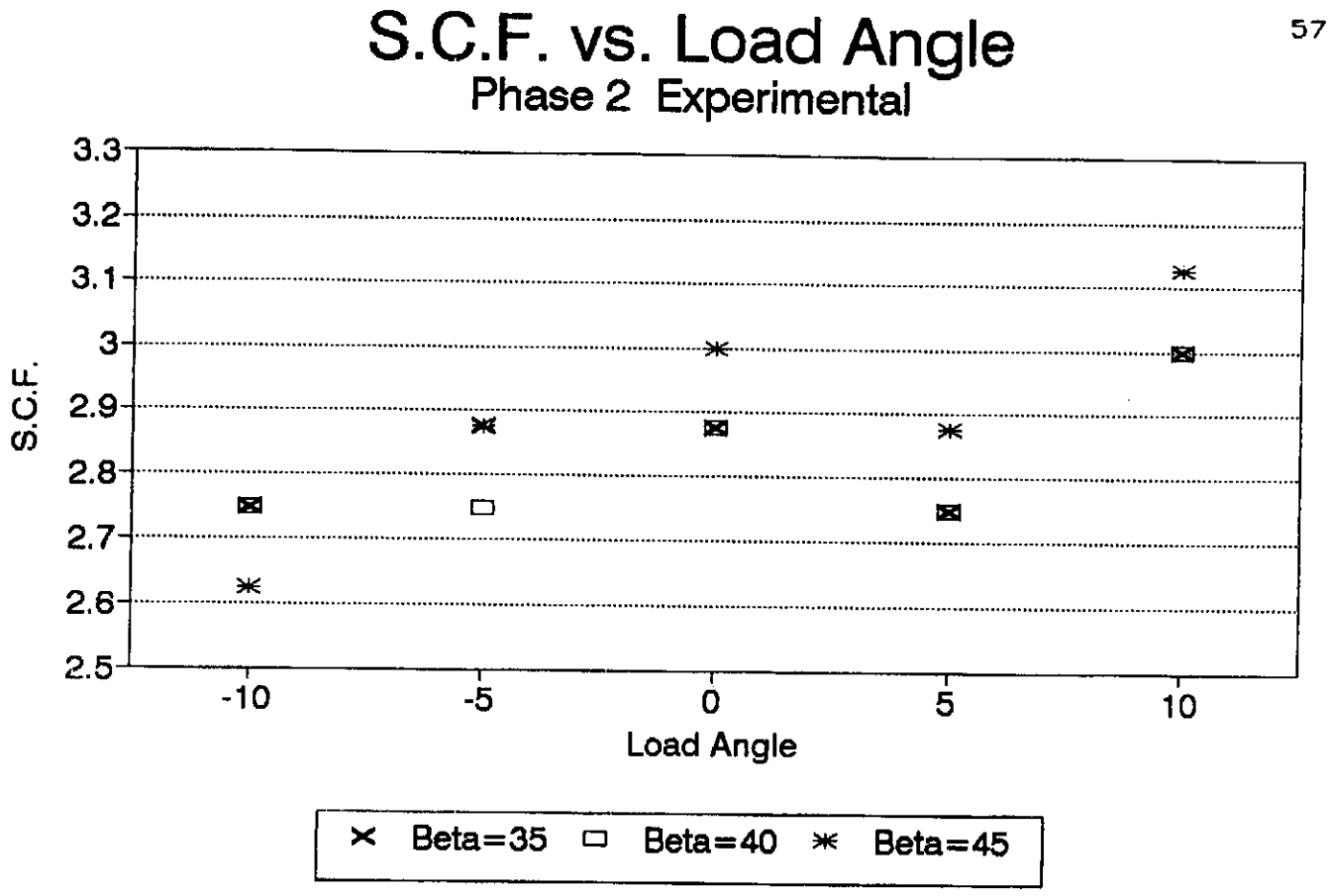

Figure 8.4

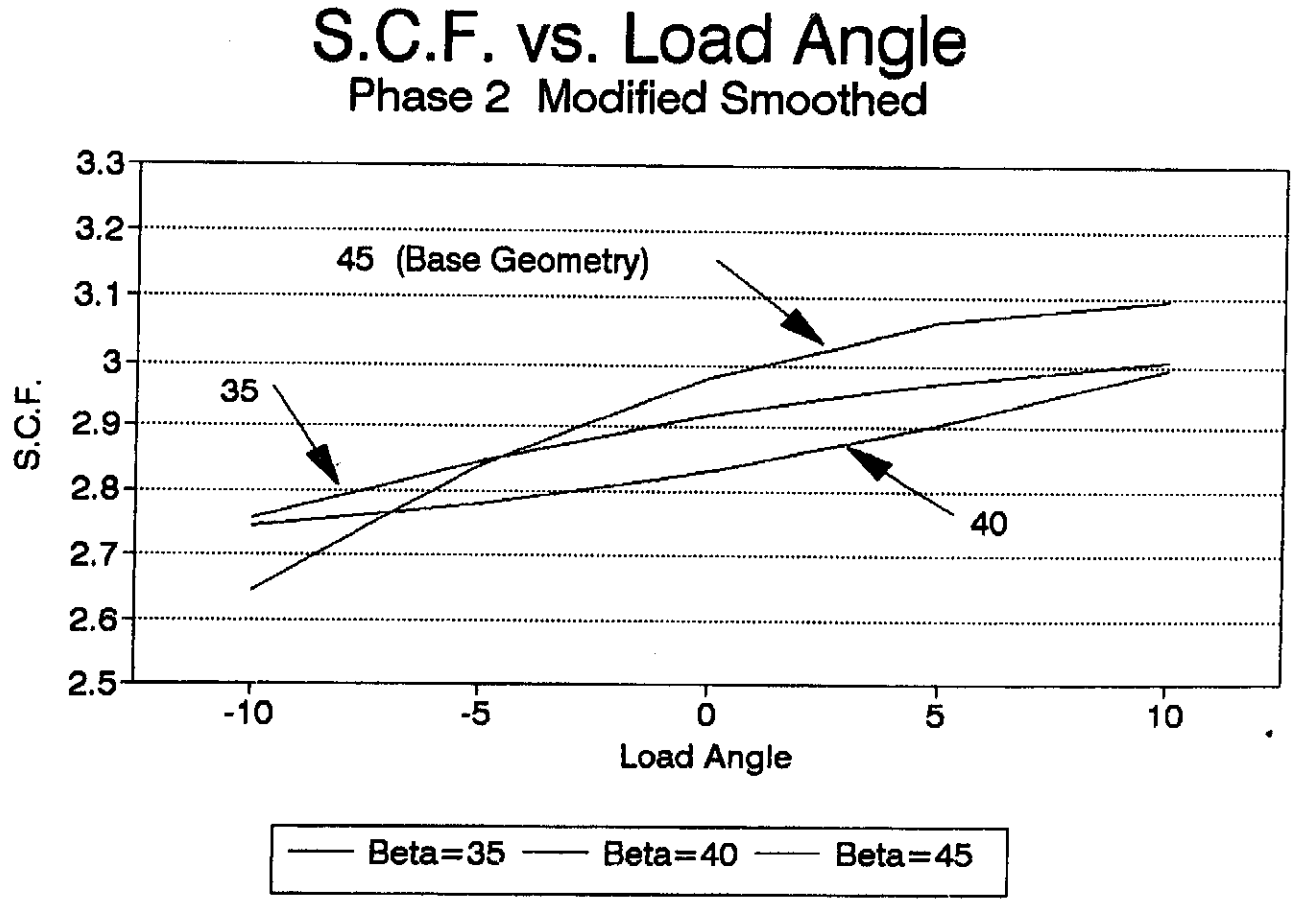

Figure 8.5

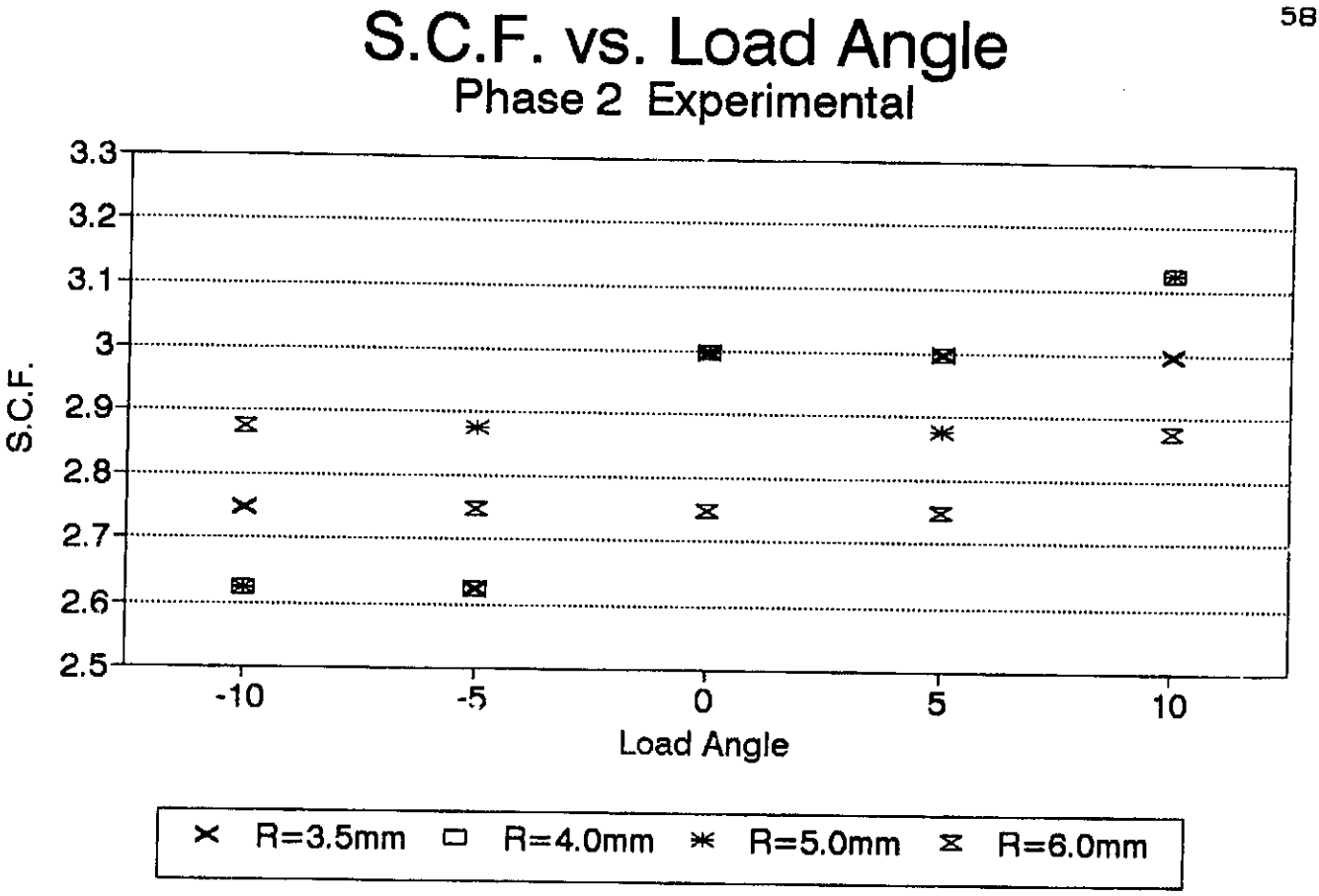

Figure 8.6

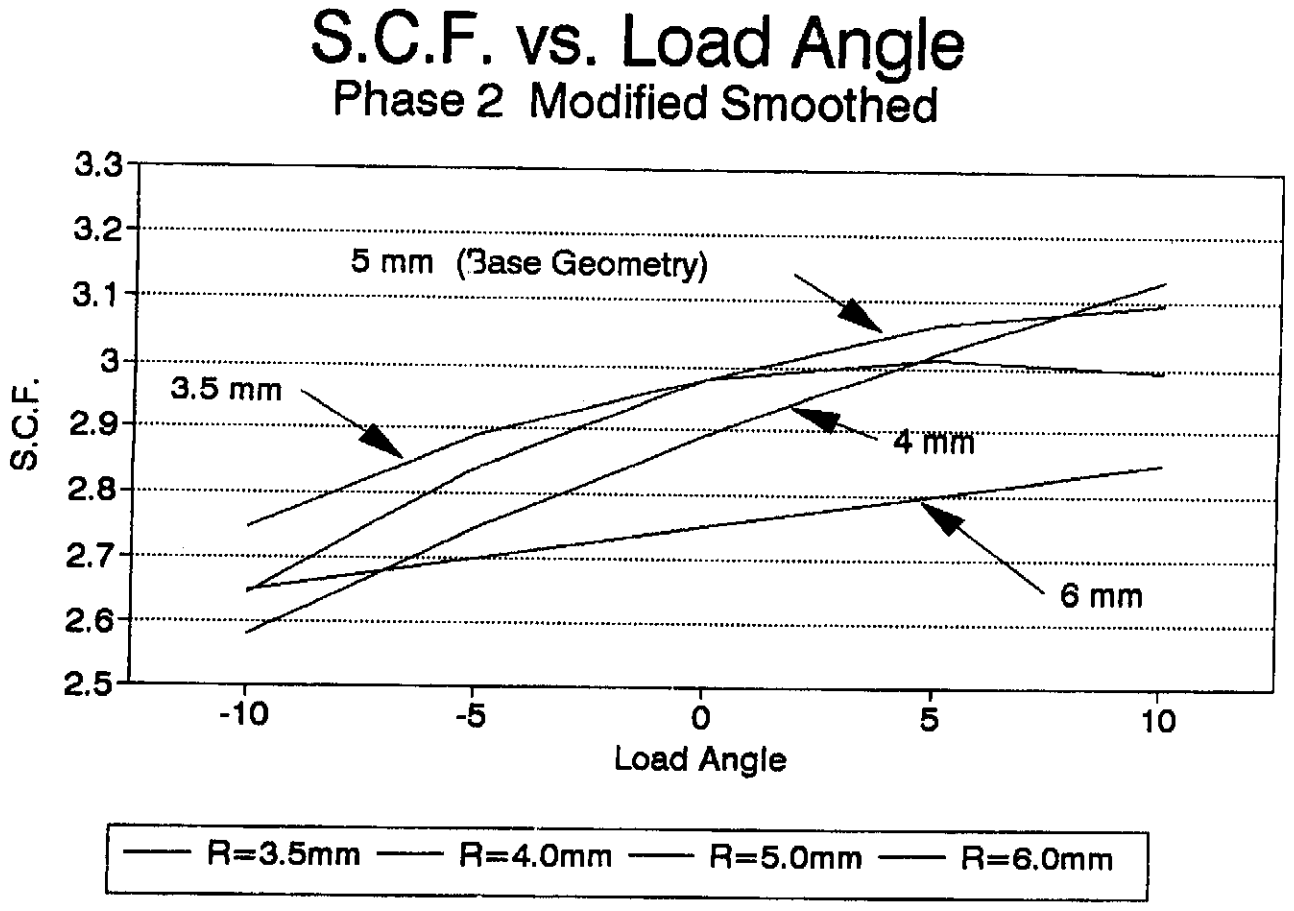

Figure 8.7

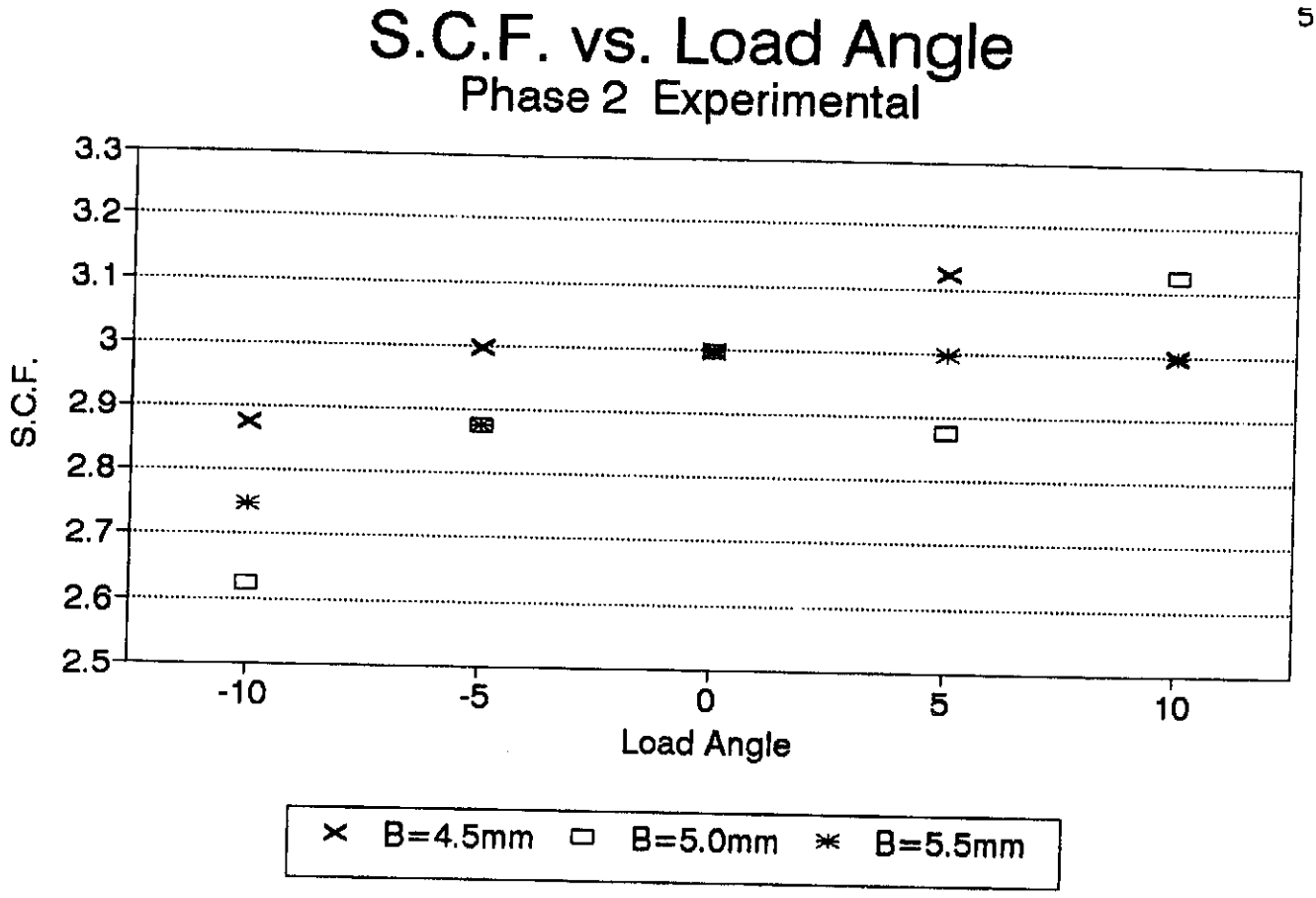

Figure 8.8

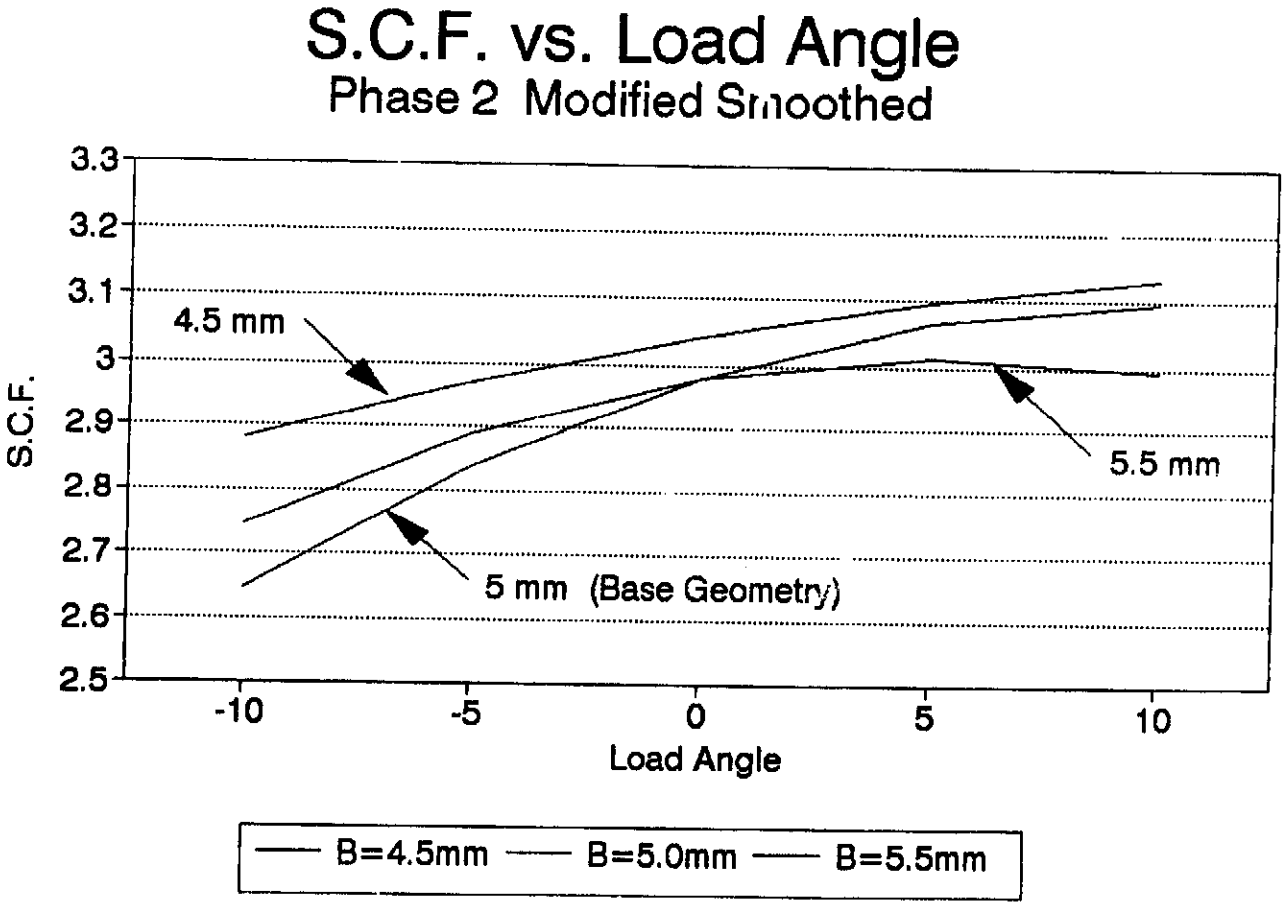

Figure 8.9

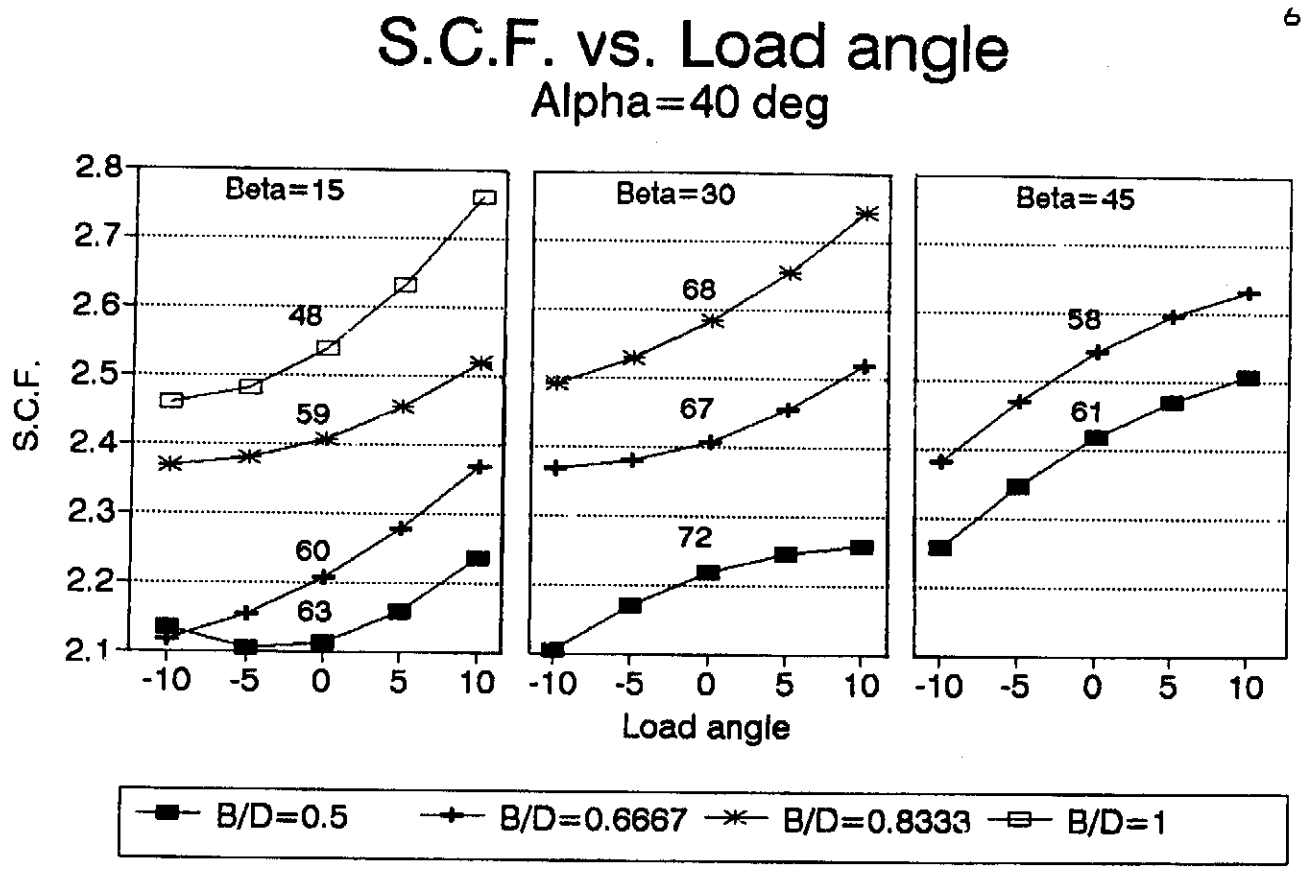

Figure 8.10

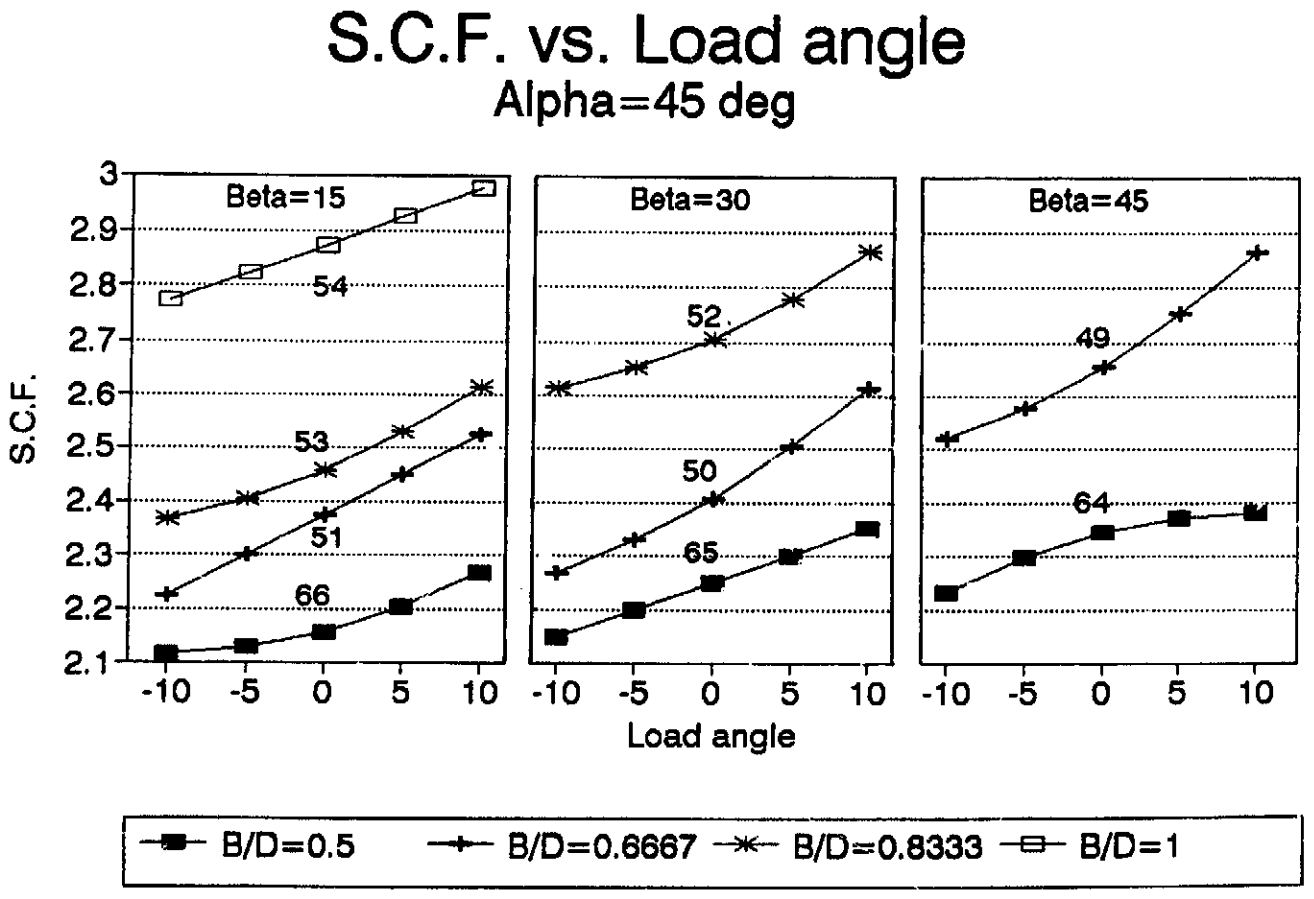

Figure 8.11

Figure 8.12

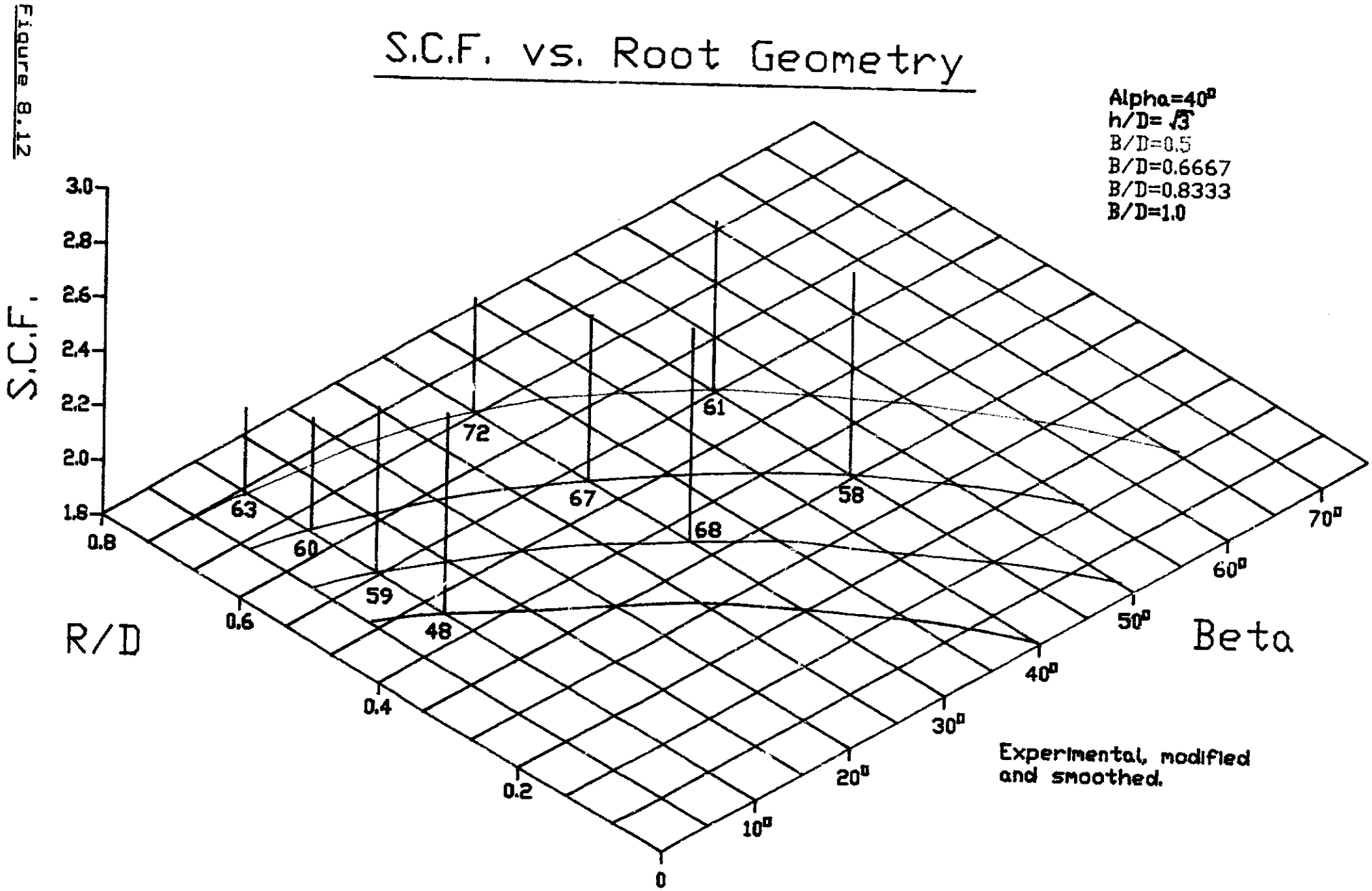
S.C.F. vs. Root Geometry
Alpha=40°
h/D= √3
B/D=0.5
B/D=0.6667
B/D=0.8333
B/D=1.0
S.C.F.
3.0
2.8
2.6
2.4
2.2
2.0
1.8
R/D
0.8
0.6
0.4
0.2
0
Beta
10°
20°
30°
40°
50°
60°
70°
63
60
59
48
72
67
68
61
58
Experimental, modified and smoothed.

Figure 8.13

S.C.F. vs. Root Geometry

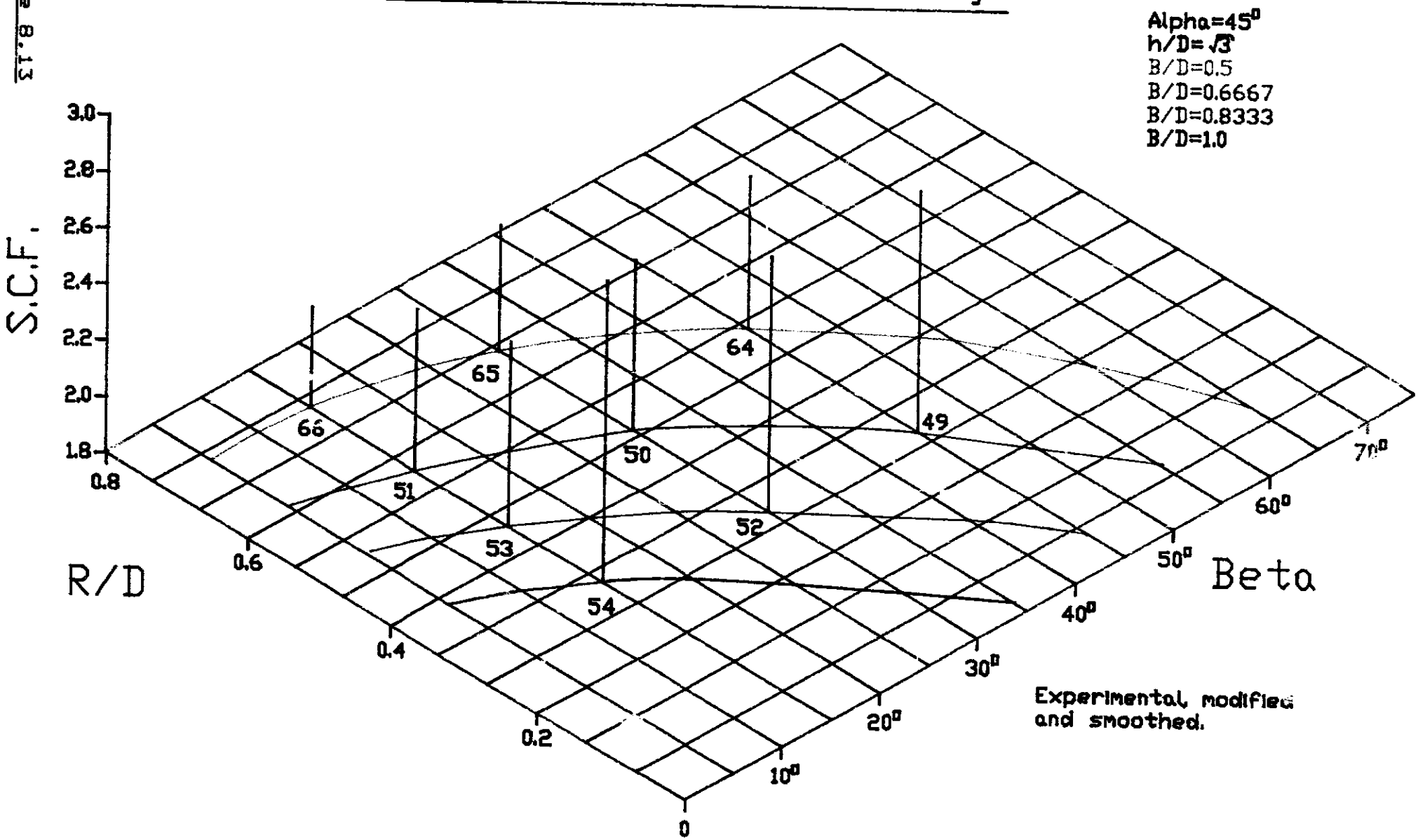

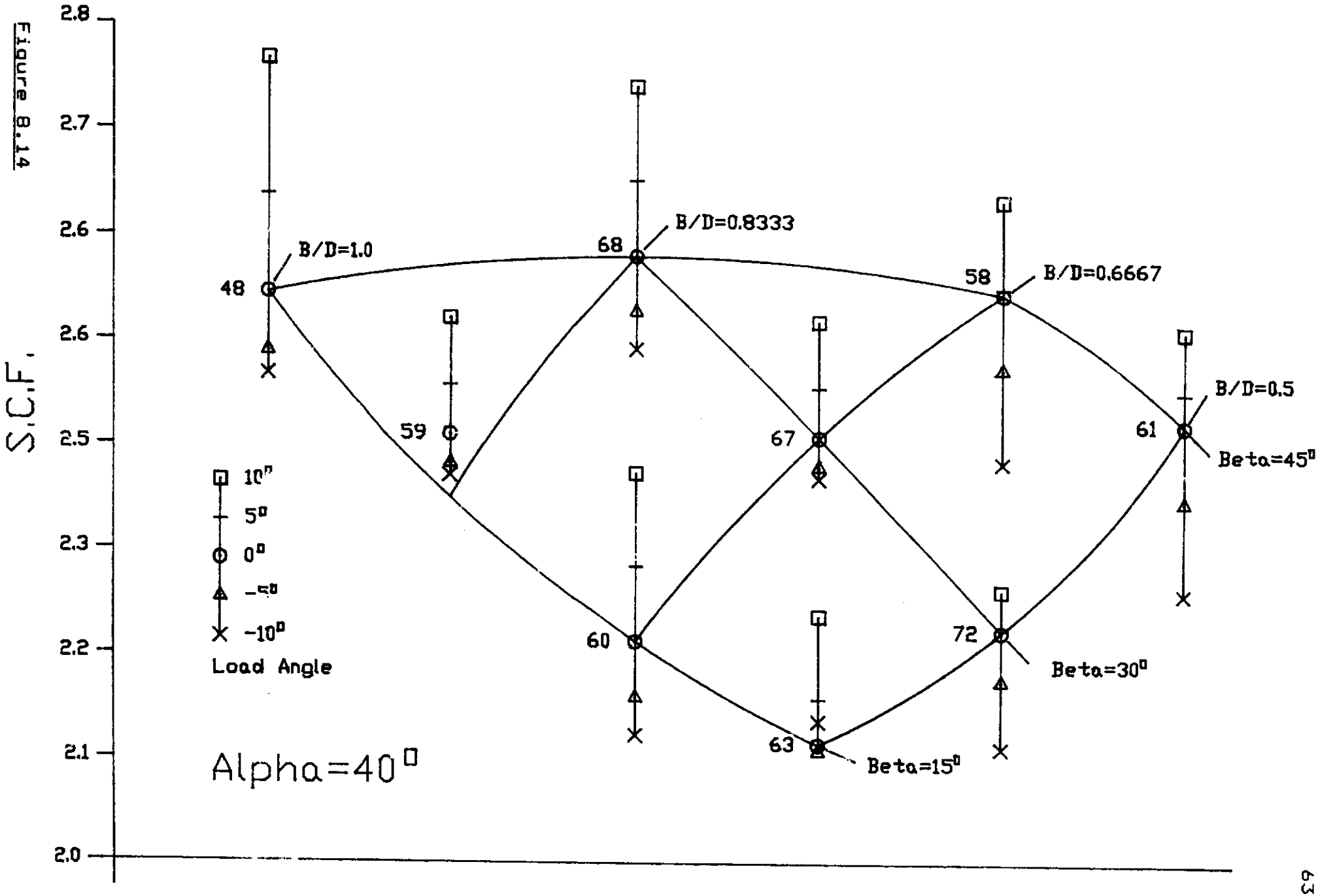
S.C.F.
2.8
2.7
2.6
2.6
2.5
2.3
2.2
2.1
2.0
B/D=1.0
B/D=0.8333
B/D=0.6667
B/D=0.5
Beta=45°
Beta=30°
Beta=15°
48
68
58
59
67
61
60
72
63
10°
5°
0°
-5°
-10°
Load Angle
Alpha=40°

Figure 8.14

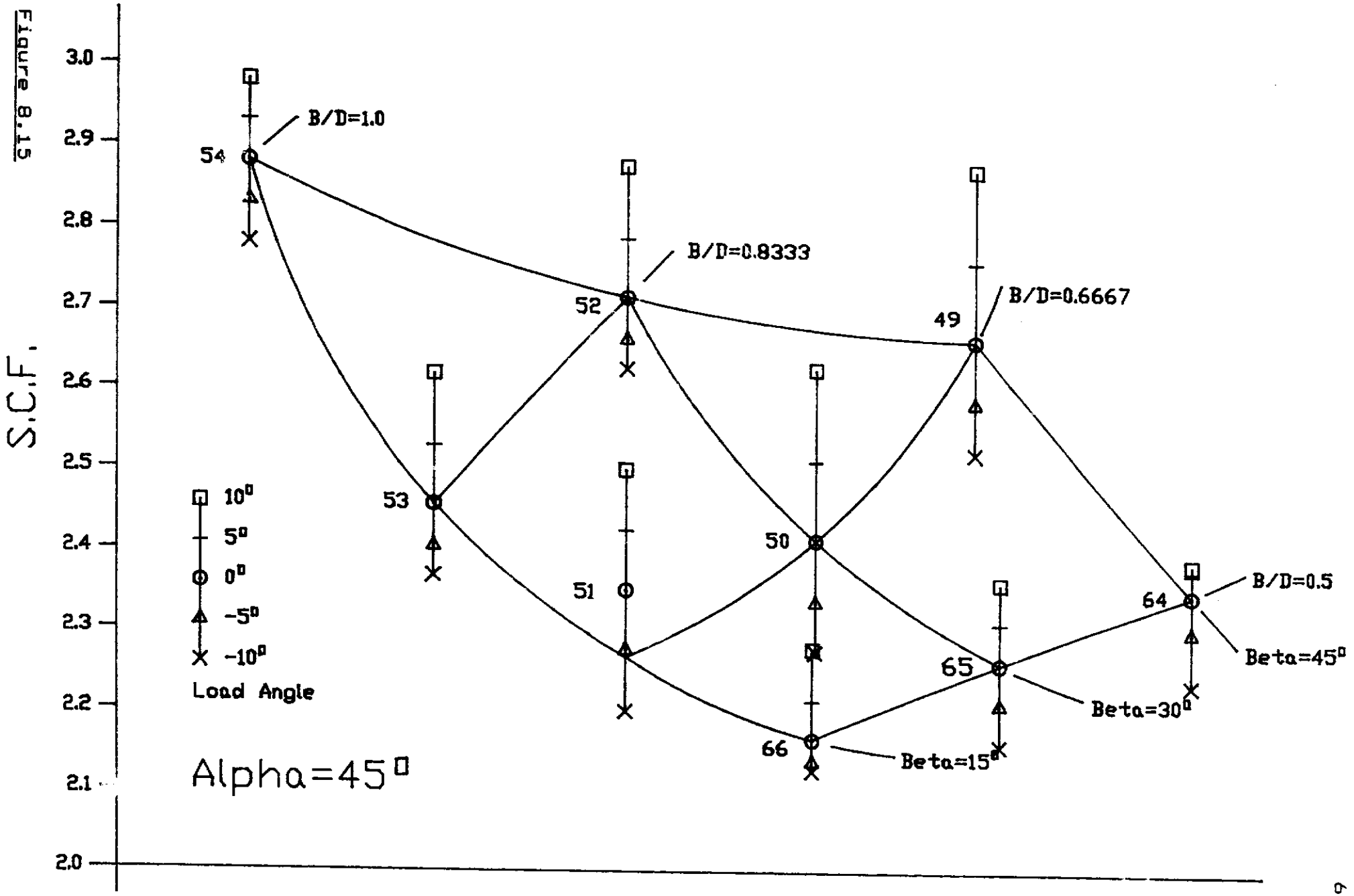
S.C.F.
3.0
2.9
2.8
2.7
2.6
2.5
2.4
2.3
2.2
2.1
2.0
B/D=1.0
B/D=0.8333
B/D=0.6667
B/D=0.5
54
52
49
53
50
51
64
65
66
Beta=45°
Beta=30°
Beta=15°
10°
5°
0°
-5°
-10°
Load Angle
Alpha=45°

Figure 8.15

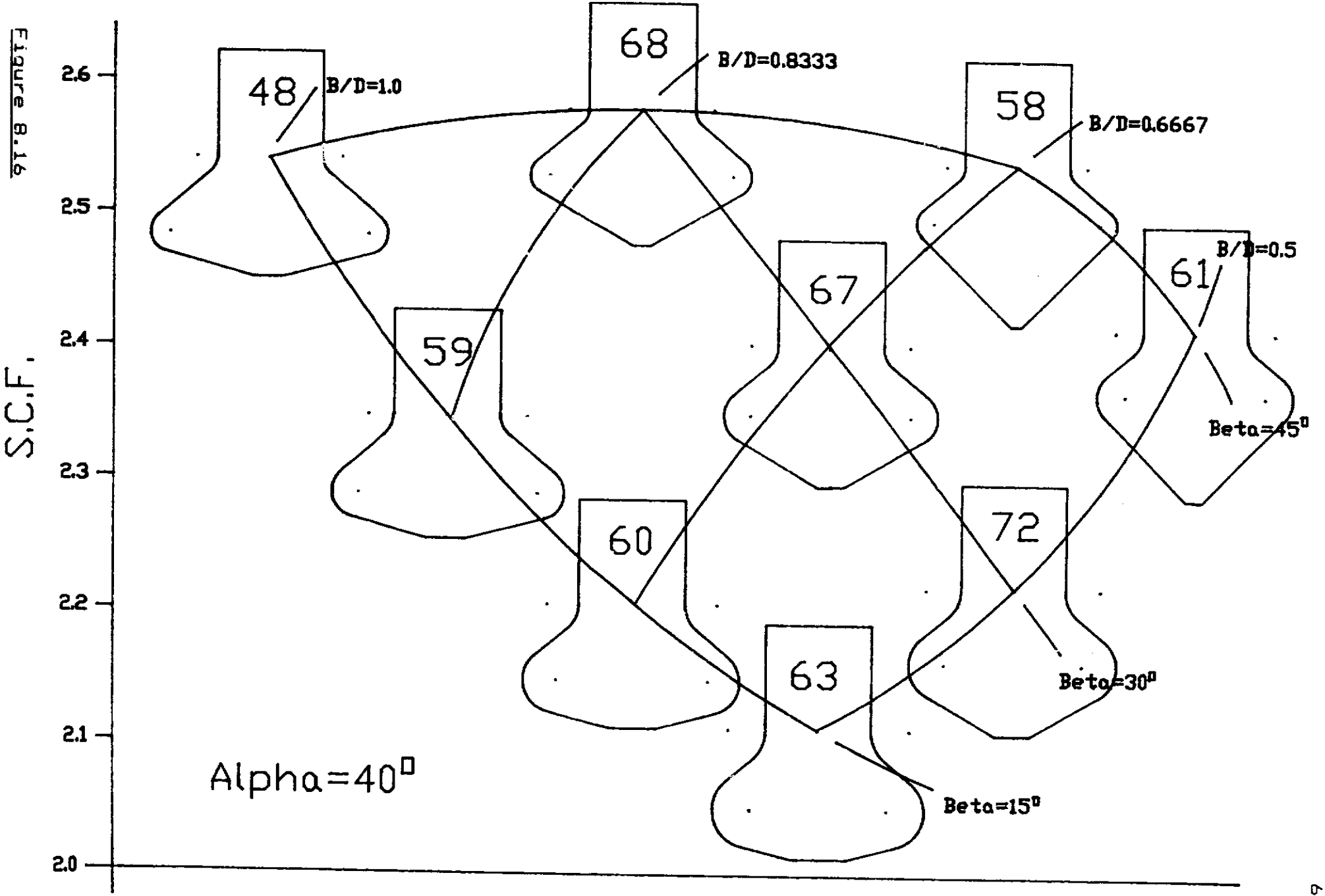
S.C.F.
2.6
2.5
2.4
2.3
2.2
2.1
2.0
48
B/D=1.0
68
B/D=0.8333
58
B/D=0.6667
61
B/D=0.5
Beta=45°
67
59
60
72
Beta=30°
63
Beta=15°
Alpha=40°

Figure 8.16

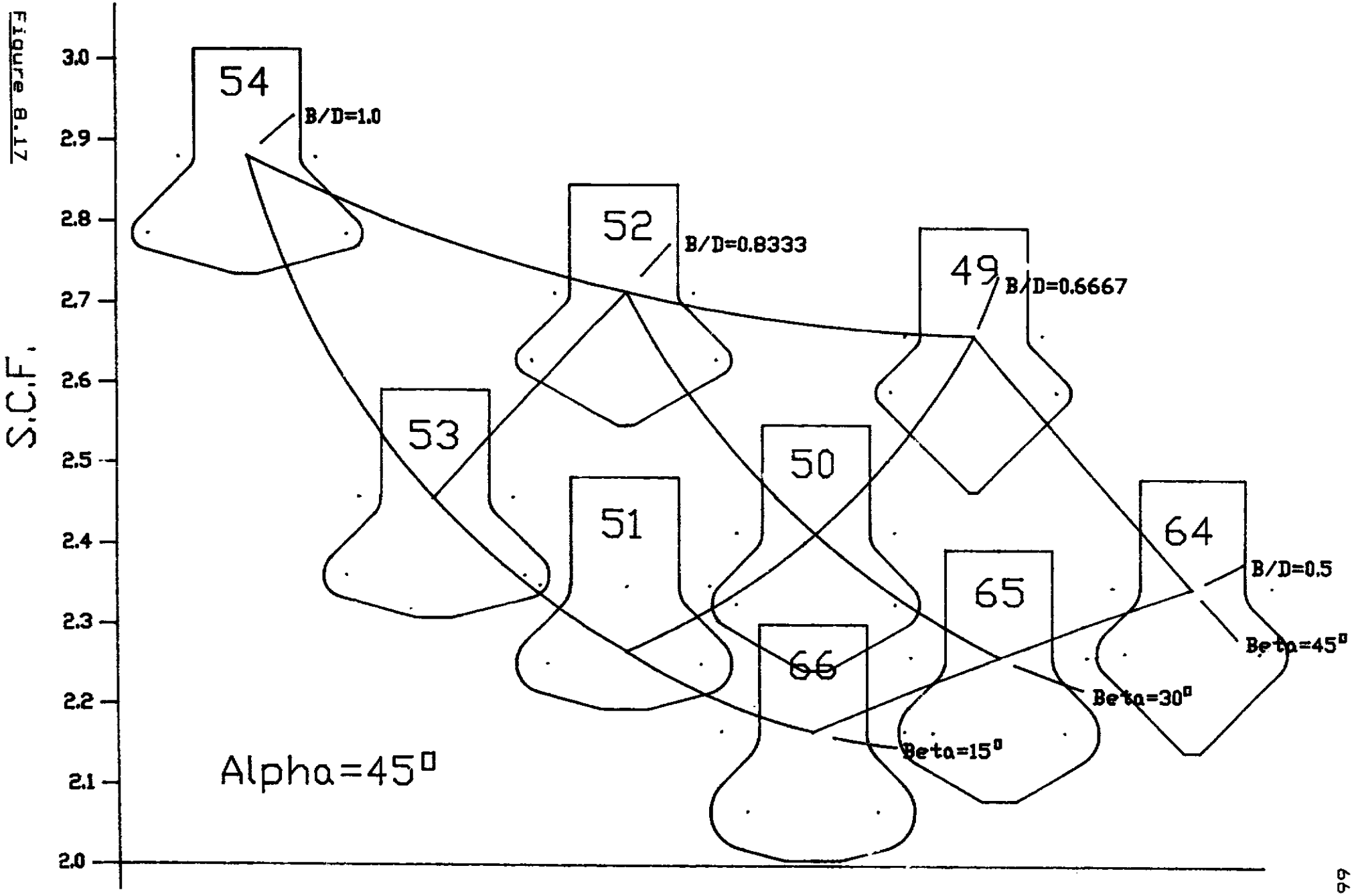
S.C.F.
3.0
2.9
2.8
2.7
2.6
2.5
2.4
2.3
2.2
2.1
2.0
54
52
49
53
51
50
64
65
66
B/D=1.0
B/D=0.8333
B/D=0.6667
B/D=0.5
Beta=45°
Beta=30°
Beta=15°
Alpha=45°

Figure 8.17

PHASE 1A

Root	Alpha	Beta	R1	R2	B	DO	Gamma	D
1	40	34	3.1	3.1	4.271	9.0805	15	5.23
2	45	34	3.1	3.1	4.271	9.0805	15	5.25
3	35	34	3.1	3.1	4.271	9.0805	15	5.24
4	40	39	3.1	3.1	4.271	9.0805	15	5.66
5	40	29	3.1	3.1	4.271	9.0805	15	4.90
6	40	34	3.6	3.6	4.271	9.0805	15	5.74
7	40	34	4.1	4.1	4.271	9.0805	15	6.24
8	40	34	3.1	3.1	4.271	6.0805	15	5.23
9	40	34	3.1	3.1	4.271	12.0805	15	5.23
10	40	34	3.1	3.1	4.271	9.0805	20	7.72
11	40	34	3.1	3.1	4.271	9.0805	10	3.20
12	40	34	3.1	3.1	3.271	9.0805	15	4.74
13	40	34	3.1	3.1	5.271	9.0805	15	5.73
14	50	34	3.1	3.1	4.271	9.0805	15	5.31
15	40	34	5.1	5.1	4.271	9.0805	15	7.25
16	40	34	3.1	3.1	4.271	9.0805	15	5.23
17	45	34	3.1	3.1	4.271	9.0805	15	5.25
18	50	34	3.1	3.1	4.271	9.0805	15	5.31
19	40	34	3.6	3.6	4.271	9.0805	15	5.74
20	40	34	4.1	4.1	4.271	9.0805	15	6.24
21	40	34	3.1	3.1	4.271	6.0805	15	5.23
22	40	34	3.1	3.1	4.271	3.0805	15	5.23
23	40	34	3.1	3.1	4.271	9.0805	15	5.23
24	40	34	3.6	3.6	4.271	9.0805	15	5.74
25	40	34	4.1	4.1	4.271	9.0805	15	6.24

Experimental S.C.F.

Load angle

-10	-5	0	5	10	AVE
2.5	2.75	2.75	2.75	2.75	2.7
2.5	2.75	3	3	3	2.85
3	3.25	3.5	3.5	3.75	3.4
2.75	2.75	3	3	3.25	2.95
3	3.25	3.25	3.25	3.25	3.2
2.75	2.75	3	3	3	2.9
2.5	2.75	2.75	3		2.75
2.25	2.5	2.5	2.75	2.75	2.55
3.5	3.5	3.75	4	3.75	3.7
3	3.25	3.25	3.25	3.5	3.25
2.5	2.75	2.75	2.75	2.75	2.7
2.75	3	3.25	3	3.25	3.05
2.75	2.75	2.75	3	3.25	2.9
2.25	2.5	2.75	2.75	3	2.65
2.5	2.75	3	3	3	2.85
3.25	3.25	3.5	3.75	3.75	3.5
2.75	3	3	3.5	3.5	3.15
2.25			3.25	3.25	2.917
3.25	3.5	3.5	3.75	3.75	3.55
3	3.25	3.25	3.25	3.5	3.25
2.75	2.75	2.75		3	2.25
2	2	2.5	2.5	2.5	2.3
2.5	2.75	3	3.25	3.25	2.95
2.25	2.5	2.5	3	3.5	2.75
2	2	2	2.5	2.5	2.2

PHASE 1B

ROOT	Experimental smoothed S.C.F. Load angle -10	-5	0	5	10
1	2.529	2.686	2.771	2.786	2.729
2	2.493	2.779	2.957	3.029	2.993
3	3.014	3.243	3.436	3.593	3.714
4	2.736	2.807	2.914	3.057	3.236
5	3.029	3.186	3.271	3.286	3.229
6	2.714	2.843	2.936	2.993	3.014
7	2.257	3.121	3.093	2.171	0.357
8	2.264	2.443	2.586	2.693	2.764
9	3.429	3.636	3.771	3.836	3.829
10	3.05	3.15	3.25	3.35	3.45
11	2.529	2.686	2.771	2.786	2.729
12	2.779	2.986	3.121	3.186	3.179
13	2.757	2.721	2.793	2.971	3.257
14	2.264	2.493	2.686	2.843	2.964
15	2.493	2.779	2.957	3.029	2.993
16	3.2	3.35	3.5	3.65	3.8
17	2.75	2.95	3.15	3.35	3.55
18	1.807	0.671	0.643	1.721	3.907
19	3.264	3.443	3.586	3.693	3.764
20	3.05	3.15	3.25	3.35	3.45
21	3.164	2.243	1.786	1.793	2.264
22	1.929	2.186	2.371	2.486	2.529
23	2.479	2.786	3.021	3.186	3.279
24	2.293	2.379	2.607	2.979	3.493
25	1.971	2.014	2.129	2.314	2.571

Experimental modified S.C.F. Load angle -10	-5	0	5	10
2.5	2.75	2.75	2.75	2.75
2.5	2.75	3	3	3
3	3.25	3.5	3.5	3.75
2.75	2.75	3	3	3.25
3	3.25	3.25	3.25	3.25
2.75	2.75	3	3	3
2.5	2.75	2.75	3	3
2.25	2.5	2.5	2.75	2.75
3.5	3.5	3.75	4	4
3	3.25	3.25	3.25	3.5
2.5	2.75	2.75	2.75	2.75
2.75	3	3	3.25	3.25
2.75	2.75	2.75	3	3.25
2.25	2.5	2.75	2.75	3
2.5	2.75	3	3	3
3.25	3.25	3.5	3.75	3.75
2.75	3	3	3.5	3.5
2.25	2.5	2.75	3	3.25
3.25	3.5	3.5	3.75	3.75
3	3.25	3.25	3.25	3.5
2.75	2.75	2.75	3	3
2	2	2.5	2.5	2.5
2.5	2.75	3	3.25	3.25
2.25	2.5	2.5	3	3.5
2	2	2	2.5	2.5

Experimental modified smoothed S.C.F. Load angle -10	-5	0	5	10
2.529	2.686	2.771	2.786	2.729
2.493	2.779	2.957	3.029	2.993
3.014	3.243	3.436	3.593	3.714
2.736	2.807	2.914	3.057	3.236
3.029	3.186	3.271	3.286	3.229
2.714	2.843	2.936	2.993	3.014
2.514	2.693	2.836	2.943	3.014
2.264	2.443	2.586	2.693	2.764
3.45	3.6	3.75	3.9	4.05
3.05	3.15	3.25	3.35	3.45
2.529	2.686	2.771	2.786	2.729
2.764	2.943	3.086	3.193	3.264
2.757	2.721	2.793	2.971	3.257
2.264	2.493	2.686	2.843	2.964
2.493	2.779	2.957	3.029	2.993
3.2	3.35	3.5	3.65	3.8
2.75	2.95	3.15	3.35	3.55
2.25	2.5	2.75	3	3.25
3.264	3.443	3.586	3.693	3.764
3.05	3.15	3.25	3.35	3.45
2.736	2.757	2.814	2.907	3.036
1.929	2.186	2.371	2.486	2.529
2.479	2.786	3.021	3.186	3.279
2.293	2.379	2.607	2.979	3.493
1.971	2.014	2.129	2.314	2.571

PHASE 2A

Root	Alpha	Beta	R1	R2	B	DO	Gamma	D
28	40	45	5	5	5	6	15	8.99
29	50	40	5	5	5	6	15	8.02
30	50	35	5	5	5	6	15	7.50
31	50	45	5	5	4.5	6	15	8.34
32	50	45	5	5	5.5	6	15	9.14
33	50	45	4	4	5	6	15	7.79
34	50	45	6	6	5	6	15	9.68
35	55	45	5	5	5	6	15	8.72
36	50	45	3.5	3.5	5	6	15	7.32
37	40	34	3.1	3.1	4.271	9.0805	15	5.23
38	50	45	5	5	5	6	15	8.74
39	45	45	5	5	5	6	15	8.84
40	46	14	7.78	4	4.89	18.67	16	7.56
41	46	14	11.5	4	4.89	18.67	16	9.34
42	46	14	4	4	4.89	18.67	16	5.76

Experimental S.C.F.

Load angle

-10	-5	0	5	10	AVE
2.875	3	3.125	3.25	3.25	3.1
2.75	2.75	2.875	2.75	3	2.825
2.75	2.875	2.875	2.75	3	2.85
2.875	3	3	3.125	3	3
2.75	2.875	3	3	3	2.925
2.625	2.625	3	3	3.125	2.875
2.875	2.75	2.75	2.75	2.875	2.8
2.75	3	3	3	3.125	2.975
2.75	2.625	3	3	3	2.875
3.5	3.5	3.625	3.625	4.125	3.675
2.625	2.875	3	2.875	3.125	2.9
2 75	3	3	3.125	3.125	3
3.875	4	4.25	4.375	4.5	4.2
4.167	4.167	4.5	4.667	4.833	4.467
3.75	4	4.25	4.5	4.75	4.25

PHASE 2B Experimental smoothed S.C.F.

ROOT	Load angle -10	-5	0	5	10
28	2.864	3.018	3.136	3.218	3.264
29	2.761	2.757	2.789	2.857	2.961
30	2.793	2.804	2.832	2.879	2.943
31	2.871	2.989	3.054	3.064	3.021
32	2.746	2.889	2.979	3.014	2.996
33	2.582	2.746	2.893	3.021	3.132
34	2.871	2.764	2.729	2.764	2.871
35	2.789	2.918	3.011	3.068	3.089
36	2.682	2.796	2.893	2.971	3.032
37	3.525	3.475	3.55	3.75	4.075
38	2.664	2.818	2.936	3.018	3.064
39	2.771	2.939	3.054	3.114	3.121
40	3.857	4.046	4.218	4.371	4.507
41	4.124	4.272	4.443	4.638	4.857
42	3.75	4	4.25	4.5	4.75

Experimental modified S.C.F.

Load angle -10	-5	0	5	10
2.875	3	3.125	3.25	3.25
2.75	2.75	2.875	2.875	3
2.75	2.875	2.875	3	3
2.875	3	3	3.125	3.125
2.75	2.875	3	3	3
2.625	2.625	3	3	3.125
2.625	2.75	2.75	2.75	2.875
2.75	3	3	3	3.125
2.75	2.875	3	3	3
3.5	3.5	3.625	3.625	4.125
2.625	2.875	3	3	3.125
2.75	3	3	3.125	3.125
3.875	4	4.25	4.375	4.5
4.1667	4.1667	4.5	4.6667	4.8333
3.75	4	4.25	4.5	4.75

Experimental modified smoothed S.C.F.

Load angle -10	-5	0	5	10
2.864	3.018	3.136	3.218	3.264
2.743	2.779	2.832	2.904	2.993
2.757	2.846	2.918	2.971	3.007
2.882	2.971	3.043	3.096	3.132
2.746	2.889	2.979	3.014	2.996
2.582	2.746	2.893	3.021	3.132
2.65	2.7	2.75	2.8	2.85
2.789	2.918	3.011	3.068	3.089
2.746	2.889	2.979	3.014	2.996
3.525	3.475	3.55	3.75	4.075
2.646	2.839	2.979	3.064	3.096
2.771	2.939	3.054	3.114	3.121
3.857	4.046	4.218	4.371	4.507
4.124	4.271	4.443	4.638	4.857
3.75	4	4.25	4.5	4.75

PHASE 3A

Root	Alpha	Beta	R1	R2	B	DO	Gamma	D
43	40	45	3.291	6.667	10	0	17.2	10.00
44	40	30	5.084	6.667	10	0	17.9	10.00
45	40	15	6.101	6.667	10	0	18.5	10.00
46	40	30	3.56	8.333	10	0	19.3	10.00
47	40	15	4.969	8.333	10	0	19.6	10.00
48	40	15	3.836	10	10	0	20.9	10.00
49	45	45	4.229	10	15	0	17.7	15.00
50	45	30	4.681	6.667	10	0	18.5	10.00
51	45	15	5.71	6.667	10	0	19.1	10.00
52	45	30	4.309	12.5	15	0	20.1	15.00
53	45	15	4.349	8.333	10	0	20.5	10.00
54	45	15	4.483	15	15	0	22.1	15.00
55	40	34	3.1	4.271	5.2345	9.0805	15	5.23
56	40	34	5.922	8.159	10	0	15	10.00
57	45	15	5.769	5.138	9.266	0.73	19	9.27
58	40	45	3.291	6.667	10	0	17.16	10.00
59	40	15	4.969	8.333	10	0	19.59	10.00
60	40	15	6.101	6.667	10	0	18.47	10.00
61	40	45	5.3	5	10	0	15.74	10.00
62	40	30	6.6	5	10	0	16.71	10.00
63	40	15	7.2	5	10	0	17.52	10.00
64	45	45	5.2	5	10	0	16.07	10.00
65	45	30	6.5	5	10	0	17.07	10.00
66	45	15	7.1	5	10	0	17.84	10.00
67	40	30	5.084	6.667	10	0	17.9	10.00
68	40	30	3.56	8.333	10	0	19.3	10.00
69	45	15	5.71	6.667	10	0	19.1	10.00
70	40	34	5.922	8.159	10	0	15	10.00
71	40	15	4.969	8.333	10	0	19.59	10.00
72	40	30	6.6	5	10	0	16.71	10.00

Experimental S.C.F.

Load angle

-10	-5	0	5	10	AVE
2.25	2.25	2.375	2.375	2.5	2.35
2.25	2.375	2.5	2.5	2.5	2.425
2.25	2.375	2.375	2.375	2.5	2.375
2.375	2.625	2.75	2.75	2.875	2.675
2.75	2.5	2.875	2.75	2.75	2.725
2.5	2.375	2.625	2.625	2.75	2.575
2.5	2.625	2.625	2.75	2.875	2.675
2.25	2.375	2.375	2.5	2.625	2.425
2.25	2.25	2.375	2.5	2.5	2.375
2.625	2.625	2.75	2.75	2.875	2.725
2.5	2.375	2.5	2.5	2.625	2.5
2.75	2.875	2.875	2.875	3	2.875
3.25	3.5	4.25	4	4.5	3.9
2.125	2	2	2	2	2.025
2.25	2.375	2.375	2.5	2.5	2.4
2.375	2.5	2.5	2.625	2.625	2.525
2.375	2.375	2.375	2.5	2.5	2.425
2.125	2.125	2.25	2.25	2.375	2.225
2.25	2.375	2.375	2.5	2.5	2.4
2	2	2	2.125	2.125	2.05
2.125	2.125	2.125	2	2.125	2.1
2.25	2.25	2.375	2.375	2.375	2.325
2.25	2.25	2.25	2.25	2.25	2.25
2.125	2.125	2.125	2.25	2.25	2.175
2.375	2.375	2.375	2.5	2.5	2.425
2.5	2.5	2.625	2.625	2.75	2.6
2.25	2.375	2.375	2.375	2.5	2.375
2.125	2.125	2.125	2.25	2.25	2.175
2.375	2.375	2.375	2.5	2.5	2.425
2.125	2.125	2.25	2.25	2.25	2.2

PHASE 3B

ROOT	Experimental smoothed S.C.F. Load angle -10	-5	0	5	10
43	2.243	2.279	2.332	2.404	2.493
44	2.246	2.389	2.479	2.514	2.496
45	2.275	2.325	2.375	2.425	2.475
46	2.396	2.589	2.729	2.814	2.846
47	2.675	2.7	2.725	2.75	2.775
48	2.461	2.482	2.539	2.632	2.761
49	2.518	2.579	2.657	2.754	2.868
50	2.268	2.329	2.407	2.504	2.618
51	2.225	2.3	2.375	2.45	2.525
52	2.618	2.654	2.707	2.779	2.868
53	2.479	2.436	2.446	2.511	2.629
54	2.775	2.825	2.875	2.925	2.975
55	3.229	3.636	3.971	4.236	4.429
56	2.111	2.032	1.989	1.982	2.011
57	2.257	2.346	2.418	2.471	2.507
58	2.382	2.471	2.543	2.596	2.632
59	2.368	2.379	2.407	2.454	2.518
60	2.118	2.154	2.207	2.279	2.368
61	2.257	2.346	2.418	2.471	2.507
62	1.993	2.004	2.032	2.079	2.143
63	2.143	2.104	2.082	2.079	2.093
64	2.232	2.296	2.343	2.371	2.382
65	2.25	2.25	2.25	2.25	2.25
66	2.118	2.129	2.157	2.204	2.268
67	2.368	2.379	2.407	2.454	2.518
68	2.493	2.529	2.582	2.654	2.743
69	2.275	2.325	2.375	2.425	2.475
70	2.118	2.129	2.157	2.204	2.268
71	2.368	2.379	2.407	2.454	2.518
72	2.107	2.171	2.218	2.246	2.257

Experimental modified S.C.F. Load angle -10	-5	0	5	10
2.25	2.25	2.375	2.375	2.5
2.25	2.375	2.5	2.5	2.5
2.25	2.375	2.375	2.375	2.5
2.5	2.625	2.75	2.75	2.875
2.75	2.5	2.875	2.75	2.75
2.5	2.375	2.625	2.625	2.75
2.5	2.625	2.625	2.75	2.875
2.25	2.375	2.375	2.5	2.625
2.25	2.25	2.375	2.5	2.5
2.625	2.625	2.75	2.75	2.875
2.375	2.375	2.5	2.5	2.625
2.75	2.875	2.875	2.875	3
3.25	3.5	4.25	4	4.5
2.125	2	2	2	2
2.25	2.375	2.375	2.5	2.5
2.375	2.5	2.5	2.625	2.625
2.375	2.375	2.375	2.5	2.5
2.125	2.125	2.25	2.25	2.375
2.25	2.375	2.375	2.5	2.5
2	2	2	2.125	2.125
2.125	2.125	2.125	2.125	2.25
2.25	2.25	2.375	2.375	2.375
2.125	2.25	2.25	2.25	2.375
2.125	2.125	2.125	2.25	2.25
2.375	2.375	2.375	2.5	2.5
2.5	2.5	2.625	2.625	2.75
2.25	2.375	2.375	2.375	2.5
2.125	2.125	2.125	2.25	2.25
2.375	2.375	2.375	2.5	2.5
2.125	2.125	2.25	2.25	2.25

Experimental modified smoothed S.C.F. Load angle -10	-5	0	5	10
2.243	2.279	2.332	2.404	2.493
2.246	2.389	2.479	2.514	2.496
2.275	2.325	2.375	2.425	2.475
2.507	2.621	2.718	2.796	2.857
2.675	2.7	2.725	2.75	2.775
2.461	2.482	2.539	2.632	2.761
2.518	2.579	2.657	2.754	2.868
2.268	2.329	2.407	2.504	2.618
2.225	2.3	2.375	2.45	2.525
2.618	2.654	2.707	2.779	2.868
2.368	2.404	2.457	2.529	2.618
2.775	2.825	2.875	2.925	2.975
3.229	3.636	3.971	4.236	4.429
2.111	2.032	1.989	1.982	2.011
2.257	2.346	2.418	2.471	2.507
2.382	2.471	2.543	2.596	2.632
2.368	2.379	2.407	2.454	2.518
2.118	2.154	2.207	2.279	2.368
2.257	2.346	2.418	2.471	2.507
1.993	2.004	2.032	2.079	2.143
2.136	2.107	2.114	2.157	2.236
2.232	2.296	2.343	2.371	2.382
2.15	2.2	2.25	2.3	2.35
2.118	2.129	2.157	2.204	2.268
2.368	2.379	2.407	2.454	2.518
2.493	2.529	2.582	2.654	2.743
2.275	2.325	2.375	2.425	2.475
2.118	2.129	2.157	2.204	2.268
2.368	2.379	2.407	2.454	2.518
2.107	2.171	2.218	2.246	2.257

CHAPTER 9

9. The "In-Rotor" experiments

9.1 Experimental objectives

The optimum geometries described in the previous chapter were obtained under artificially controlled loading conditions. The experiments described in this chapter are aimed at assessing the stresses in the optimum roots under simulated operating conditions without artificial constraints. The friction angle and load position are not controlled but are free to move as the forces generated in the assembly dictate. This models the situation found in an operating turbine. As in the previous chapter the modeling was done using simple photoelastic experimentation. To ease the discussion the two root geometries tested will be referred to by their contact surface angles only ie. Alpha=40° is Alpha=40°, Beta=30°, B/D=0.5, h/D=√3, D_o=0 and Alpha=45° is Alpha=45°, Beta=15°, B/D=0.6667, h/D=√3, D_o=0

9.2 The loading rig

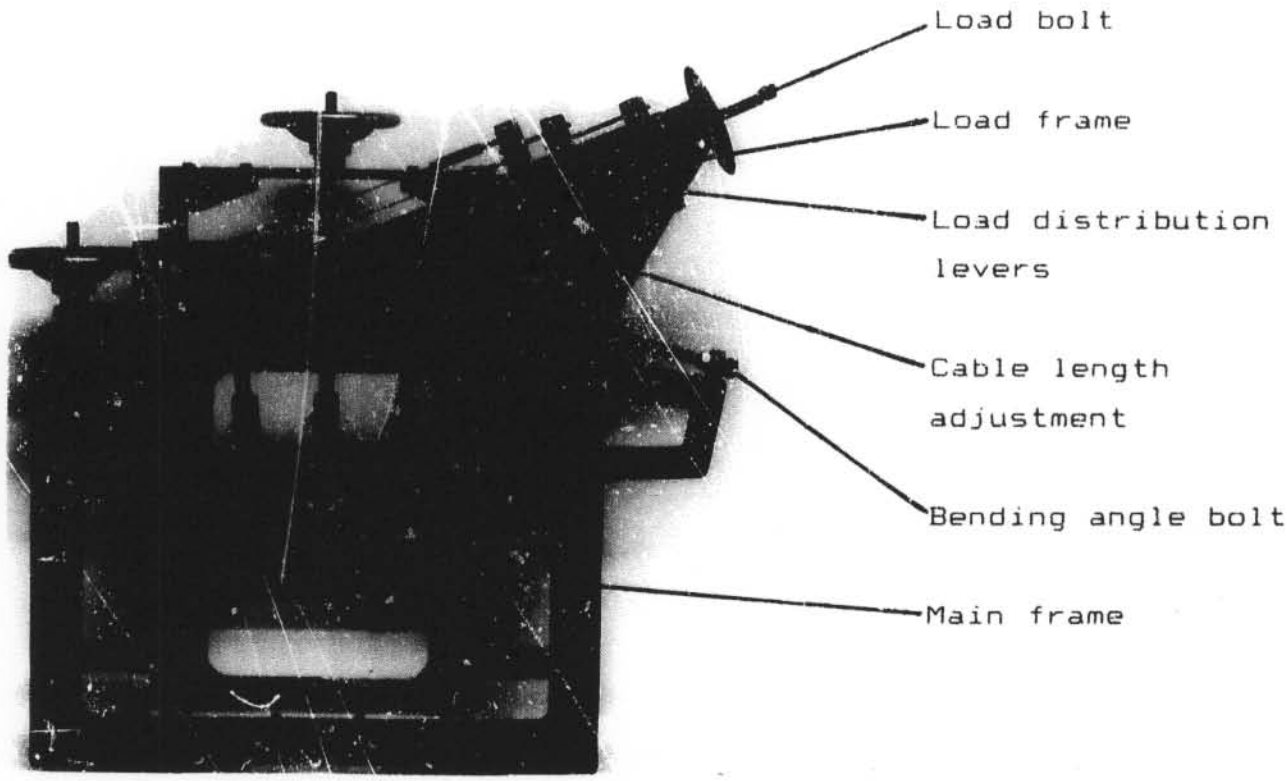

Figure 9.1 The "In-Rotor" test rig.

To simulate the internal load conditions as well as the external boundary conditions existing in the rotor a section of the rotor comprising 5 root notches was used of which only the middle one was used to take readings. The four outer roots and notches served to establish realistic boundary conditions for the center notch. The roots were arranged in an arc with an angle of 6° between the roots thus representing a rotor with 60 blades. The dimensions of the roots were chosen to give a "symmetrical" assembly in which the root shank and the rotor "shank" have the same width as seen in figure 9.5. The bottom of the Araldite rotor section was clamped onto the main frame. A movable load frame was attached to the top of the main frame. This frame carried a set of levers to distribute the load applied by the loading bolt between the blades to which they were attached by stainless steel cables running over ball bearing supported pulleys. The levers and the pulleys were positioned to apply the force circumferentially to the blades. The loading frame could be moved in an arc on the main frame to change the angle at which the blades were pulled thus simulating a combined centrifugal and bending force. A photograph of the rig with a test section in position is given in figure 9.1. The test rig was mounted on the polariscope load frame (also shown in Fig 9.1) which allowed the whole test rig to be moved easily in relation to the polariscope light beam thus permitting the viewing of different parts of the test section.

9.3 Experimental method

Using the Pascal programs listed in Appendix 3, control programs for the numerical milling machine to cut the rotor section and the roots were generated. After cutting the root and rotor contact surfaces were smoothed by hand using 1200 grit emery paper (as described in appendix 2) to minimize surface roughness generated by the cutting action. After fixing the model in the test rig, the rig was adjusted to ensure equal distribution of force between the roots by adjusting the cable lengths and to eliminate any bending in the roots caused by misalignment of the pulleys.

Centrifugal loads were applied incrementally until the shank fringe order was 4 (as in the fixed friction angle tests). During the loading the movement of the contact surfaces over each other could be heard as popping and creaking sounds. This incremental movement creates a problem in that the actual contact surface load distribution when measurements are taken may differ from load application to load application. The load distribution is dependent on the state of the contact surface in its stick-slip cycle. The load distribution may also vary from tang to tang.

Fringe orders in the root fillet and the rotor fillet were recorded and photographs taken at each step. Various amounts of bending were then applied by moving the loading frame with the bending moment load bolt. At first an attempt was made to measure the angle of the applied force (angle of the cable) but it was found that the swivel points joining the cables and the blade shanks had to much rotational friction, resulting in unreliable readings. As with the load measuring it was decided to measure the bending moment photoelastically. Increments were set when the fringe order at the edge of the shank, one shank width (2 * D), above the contact surface was 1, 2 or 3 fringes higher (or lower) than the fringe order at the center of the shank. The fillet fringes for both the rotor and the root on the high and low load tensile stress sides were recorded and photographs taken.

9.4 Experimental results

Due to the nature of the experiments no scientifically justifiable data manipulation could be performed on the results. The data was however verified by experiment duplication. This was not intentional but certain problems where experienced with the programing of the numerically controlled milling machine resulting in one slightly incorrect set of models. These were tested and the results compared with the results of the subsequently cut correct models. Although the "incorrect" models only had marginal dimensional errors it was decided to cut new models to eliminate any uncertainty about the accuracy

of the results. The results obtained from the second (correct) set of experiments are presented and discussed below. The result of the 0° fixed load-angle test of the roots from the previous chapter are also shown on the graphs to enable easy comparison.

9.4.1 Centrifugal load Alpha = 40°

Starting with the Alpha = 40° root in the centrifugally loaded case it can be seen from figure 9.2 (at the end of the chapter) that the S.C.F. rises rapidly with applied load, quickly reaching a steady value of 2.25 which is independent of load at higher loads.

The value obtained from the 0° fixed load angle test after smoothing is 2.218. This indicates a very good correlation between the 0° fixed angle test and the in-rotor test which was not expected due to the friction effects in the in-rotor test case. Returning to the fixed load angle test results however shows that the maximum range of S.C.F. for the different load angles (-10° to +10°) is only 0.125 for this geometry which is the measuring accuracy of the experimental method. The other result emerging from the test is that the rotor S.C.F. is the same as the root S.C.F. for all the load angles. This result is not expected due to the theoretically higher notch S.C.F. of the rotor compared to the root. A slightly higher notch S.C.F. could be expected due to the lower included angle of the rotor notch as can be seen from the drawing in figure 9.2. Once again the accuracy of the experiments could be the cause for the apparent equality in stress concentration factors.

9.4.2 Bending load Alpha = 40°

In contrast to the above, the results of the bending test on the Alpha=40° root, as seen in figure 9.4 below show a difference in S.C.F. between the root and the rotor for all but one case. As expected the S.C.F. in the rotor is lower on the high tensile stress side (left). On the low tensile stress side however the trend is reversed. This is due to the shift in the force

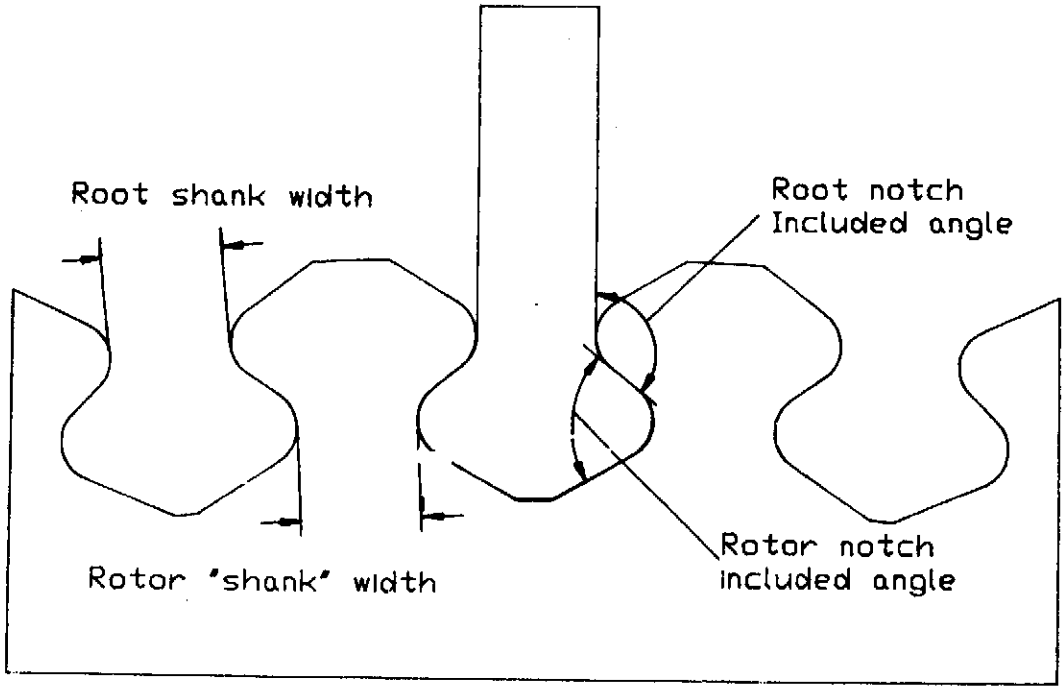

Figure 9.2 A blade root in position showing some dimensions.

distribution along the contact surface. On the low tension side the point of maximum force is shifted towards the shank, thus reducing the tang leverage in the root and increasing it in the rotor. On the high tensile stress side the reverse occurs. The same argument can be falsely put forward to explain the discrepancy with the theory which arose in the centrifugal tests. The error in this assumption lies in the fact that no relative rotation occurs in the contact area and that tang rotation is equal on both sides of the root, as opposed to the situation experienced in the bending test. From this it can be seen that bending loads are more damaging to the root than to the rotor. The observation being valid for stress magnitude as well as stress fluctuation.

9.4.3 Centrifugal load Alpha = 45°

The basic observations made for the Alpha = 40° case can also be made for the Alpha = 45° case, some details do however differ.

The centrifugal S.C.F. shown in figure 9.5, is higher than the fixed load angle 0° result. Compared to the Alpha = 40° root, the Alpha = 45° root has a wider (0.3 versus 0.15) S.C.F. variation with load angle which accounts for the difference between the fixed load angle test and the in rotor test.

9.4.4 Bending Load Alpha =45°

The bending test conducted on the Alpha = 45° root (figure 9.6) showed the same tendencies as the Alpha = 40° root. The unloading of the rotor on the high tensile stress side does not occur. The S.C.F. variation between the high and low stress sides of the root and the rotor are almost equal for the two roots. (Alpha =40° : Root S.C.F. variation = 2.63 Rotor S.C.F. variation = 1.5 Alpha = 45° : Root S.C.F. variation = 2.75 Rotor S.C.F. variation = 1.75) This gives the Alpha = 40° root a slight operating advantage over the Alpha =45° root.

9.5 Cyclic Centrifugal Test

Due to the contact surface slip which occurs when roots are loaded and unloaded it was decided to look at the change in stress concentration as loads are applied and released cyclically. Only the Alpha=45° root was used for this experiment. The slipping could be heard as a popping, creaking sound when the root was loaded and unloaded in the laboratory.

As can be seen from figure 9.7 the cyclical loading results show very little fluctuation in the value of the S.C.F. . It was found in the previous chapter that the effect of load-angle (friction angle) fluctuations on the fillet S.C.F. of this root is relatively large (0.3). This result is not reflected by the results obtained here which only show a small variation in S.C.F. if the first point at shank order 1 is ignored.. The lower S.C.F. obtained for shank order 1 during initial increase of load is probably due to the fact that the root was not seated properly in its equilibrium position. The fact that the relative S.C.F. variation of the cyclic experiment is less than the that of the fixed friction angle experiment, combined with

the fact that the average cyclic S.C.F. exceeds the maximum (+10°) fixed friction angle S.C.F. is probably as a result of the root having wedged itself into the rotor.

If this result were to be extrapolated to the Alpha = 40° (root 72) case the following would have to be kept in mind. 1) The S.C.F. variation for a range of load (friction) angles is less for the Alpha =40° root than for the Alpha = 45° root as can be seen in the previous chapter . 2) The lower contact angle Alpha results in lower tangential forces in the contact surface which results in a lower possibility of slip taking place. With a lower slip probability the load transfer along the contact angle should be small. The combination of these factors should result in the Alpha = 40° root showing even less fillet S.C.F. variation in cyclical loading than the Alpha = 45° root.

9.6 Experimental Conclusions

The results show that the fixed load-angle data can be extrapolated to the centrifugal in-rotor situations as long as S.C.F. variations, as they are influenced by friction, are taken into consideration. Care should however be taken when projecting the fixed load-angle results to the bending load situation because force distribution changes which result from the bending force result in significant changes in S.C.F. profiles in both the root and the rotor. Here it important to note that the rotor experiences a lower change in fillet S.C.F. than the root.

From the results it can be seen that the Alpha = 40° root has the lower S.C.F. under centrifugal load and a slightly lower S.C.F. and S.C.F. variation under bending load. The Alpha = 40° root thus provides a practical solution to the optimization problem.

9.7 In Rotor Results

Alpha=40° Centrifugal loading

Shank load (orders)	Root S.C.F.	Rotor S.C.F.
0.00	0.00	0.00
1.00	2.00	2.00
2.00	2.25	2.25
3.00	2.25	2.25
4.00	2.25	2.25

Alpha=40° Bending loading

Bending load (orders)	Root S.C.F.		Rotor S.C.F.	
0.00	2.25	2.25	2.25	2.25
1.00	1.88	2.63	1.88	2.50
2.00	1.38	3.13	1.63	2.75
3.00	0.75	3.38	1.38	2.88

Alpha=45° Centrifugal loading

Shank load (orders)	Root S.C.F.	Rotor S.C.F.
0.00	0.00	0.00
1.00	2.00	2.00
2.00	2.50	2.50
3.00	2.83	2.83
4.00	2.75	2.75

Alpha=45° Bending loading

Bending load (orders)	Root S.C.F.		Rotor S.C.F.	
0.00	2.75	2.75	2.75	2.75
1.00	2.25	3.00	2.25	3.00
2.00	1.75	3.25	2.25	3.25
3.00	1.00	3.75	2.00	3.75

Alpha=45° Cyclical centrifugal loading

Shank load (orders)	Root S.C.F.	Rotor S.C.F.
0.00	0.00	0.00
1.00	2.00	2.00
2.00	2.50	2.50
3.00	2.83	2.83
4.00	2.75	2.75
3.00	2.67	2.67
2.00	2.75	2.75
1.00	3.00	3.00
2.00	2.75	2.75
3.00	2.83	2.83
4.00	2.63	2.75

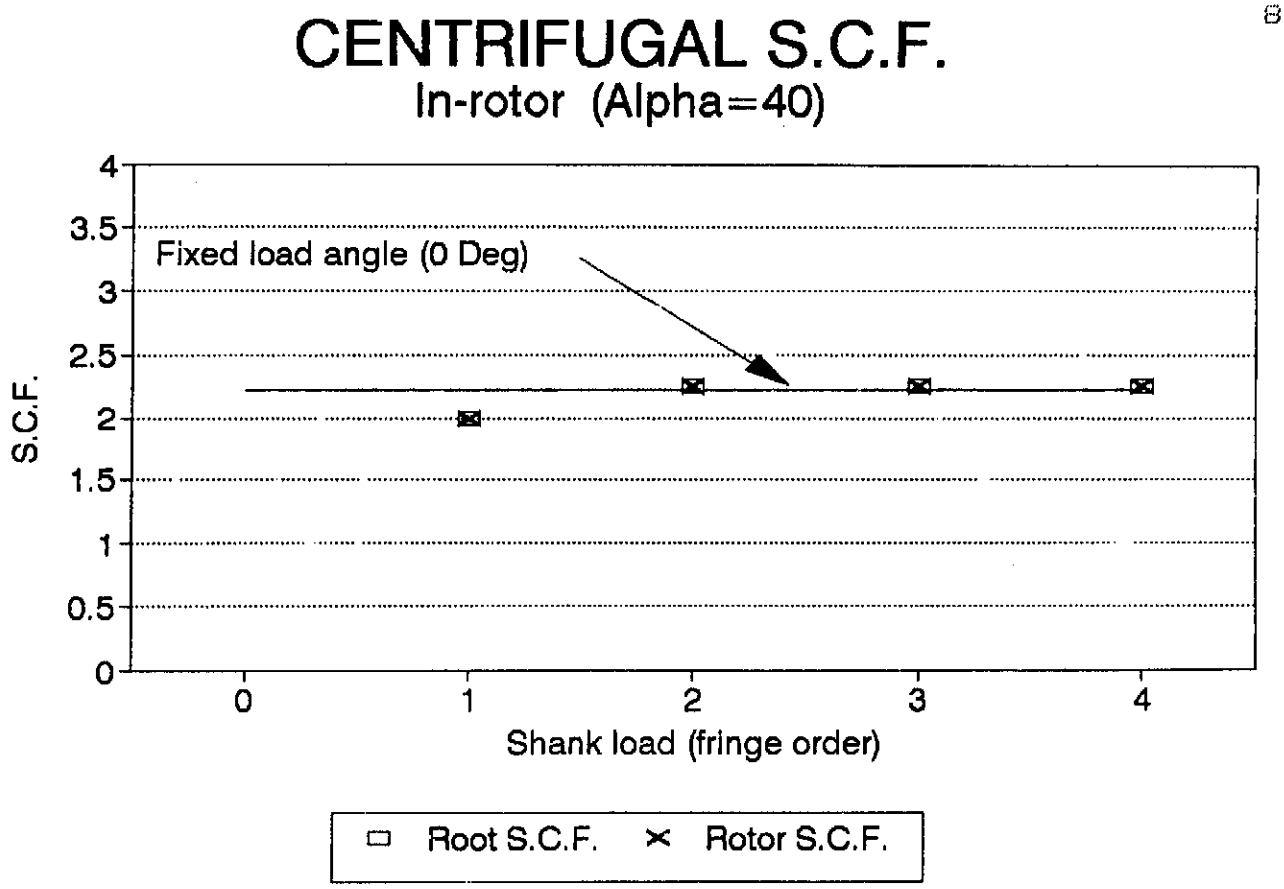

Figure 9.3 In-rotor centrifugal loading results for Alpha=40°

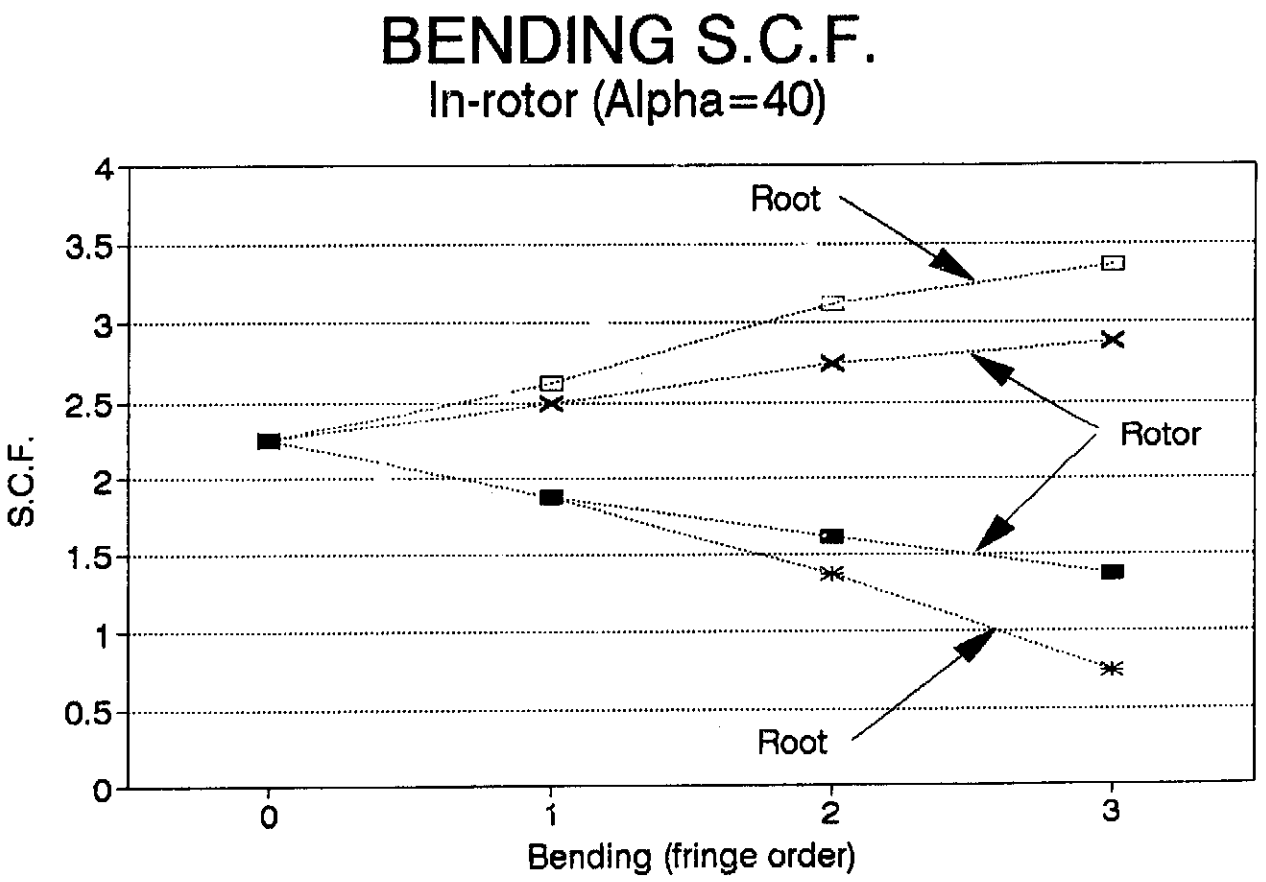

Figure 9.4 In-rotor bending load results for Alpha=40°

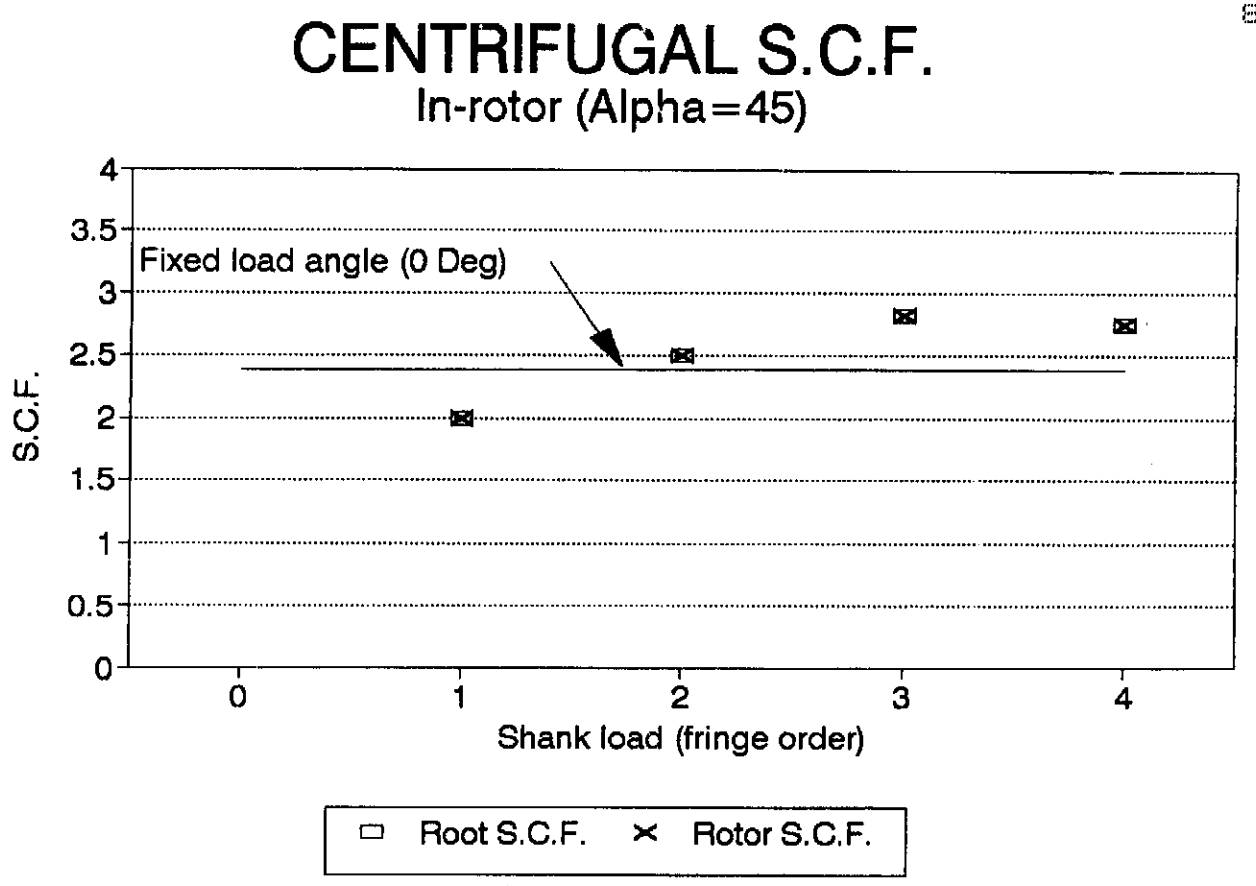

Figure 9.5 In-rotor centrifugal loading results for Alpha=45°

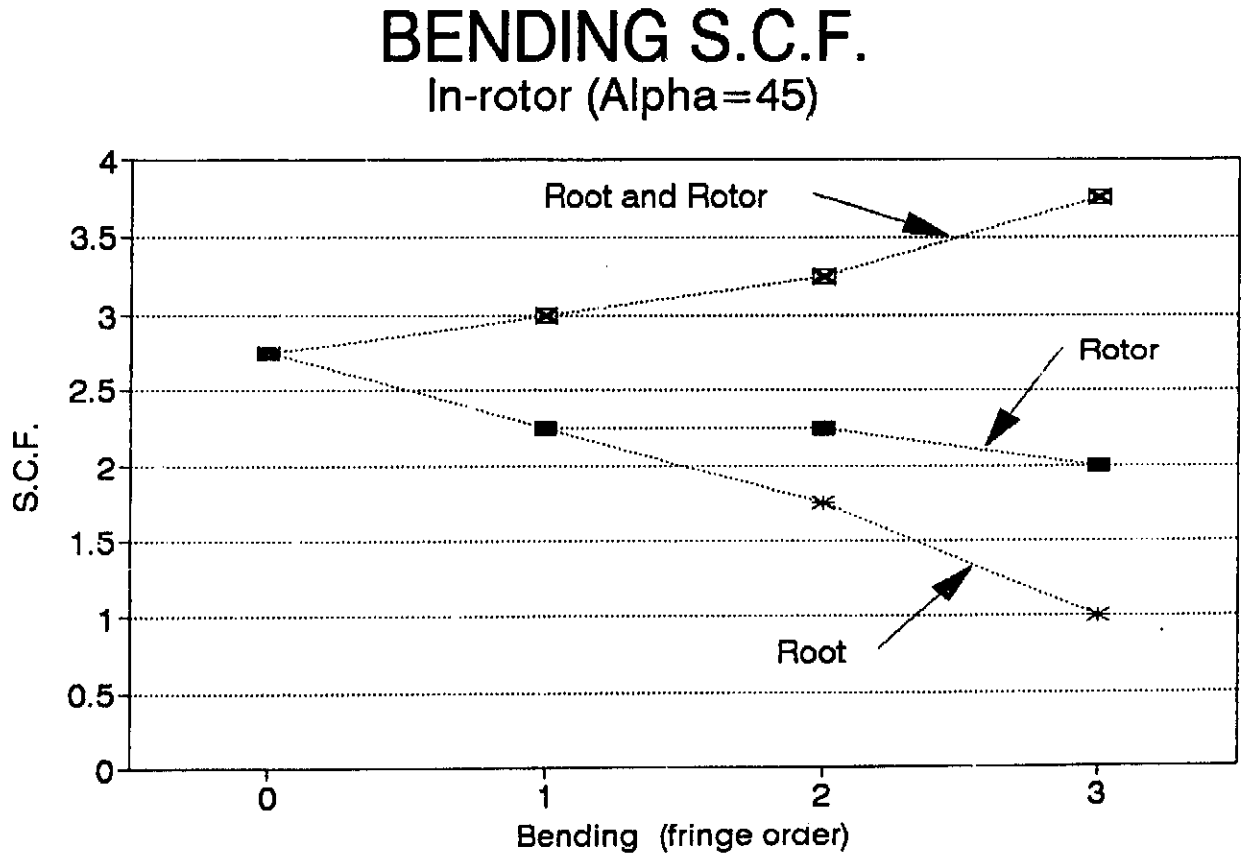

Figure 9.6 In-rotor bending test results for Alpha=45°

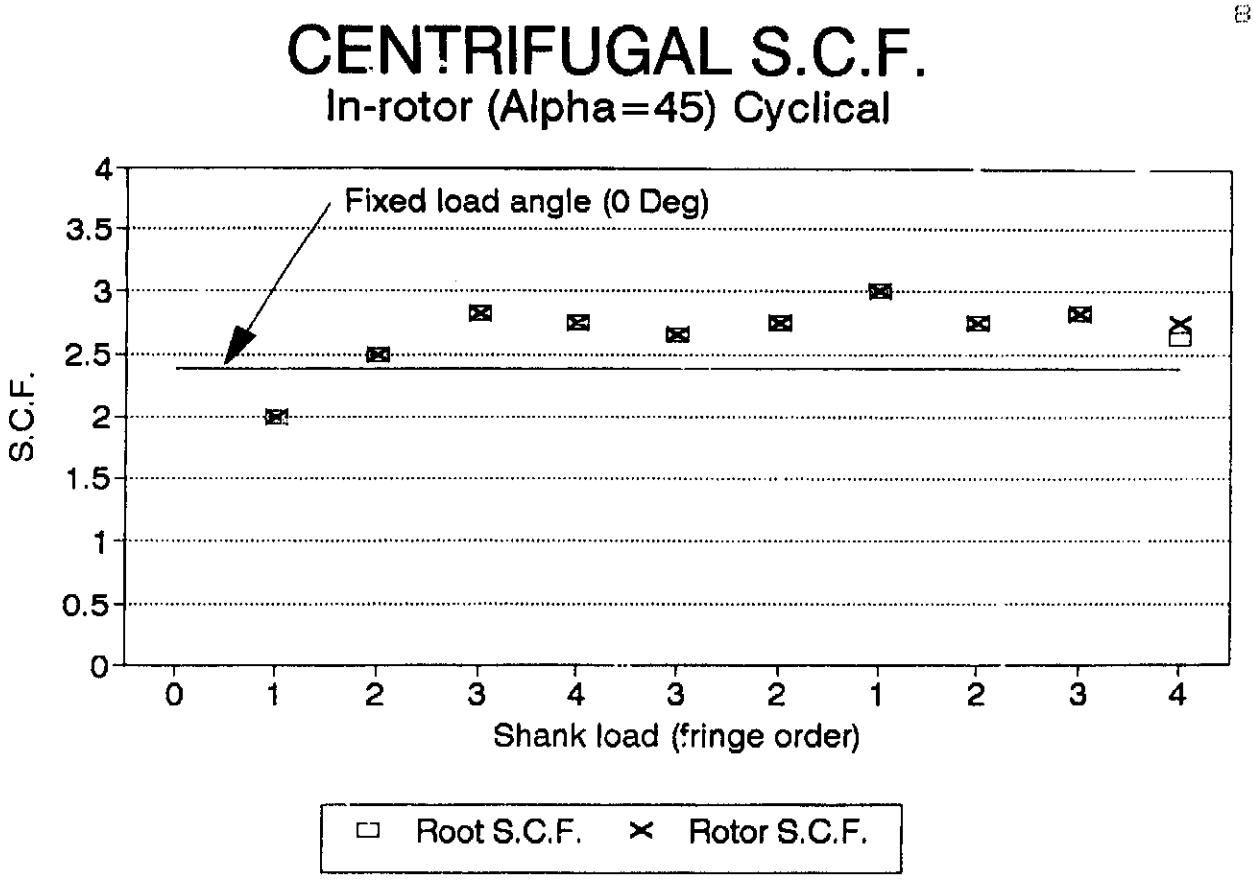

Figure 9.7 In-rotor cyclical centrifugal tests for Alpha=45°

CHAPTER 10

10. Multiple tang tests

10.1 Experimental aim

Having found a satisfactory optimum single tang root, the result of expanding the single tang geometry downwards to form a 3 tang root, was to be investigated. Modeling of centrifugal as well as bending forces in the in-rotor position was undertaken. The experiments presented in this chapter are not intended to represent an optimization as in the previous chapter but are intended to serve as a culmination of the study of the optimal single tang root. The experiments also serve to show how the optimization process can be continued and what aspects are important.

10.2 The 3 tang root

As described in chapter 4, the 3 tang root used in this study is simply a single tang root propagated downwards at an angle Gamma which is dependant on the choice of D and DO. In the single tang root Gamma was artificially defined but in the 3 tang root it is a real physical characteristic. With a multiple tang root, manufacturing becomes more difficult due to the length and torsional strength and stiffness that a milling cutter shaft must have to machine the deepest rotor notches. This, fundamentally cutting force and precision based problem, is often overcome by manufactures increasing the width of the shank, termed DO in this report (see figure 4.1). A similar but less severe problem also arises when broaching instead of milling is used. For the purposes of the tests at hand DO was chosen as 0 which in all probability represents the optimal choice. The effect of increasing DO, varying Gamma and similar geometric changes, as well as the effect these changes have on the rotor stresses would form the subject matter of a multiple tang investigation. The optimal single tang root (from chapters 8 and 9) can be used as a basis for such a study.

10.3 Experimental procedure

The rig employed for the in-rotor tests as described in the previous chapter was also used for the 3 tang blade root tests. The tests were carried out similarly to the single tang in-rotor tests described in the previous chapter but shank loads were limited to order 3 and not taken to order 4 as in all the other experiments. This was done to limit stresses in the loading rig which are much higher due to the larger shank size of the 3 tang roots tested. The tests were done on a root with the basic tang geometry of the Alpha = 40° root discussed in the previous chapter, that is :

Alpha = 40°
Beta = 30°
B/D = 0.5
h/D = $\sqrt{3}$ = 1.732
Gamma = 16.71°

A test to assess the effectiveness, in terms of S.C.F. decrease, of modifying the top fillet of the 3 tang root was also undertaken. The modification was made as described by Durreli [8].

10.4 Experimental results

The accuracy of the experimental results were reduced due to the lower stress in the shank and the unchanged fringe counting accuracy. The loss of accuracy was made worse by the fact that no smoothing of the results was possible as in chapter 8. The full results are included in tabular form at the end of the chapter. The stress concentration factors of the root and the rotor are given for each tang and are arranged in the same way as they would be physically. A graphical representation of the results was not attempted due to the nature of the tests.

10.4.1 Centrifugal load

The average root fillet S.C.F. of 2.5 for the 3 tang root is 11% higher than the value of 2.2 obtained for the single tang root. Taking the maximum value of 2.7 encountered in the top tangs into account makes a comparison with the single tang root even

more difficult. The reason for this large discrepancy between the single and the multiple tang root is can be attributed to limited measuring accuracy, friction effects and unequal loading of individual tangs due to manufacturing accuracy. All of these effects require further investigation.

Of considerable interest in multiple tang roots is the load distribution which occurs between the different tangs. The deviations from a uniform load distribution are caused by the inherent stress distribution in the root, and by manufacturing tolerances causing a lack of simultaneous contact on all the contacting surfaces as the load is applied. Which factor is responsible for which effect is difficult to distinguish, the effect is however clearly seen in the experimental results. The effect of manufacturing tolerances would normally be lost in a finite element analysis a fact which losses its importance in practice because unequal tang loading is minimized by plastic deformation in overspeed spinning. The results also show a decrease in S.C.F. from the top tang to the bottom tang. The possibility of distributing the stress evenly by changing DO and Gamma would be an important part of a future study.

10.4.2 Bending load

Given the stress distribution of the centrifugal load tests and the load transfer observed in the single tang bending tests the results of the three tang bending tests are as expected. The root S.C.F. on the high load side is higher than the single tang result (an average of 4.3 compared to 3.4) and decreases from the top tang to the bottom tang, as seen with the centrifugal loads. The load transfer which occurs as a result of the bending force is seen clearly on both sides of the root. On the low load side the average rotor S.C.F. is 2.7 compared to the average root S.C.F. of 0.4. On the high load side the average rotor S.C.F is 2.6 and the average root S.C.F. is 4.3. Although these figures are higher than those obtained for the single tang roots it should be remembered that the single tang roots were initially loaded to shank order 4 and the 3 tang root was only loaded to shank order 3. The subsequent bending was however the

same resulting in the higher S.C.F. changes experienced in the three tang root test.

10.5 Top fillet modification

The fillet modification experiments were undertaken some time after the original three tang experiments. This time delay resulted in considerable model aging, causing severe time edge effects to develop in the model. A quantitative analysis of S.C.F. decrease was thus ruled out but the qualitative analysis of the results proved useful. The modifications were made as described by Durreli [8]. Removing the material in the fillet where the highest stress occurs, results in flattening of the stress peak and a reduction of the stress.

Referring to the series of photographs in appendix A3.4 it can be seen how the sharp fillet peak stress is gradually smoothed and decreased as more material is removed from the fillet. The change in fillet geometry is seen to have a marked effect on the length and position of the maximum stress peak, flattening it and moving it away from the contact region.

10.6 Experimental conclusions

The results show that the single tang S.C.F. cannot simply be extrapolated to the multiple tang situation as the multiple tang root returns higher average stress concentration factors. The load distribution between the tangs of the multiple tang root also complicate the situation. When subjected to bending loads, the same type of load transfer is found as in the single tang root. As in the single tang root the load transfer has the effect of protecting the rotor against bending forces to a certain extent.

Modifying the fillet radius showed that the sharp stress peak in the fillet, can be flattened and moved away from the contact region.

10.7 Three Tang Root Test Results

Centrifugal S.C.F

Tang	Rotor	Root	Shank order	Root	Rotor
Top	2.5	2.5	1.0	2.5	2.5
Middle	2.5	3.0	1.0	2.5	2.5
Bottom	2.5	2.5	1.0	2.5	3.0

Tang	Rotor	Root	Shank order	Root	Rotor
Top	2.0	2.8	2.0	2.5	2.3
Middle	2.8	2.8	2.0	2.8	2.3
Bottom	3.0	2.8	2.0	2.5	3.0

Tang	Rotor	Root	Shank order	Root	Rotor
Top	2.0	2.7	3.0	2.7	2.5
Middle	2.3	2.5	3.0	2.5	2.2
Bottom	2.8	2.3	3.0	2.3	2.5

Bending S.C.F.

Tang	Rotor	Root	Shank order	Root	Rotor
Top	2.3	3.2	4,3,2	1.5	1.5
Middle	2.5	2.8	4,3,2	1.8	2.2
Bottom	2.8	2.5	4,3,2	2.2	3.0

Tang	Rotor	Root	Shank order	Root	Rotor
Top	2.7	3.8	5,3,1	0.7	1.8
Middle	2.3	3.7	5,3,1	1.2	2.3
Bottom	2.7	2.8	5,3,1	1.8	3.2

Tang	Rotor	Root	Shank order	Root	Rotor
Top	2.5	4.7	6,3,0	0.3	2.5
Middle	2.7	4.3	6,3,0	0.7	2.3
Bottom	2.5	4.0	6,3,0	0.3	3.2

CHAPTER 11

11. Comparison between experimental and analytical results

11.1 The Heywood formula compared to experimental results

After completion of the experimental phase of the study the experimental results were compared to the results obtained from the Heywood formula described in chapter 6. The two sets of results are shown graphically at the end of the chapter.

The experimental results of the roots with a nonzero value of DO showed the best correlation with the Heywood formula when a reverse linear force distribution was used in the Heywood analysis. The experimental results of the roots with DO = 0 showed the best correlation with the linear force distribution Heywood results. Graphs of the two cases are given in figure 11.1 and 11.2. This observation uncovers a serious flaw in the Heywood formula when applied to turbine blade roots. The reasons for this flaw are twofold. 1) The Heywood formula was derived from experiments in which the loaded projections (tangs) were supported by a semi-infinite plate while the blade roots were subject to loads on symmetrically opposite tangs supported by a central shank. 2) The other factor which makes the Heywood formula inaccurate for the application at hand is the formulas sensitivity to variations in Gamma. This can be demonstrated by calculation but can also be seen directly from the geometry where a decrease in Gamma results in a increase of "e" and a decrease of "a" (Refer to figure 6.2). This results in the $1.5*e/a^2$ term in the stress equation showing a sharp increase in the fillet stress. This makes a accurate determination of Gamma very important. In a multiple tang root this presents no problem but in the case of a single tang root Gamma is not a true geometric parameter and has to be artificially defined.

11.2 Mathematical result modeling

In the light of the unsatisfactory results obtained from the Heywood formula for the turbine blade root it was decided to develop two formulas which would accurately model the results obtained in the experimentation phase. The models were to be simple and accurate for range of available test data. To develop the models the results of the single tang investigation, as described in chapter 8, were used as a data base. The first formula, called Form0 for reference purposes uses DO=0 results from the phase 3 experiments. These result were the most accurate experimental results and cover a variety of geometries. The second formula, called Form1, is not as accurate as Form0 but was fitted to all the available experimental data (excluding repeat tests). The formula is valid for roots with DO=0 and DO>0. Only the 0° load angle data was used to fit the formulas.

11.3 Form0 (Formula for roots with DO=0)

The model is made up of a single combined geometric variable which is calculated from the main geometric variables of the blade root, namely: Alpha, Beta, R, B and D. The combination of variables that gave the best overall representation of the geometry was

$$G = \frac{(\text{Alpha} + 3 * \text{Beta}) * 0.01745 * B^{2.2}}{R * D^{1.2}}$$

Were Alpha and Beta are given in radians and the lengths can be given in any convenient unit as the formula is dimensionless. In chapter 8 and 9 use was made of dimensionless variables B/D and R/D. The $B^{2.2} / (R * D^{1.2})$ part of the combined geometric variable can be written as $(B/D)^{1.2} * (B/D) * (D/R)$, thus resolving it back into dimensionless geometric variables. The physical justification of the formula is seen in the (Alpha + 3 * Beta) part representing the relative projection beam height while the $B^{2.2} / (R1 * D^{1.2})$ part represents the combined influence of the fillet radius and the vertical projection of the contact angle length in relation to the shank width.

This geometric variable was then fitted to the experimental data using a least squares fitting. The formula which was found to give the best fit was:

$$S.C.F. = \frac{1}{0.4379-0.0383*Ln\ G}$$

Were G is the combined geometric variable described in the previous section.

The maximum errors were found to be +7.051% and -3.47% when compared with the experimental data. If one data point (Root 54) is not included in the error analysis the maximum positive error drops to 3.618%. No explanation could be found for the deviation of root 54.

Table 11.3 and the graph in figure 11.4 present a comparison between the experimental results and the S.C.F. values obtained from the formula.

11.3.1 Form0 formula limitations

As the data base used to develop the formula is limited, the formula should not be used beyond these limits. The possibility that the formula provides good results beyond these limits does exist but this possibility should be verified before being applied. The limits are:

$40° < Alpha > 45°$
$15° < Beta > 45°$
$0.5 < B/D > 1.0$
$h/D = \sqrt{3}$
Load Angle = 0°

As these limits also represent the limits of most practical blade root geometries they should not place a serious limitation on the practical usefulness of the formula.

11.4 Form1 (Formula for all roots with decreased accuracy)

The development of this formula presented far greater problems than the development of Form0. The problems arose from the extra variable (D0) which had to be modeled and the overall

lower integrity of the experimental data, most of which was established before the experimental technique was perfected. The DO component was considered as strengthening the shank by a factor (DO+D)/D. This factor was combined with the previously established variable G to form another dimensionless variable Eta defined as

$$Eta = G^2 - 2*G + 2 - 2*(DO+D)/D + ((DO+D)/D)^2$$

This variable was then fitted to various functions using a least squares fitting method. The function which was found to give the best practical fit was

$$S.C.F. = 2.267 + 0.565*Eta^2 - 0.106*Eta^4$$

The maximum error was 23.8% and the average error is 9.2%. These errors are large and it can be seen from figure 11.6 the fitting shows an unrealistic drop in S.C.F. with an increase of Eta above 2.5. The limited geometry range across which the data was obtained is an important factor in producing this unrealistic fit.

Table 11.5 and the graph in figure 11.6 show the comparison between the experimental results and the formula Form1.

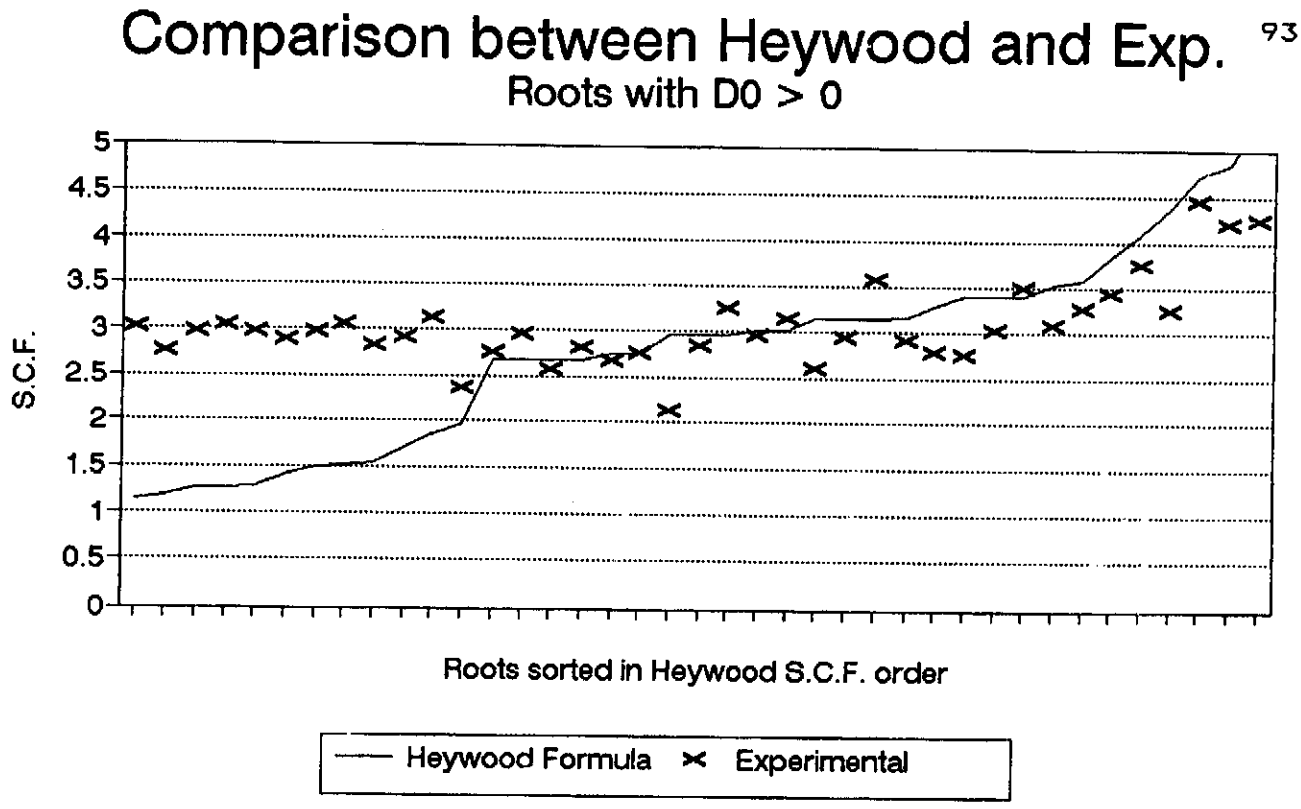

Figure 11.1 Comparison between Heywood and experimental results for DO > O roots

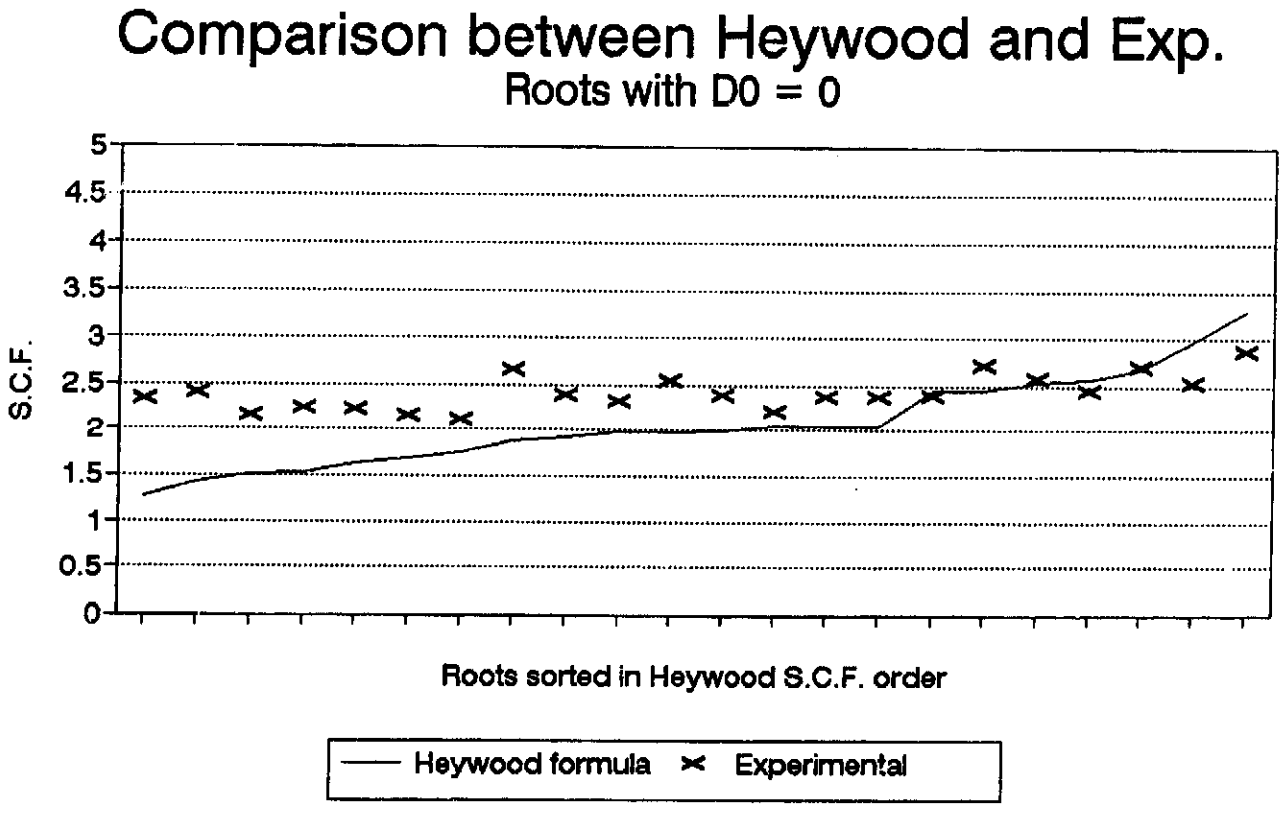

Figure 11.2 Comparison between Heywood and experimental results for DO = O roots

Root	Alpha	Beta	R1	B	D	Gamma	Exp	"G"	Formula	% Error
48	40	15	3.836	10	10	20.9	2.539	221.58	2.591	-2.05
49	45	45	4.229	10	15	17.7	2.657	261.65	2.634	0.85
50	45	30	4.681	6.667	10	18.5	2.407	118.19	2.439	-1.32
51	45	15	5.71	6.667	10	19.1	2.375	64.59	2.309	2.80
52	45	30	4.309	12.5	15	20.1	2.707	314.67	2.684	0.84
53	45	15	4.349	8.333	10	20.5	2.457	138.55	2.476	-0.76
54	45	15	4.483	15	15	22.1	2.875	301.14	2.672	7.05
58	40	45	3.291	6.667	10	17.16	2.543	217.92	2.587	-1.72
59	40	15	4.969	8.333	10	19.59	2.407	114.54	2.432	-1.03
60	40	15	6.101	6.667	10	18.47	2.207	57.10	2.284	-3.47
61	40	45	5.3	5	10	15.74	2.418	71.86	2.331	3.62
63	40	15	7.2	5	10	17.52	2.114	25.69	2.135	-0.97
64	45	45	5.2	5	10	16.07	2.343	75.34	2.340	0.11
65	45	30	6.5	5	10	17.07	2.25	45.20	2.238	0.54
66	45	15	7.1	5	10	17.84	2.157	27.59	2.147	0.46
67	40	30	5.084	6.667	10	17.9	2.407	104.79	2.412	-0.20
68	40	30	3.56	8.333	10	19.3	2.582	244.51	2.617	-1.34
72	40	30	6.6	5	10	16.71	2.218	42.87	2.228	-0.44

Table 11.3 Comparison between the formula and the experimental results for DO = 0

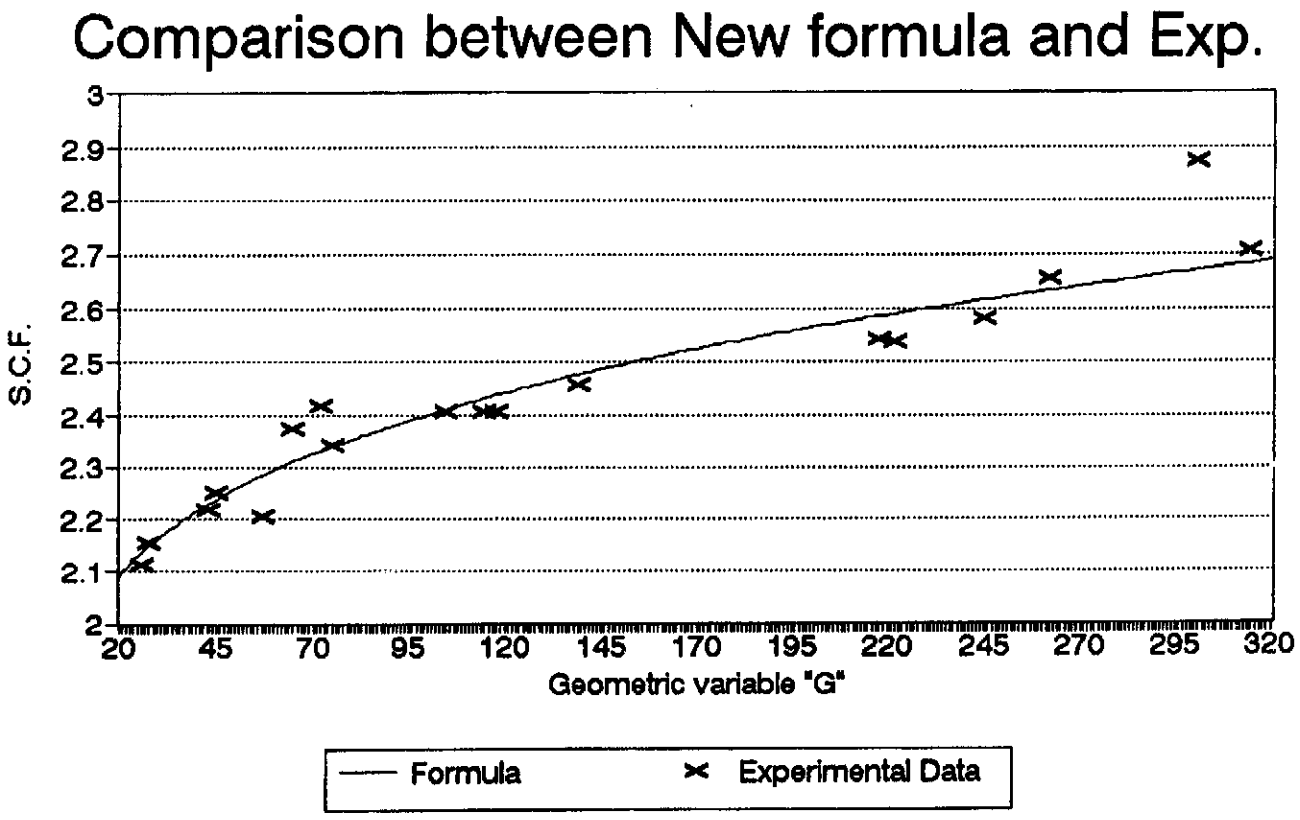

Figure 11.4 Comparison between the formula Form0 and the experimental results

Table 11.5 Comparison between the formula Form1 and the experimental results for all root geometries tested

Root	Alpha	Beta	R1	B	D	Gamma	DO	Exp	(DO+D)/D	'G'	'Eta'	Formula	% Error
3	35	34	3.100	4.271	5.243	15.000	9.081	3.436	2.732	2.576	2.342	3.009	12.422
4	40	39	3.100	4.271	5.661	15.000	9.081	2.914	2.604	2.692	2.332	3.008	-3.242
5	40	29	3.100	4.271	4.903	15.000	9.081	3.271	2.852	2.588	2.439	3.015	7.829
9	40	34	3.100	4.271	5.234	15.000	12.081	3.750	3.308	2.675	2.852	3.017	19.554
10	40	34	3.100	4.271	7.721	20.000	9.081	3.250	2.176	1.678	1.358	2.839	12.650
11	40	34	3.100	4.271	3.203	10.000	9.081	2.771	3.835	4.823	4.759	2.557	7.738
12	40	34	3.100	3.271	4.739	15.000	9.081	3.086	2.916	1.676	2.032	2.978	3.511
13	40	34	3.100	5.271	5.729	15.000	9.081	2.793	2.585	3.813	3.228	2.987	-6.944
14	50	34	3.100	4.271	5.309	15.000	9.081	2.686	2.711	2.815	2.494	3.017	-12.331
15	40	34	5.100	4.271	7.247	15.000	9.081	2.957	2.253	1.100	1.257	2.810	4.974
16	40	34	3.100	4.271	5.234	15.000	9.081	3.500	2.735	2.675	2.411	3.013	13.901
17	45	34	3.100	4.271	5.252	15.000	9.081	3.150	2.729	2.758	2.466	3.016	4.251
20	40	34	4.100	4.271	6.241	15.000	9.081	3.250	2.455	1.638	1.589	2.897	10.853
21	40	34	3.100	4.271	5.234	15.000	6.081	2.814	2.162	2.675	2.038	2.979	-5.848
22	40	34	3.100	4.271	5.234	15.000	3.081	2.371	1.589	2.675	1.775	2.936	-23.840
24	40	34	3.600	4.271	5.738	15.000	9.081	2.607	2.583	2.063	1.907	2.959	-13.509
28	40	45	5.000	5.000	8.993	15.000	6.000	3.136	1.667	1.510	0.840	2.667	14.958
29	50	40	5.000	5.000	8.022	15.000	6.000	2.832	1.748	1.682	1.012	2.731	3.581
30	50	35	5.000	5.000	7.498	15.000	6.000	2.918	1.800	1.664	1.040	2.740	6.099
31	50	45	5.000	4.500	8.335	15.000	6.000	3.043	1.720	1.387	0.817	2.658	12.647
32	50	45	5.000	5.500	9.138	15.000	6.000	2.979	1.657	1.931	1.140	2.773	6.901
33	50	45	4.000	5.000	7.791	15.000	6.000	2.893	1.770	2.370	1.572	2.893	-0.014
34	50	45	6.000	5.000	9.681	15.000	6.000	2.750	1.620	1.218	0.657	2.593	5.724
35	55	45	5.000	5.000	8.721	15.000	6.000	3.011	1.688	1.701	0.982	2.720	9.669
36	50	45	3.500	5.000	7.319	15.000	6.000	2.979	1.820	2.920	2.088	2.985	-0.197
48	40	15	3.836	10.000	10.000	20.900	0.000	2.539	1.000	3.867	2.867	3.016	-18.791
49	45	45	4.229	10.000	15.000	17.700	0.000	2.657	1.000	4.567	3.567	2.935	-10.447
50	45	30	4.681	6.667	10.000	18.500	0.000	2.407	1.000	2.063	1.063	2.748	-14.165
51	45	15	5.710	6.667	10.000	19.100	0.000	2.375	1.000	1.127	0.127	2.338	1.578
52	45	30	4.309	12.500	15.000	20.100	0.000	2.707	1.000	5.492	4.492	2.668	1.458
53	45	15	4.349	8.333	10.000	20.500	0.000	2.457	1.000	2.418	1.418	2.855	-16.211
54	45	15	4.483	15.000	15.000	22.100	0.000	2.875	1.000	5.256	4.256	2.753	4.246
58	40	45	3.291	6.667	10.000	17.160	0.000	2.543	1.000	3.803	2.803	3.018	-18.694
59	40	15	4.969	8.333	10.000	19.590	0.000	2.407	1.000	1.999	0.999	2.726	-13.247
60	40	15	6.101	6.667	10.000	18.470	0.000	2.207	1.000	0.997	0.003	2.269	-2.821
61	40	45	5.300	5.000	10.000	15.740	0.000	2.418	1.000	1.254	0.254	2.404	0.577
63	40	15	7.200	5.000	10.000	17.520	0.000	2.114	1.000	0.448	0.552	2.547	-20.464
64	45	45	5.200	5.000	10.000	16.070	0.000	2.343	1.000	1.315	0.315	2.435	-3.911
65	45	30	6.500	5.000	10.000	17.070	0.000	2.250	1.000	0.789	0.211	2.382	-5.858
66	45	15	7.100	5.000	10.000	17.840	0.000	2.157	1.000	0.481	0.519	2.532	-17.370
67	40	30	5.084	6.667	10.000	17.900	0.000	2.407	1.000	1.829	0.829	2.663	-10.624
68	40	30	3.560	8.333	10.000	19.300	0.000	2.582	1.000	4.267	3.267	2.982	-15.497
72	40	30	6.600	5.000	10.000	16.710	0.000	2.218	1.000	0.748	0.252	2.403	-8.332

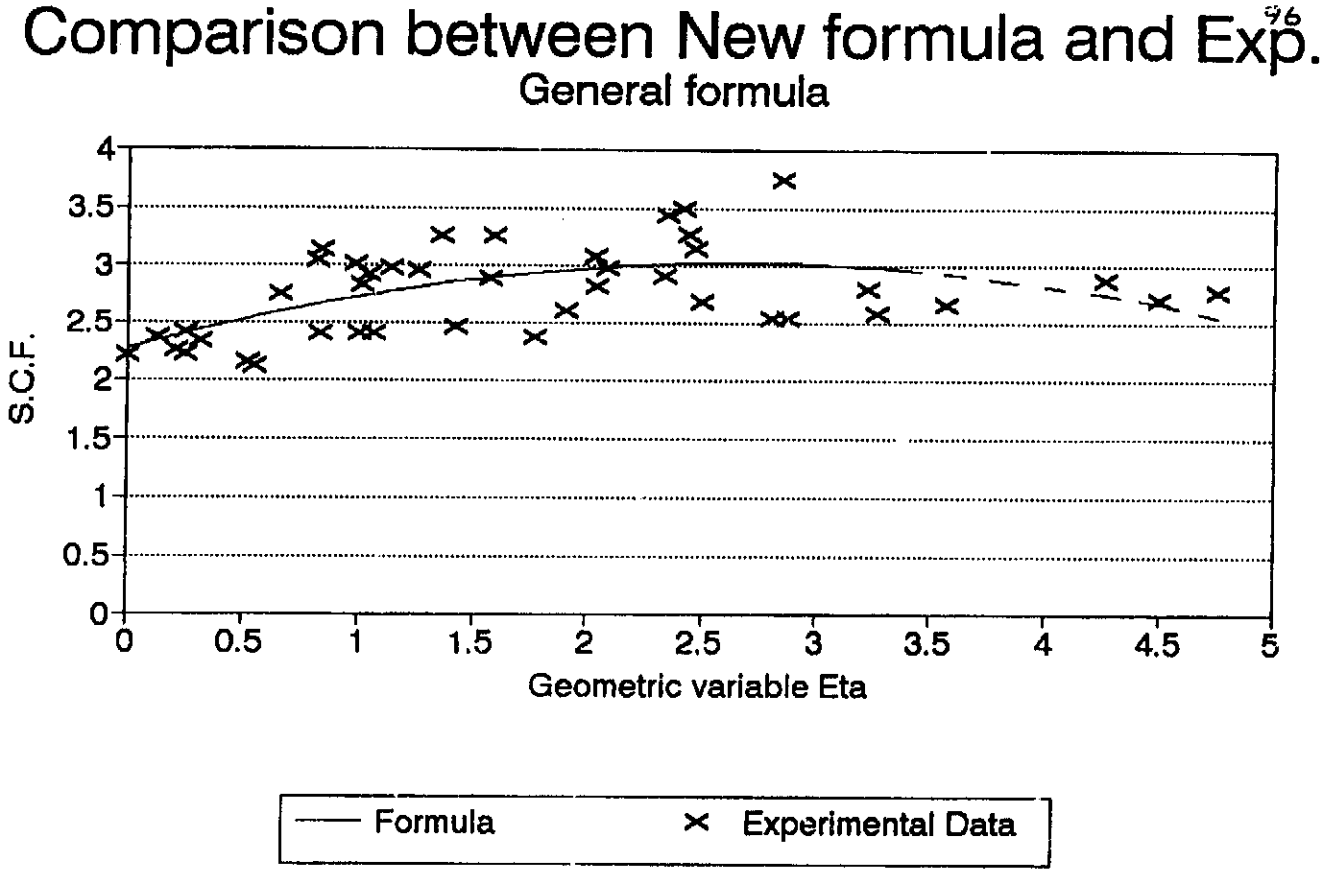

Figure 11.6 Comparison between the formula Form1 and the experimental results

CHAPTER 12

12. A single tang blade root design rule

From the experimental results the following points which serve as guidelines for single tang blade root design were developed

1) Alpha should be between 40° and 45°. Larger roots must have a smaller Alpha i.e. 40° to minimize slip and prevent the root "walking" out of the rotor notch. Smaller roots can have larger Alpha but the larger angle does not reduce the fillet S.C.F. and must be chosen in answer to other requirements.

2) B/D which represents the contact surface length to shank width ratio should be chosen as low as possible. Choice of materials as well as surface treatment such as shotpeening, influences the surface strength of the root. Due to the plastic deformation which is partially permissible in the contact region stress spikes are smoothed thus giving the surface a higher loading capacity than would normally be the case.

3) The angle Beta should be in the region of 15°. The main factor determining the size of Beta is the tang base height, h (fig. 4.1). An angle of Beta = 15° was found to give the best results but lower angles could also be tried if the tang base height can withstand the shear stress.

4) The ratio of R/D should be kept between 0.7 and 0.8 to stay within the maximum material utilization criterion. It was also found that increasing the fillet radius beyond this region does not benefit the S.C.F. A modification as done on the top fillet of the 3 tang root (Section 10.5) is useful, especially in moving the stress peak away from the contact region.

5) Material utilization optimization should always be kept in mind as it was found to provide a good base to work from.

6) Surfaces should be treated to minimize the danger on fretting and crack initiation. Dry lubricants which can reduce the friction coefficient to 0.1 should be used to minimize the surface shear stress when unavoidable slip does take place. Shotpeening and other treatments which enhance the surface characteristics are also useful.

7) The combination of root, shank and airfoil should be chosen to minimize the risk of the load resultant ever going outside the critical area as described in section 4.3.

8) DO, the manufacturing concession should be kept as low as possible as an increase in DO increases the strength of the shank above that of the optimum root.

CHAPTER 13

13. Conclusion and recommendations for further research

13.1 Conclusion

Turbo-machinery blade roots are subject to two principal loads. A centrifugal load resulting from the mass of the blade and the rotation of the machine and a bending load caused by gas forces and vibrations of the blade. An optimized blade root geometry was defined as the geometry in which the fillet stress concentration factor was minimized under typical practical loading conditions.

The literature survey highlighted various important facets of the blade root optimization problem. The importance of modeling the contact surface conditions accurately led to the decision to use photoelasticity in the experimental phase instead of finite element analysis with which contact surface problems cannot be reliably solved to date.

Various methods were used to solve the optimization problem of which the material utilization optimization method produced the best results. Using this approach a fixed load analysis of various turbo-machinery blade root geometries was made which showed that the stress concentration factor distribution in the region a of practical optimum geometry was relatively flat. This explains the large variety of different root geometries used in industry where the blade root geometries are adapted to suite particular applications.

A general optimum single tang blade root geometry was defined using the experimental results. The subsequent centrifugal load in-rotor results corresponded well to the fixed friction angle test results. When subjected to combined bending and centrifugal loads a load transfer takes place in the contact region. This load transfer produces larger stress fluctuations in the blade root than in the rotor making the rotor less susceptible to fatigue damage. A mathematical model which

predicts the fillet stress concentration factor from a given root geometry was developed.

It was found that the single tang results cannot be directly extrapolated to the multiple tang root.

13.2 Recommendations for continuing the project

A continuation of the single tang investigation would comprise the following:

1) Modification of the maximum material utilization theorem to include the effect of the fillet stress concentration , contact area stress distribution and shear force distribution in the tang base.

2) The effect of using a non-zero value for DO to quantify the compromise which is made to facilitate manufacture.

3) Broadening the geometric limits to include roots with Alpha < 40° etc.

4) The relative danger of roots "walking" out of the rotor

5) Contact surface fatigue effects.

6) Verification and possible modification of the mathematical model to include areas outside the limits of the present study and a friction angle variable.

7) Comparison of experimental resultswith finite element analysis techniques.

The development of the a multiple tang root optimum forms the second important area for further research. Facets to be studied include:

1) The effect of Gamma and DO on the fillet S.C.F..

2) Root interaction with the rotor and with the rest of the blade.

3) The distribution of the loads between the tangs including manufacturing tolerance effects.

4) The tang geometry should also be studied further because the optimum single tang geometry may not be the optimum tang geometry for multiple tang roots.

Friction coeficients at the level of contact stress experienced in blade root attachments are still largely unknown. Experiments investigating the friction effects using self loading devices and repeated loading of surfaces as used by Hattori et al. [13], should form an important part of any future blade root investigation.

The possibility of using a finite element analysis based on the method developed by Ruiz et al [3], [15] and [26] to enable faster and more flexible optimization methods to be employed should be investigated.

List of references

1. Albrecht, C., "Transmission design using finite element method analysis techniques.", Journal of the American Helicopter Society, April 1988, pp 3-14.

2. Benham, P.P., and Warnock F.V., "Mechanics of solids and structures.", Pitman Publishing, London, 1984.

3. Boddington, P.H.B., Chen, K. and Ruiz, C., "The numerical analysis of dovetail joints.", Computers and structures, Volume 20, Number 4, 1985, pp 731-735.

4. Buchan, L., "Bending stresses in the single tang turbine blade attachment.", Unpublished undergraduate thesis, University of Stellenbosch, 1991.

5. Durelli, A.J. and Riley, W.F., "Introduction to photoelasticity.", Prentice-Hall, London, 1965.

6. Durelli, A.J., "Applied stress analysis.", Pentice-Hall, New Jersey.

7. Durelli, A.J., Dally, J.W. and Riley, W.F., "Stress and strength studies on turbine blade attachments.", Proceedings of the society for experimental stress analysis, Volume XVI Number 1, pp 171-186.

8. Durelli, A,J, and Rajaiah, K., "Lighter and stronger.", Proceedings of the society for experimental stress analysis, Volume XXXVII, Number 2, 1980, pp 369-380.

9. Endres, W., "Cracks in plates under shear and compression.", R&D Journal, Volume 8, Number 1, April 1992, pp 29-34.

10. Endres, W., "Rotor design for large industrial gas turbines.", Intenational gas turbine and aero engine congress, Cologne, 1992, Paper number 92-GT-273.

11. Föppl, L., "Drang und Zwang", Leibniz Verlag, München, 1947.

12. Frocht, M.M., "Photoelasticity", Volumes 1 and 2, John Wiley and Sons, New York.

13. Hattori, T., Sakata, S. and Ohnishi, H., "Slipping behavior and fretting fatigue in the disk/blade dovetail region.", Proceedings of Tokyo International Gas Turbine Congress, 83-Tokyo-IGTC-122, 1984, pp 945-952.

14. Herschel, D., "Inert high temperature thread compounds - a new alternative.", The South African Mechanical Engineer, Volume 39, June 1989, pp 269-270.

15. He, M.J. and Ruiz, C., "Fatigue life of dovetail joints: verification of a simple biaxial model", Proceedings of the Society for Experimental Mechanics, Volume XLVI, 1989, pp 126-131.

16. Hetenyi, M., "Handbook of experimental stress analysis.", John Wiley & Sons, London, 1950.

17. Heywood, R.B., "Designing by photoelasticity.", Chapmann & Hall, London, 1952.

18. Heywood, R.B., "Photoelasticity for designers.", Pergamon Press, Oxford, 1965.

19. Heywood, R.B., "Tensile fillet stresses in loaded projections.", Proceedings of The Institution of Mechanical Engineers", Volume 159, War Emergency Issues, 37-46, 1948, pp 384-398.

20. Kashiwabara, Y., Matsuura, Y., Katoh, Y., Hagiwara, N., Hattori, T. and Tokunaga, K., "Development of a high-pressure-ratio axial flow compressor for a medium-size gas turbine.", Transactions of the American Society of Mechanical Engineers Journal of Turbomachinery, Volume 108, Number 2, October 1986, pp 233-239.

21. Kenny, B., Patterson, E.A. Said, M., and Aradhya, K.S.S., "Contact stress distributions in a turbine disc dovetail type joint - a comparison of photoelastic and finite element results.", Strain, February 1991, pp 21-24.

22. Kuske, A. and Robertson, G., "Photoelastic stress analysis", John Wiley & Sons, London, 1974.

23. Parks, V.J. and Sanford, R.J., "Photoelastic and holographic analysis of a turbine-engine component.", Proceedings of the Society for Experimental Stress Analysis, VolumeXXXV, number 2, 1978, pp 328-334.

24. Peterson, R.E., "Stress concentration factors.", John Wiley and Sons, New York, 1974.

25. Post, D., "Photoelasticity.", Proceedings of the Society for Experimental Stress Analysis, Volume XXVI, Number 1, 1979.

26. Ruiz, C., Boddington, P.H.B. and Chen, K.C., "An investigation of fatigue and fretting in a dovetail joint.", Proceedings of the Society for Experimental Mechanics, Volume XLI, 1984, pp 208-217.

27. Rust, N.A., "Investigation of stresses in blade root attachments.", Unpublished undergraduate thesis, University of Stellenbosch, 1989.

28. Smith, J.O., and Liu, C.K., "Stresses due to tangential and normal loads on an elastic solid with application to some contact stress problems.", Journal of Applied Mechanics, June 1953, pp 157-166.

29. Tredoux, J.N., "Photoelastic investigation of turbomachinery blade attachments", Unpublished undergraduate thesis, University of Stellenbosch, 1989.

30. Traupel, W., "Thermische Turbomaschinen.", Springer Verlag, Berlin, 1960, (Two Volumes).

APPENDIX 1

Three main Pascal programs were written to do repetitive calculations, each of which is discussed below. The source code together with input files, output files and executable programs are supplied on the 360 kB floppy disk inside the back cover. The programs were written in Turbo Pascal (ver 4) and will run on most IBM compatible personal computers. All the typical inputs and outputs that are given pertain to fig. A1.1 which depicts root 72.

A1.1 The stress calculation program (Program ROOTSTRE)

This program formed the basis for all geometric and stress calculations. The input for the program consists of the geometric variables describing the root geometry to be studied (Alpha, Beta, B, R1, R2, DO and D or Gamma or C). The load (friction) angle and load distribution also form part of the program input. The program then converts the given load and geometric variables to the variables used by Heywood to describe the loaded geometry. The program then calculates the Heywood fillet stress and various other force and stress components acting in and on the root geometry.
In addition the program calculates h, the tang height, which is not a variable used to specify the geometry but is important for other calculations. A simple slip criticality analysis is also carried out by the program. This routine calculates the angle at which the combined centrifugal and bending load must be applied to the root in order to cause slip in the contact surfaces given a contact surface friction coefficient. A typical output listings generated by the program is given below.

ALPHA	(deg)	:	40.00000	BETA	(deg)	:	30.00000
R1	(mm)	:	6.60000	R2	(mm)	:	6.60000
B	(mm)	:	5.00000	BO	(mm)	:	6.52704
C	(mm)	:	13.11520	CO	(mm)	:	15.14413
D	(mm)	:	10.00000	DO	(mm)	:	0.00000
GAMMA	(deg)	:	16.70987	RHO	(deg)	:	0.00000
H	(mm)	:	17.30982	GB	(mm)	:	9.83468
E	(mm)	:	11.76728	A	(mm)	:	4.44243
RR	(mm)	:	6.60000	SIGHEY		:	0.00047
H/D	(1.732)	:	1.73098	B/D	(0.833)	:	0.50000
Force points		:	30	Distribution		:	P

CRITICAL WIDTH (mm)	:	18.5835
CRITICAL HEIGHT (mm)	:	23.8905
HEIGHT BELOW SHANK (mm)	:	23.2219
CRITICAL ANGLE (deg)	:	21.81

VERTICAL FORCE :	0.76604	Vertical on contact area (Force units)
NORMAL FORCE :	1.00000	Normal on contact area (Force units)
AVERAGE NORMAL STRESS :	0.07660	Average shank stress (force units / mm)
SIGMA HEYWOOD NORMAL STRESS :	0.11526	Sum of Heywood filet stresses (force units / mm)
AVERAGE SHEAR STRESS	0.04425	Ave. shear in tang base (Force units / mm)
AVERAGE SURFACE PRESSURE :	0.15321	Ave. contact surface pressure (Force units / mm)
FRICTIONAL SHEAR FORCE :	0.00000	Tangential force on contact surfaces (Force units)
STRESS CONCENTRATION :	1.50467	Effective Heywood stress concentration factor
PRESSURE / FILET STRESS :	1.32919	Ave. contact surface pressure / fillet stress

A1.2 The NC generation program for the blade root

(Program NCROOT)

Using the same geometric inputs as the program described above together with machining information such as cutter diameter and shank length this program generates the numerical control code needed to cut the roots on a NC milling machine. As many different root geometries as needed can be specified for one program run. The output file generated by the program could be used directly to punch a control tape for the milling machine. The program also generates an file in tne which can be used as an input file instead of typing all variables in by hand (.INP) and a input information file which is a user friendly version of the input information (.INF). The listing of a typical input information file is given in section A1.3 below.

A1.3 The input information file

X offset (mm)	:	0.00000	Y offset (mm)	:	0.00000
ALPHA (deg)	:	40.00000	BETA (deg)	:	30.00000
R1 (mm)	:	6.60000	R2 (mm)	:	6.60000
B (mm)	:	5.00000	DO (mm)	:	0.00000
D (mm)	:	10.00000	C (mm)	:	13.11520
GAMMA (deg)	:	16.70987	No. of Tangs	:	1
Shank (mm)	:	100.00000	Cut dia. (mm)	:	6.00000

A1.4 The NC generation program for the rotor

(Program NCROTOR)

This program is the structured identically to the program described above. Instead of generating NC code to cut roots however, it generates the NC codes to cut the matching rotor. Only one rotor notch geometry can be specified for the 5 rotor notches which are cut into the blank. The angle between the notches is set at 6° but the rotor pitch diameter can be specified. The program also calculate what the pitch diameter for a "symmetric" root-rotor match should be.

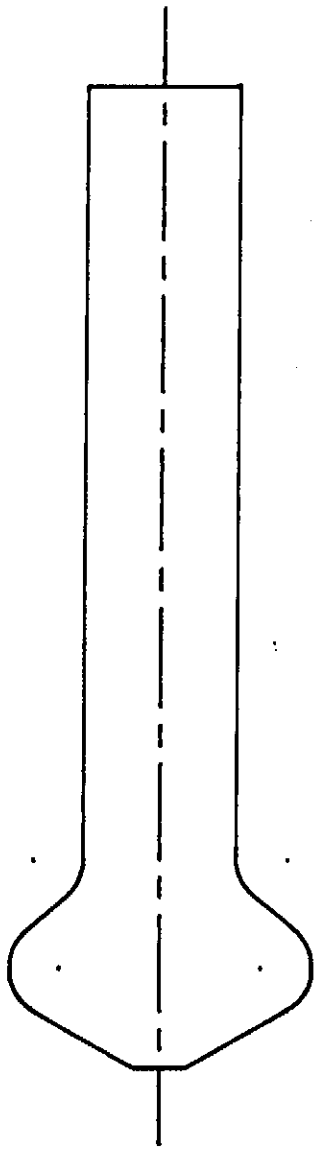

Figure A1.1 Root 72, used for all examples given in appendix 1

APPENDIX 2

A2 Preparation of the Araldite D models

The models used in the photoelastic analysis were made of a photoelastic epoxy based resin called Araldite D. The resin was cast into sheets. After curing the sheets were cut on a numerically controlled (NC) milling machine into the required model geometries.

Araldite D displays various properties which make it difficult to work with. 1) The material becomes hard and brittle with age to the point were chipping of milling cutters occurs. Even "young" material is prone to chipping. 2) Edge effects develop if the material is exposed to heat and (atmospheric) moisture. 3) Cast Araldite D may not be fully cured although it is hard and will only cure if kept at an elevated temperature for some time. The curing time decreases as the temperature increases. 4) Edge effect development can be retarded by storing the cast sheets in a cold dry place but this does not solve the embrittlement problem.

All these factors called for a special handling technique to be developed to optimally use the excellent photoelastic properties of the material. The ideal way of experimentation with Araldite D (and similar materials subject to aging) is a type of "just in time" approach. This method was used in the final experiments. The procedures involved getting the sheet straight out of the mould onto the NC machine, cutting the model and testing it immediately. This eliminated all necessity for storage and the resultant aging.

A2.1 Casting Araldite D

The care starts with the casting process in which all air bubbles must be eliminated. The temperature of the cast must also be controlled to eliminate uneven curing and thermally induced stresses in the final sheet. The curing must also be carefully checked because if the cast was slightly to cool or

the curing process was undertaken at inadequate temperatures or not enough time was allowed for the curing process or a combination of these factors the sheet seems fully cured and can be cut but reacts rather like a frozen stress model photoelastically.

A2.1.1 The mould

The mould consisted of two thick glass plates kept apart on three sides of the periphery by a aluminium spacer. The spacer was sealed to one plate using silicon sealant. The other plate was covered by a plastic film on the edges. Using silicon sealant to fill the gap between the aluminium spacer and the plastic film, the two plates were brought together with a 7 mm space between them. After the silicon sealant had cured, the two glass plates could be separated and the plastic film trimmed. The resulting gasket provided a good seal and allowed the mould to be taken apart easily when the Araldite D had cured. After spraying the inside of the mould with mould release the two glass plates were clamped in a steel frame. The mould release tends to form droplets on the glass surface. These droplets must be wiped smoothly over the glass with a paper swab to prevent dents and streaks in the surface of the casting.

A2.1.2 The mixing pot

The Araldite is extremely sticky and is very difficult to clean so it was decided to opt for a disposable mixing pot. A submerged casting process had to be used to prevent air bubbles being cast into the Araldite sheet. To combine these requirements a rubber tube was sealed into the bottom of a 2 liter soft drink bottle. The top of the bottle was cut of to facilitate filling. The outside diameter of the tube had to be chosen to fit between the glass plates of the mould. A wooden plug with a sting attached was fitted in the tube in the bottom of the bottle to prevent unmixed resin flowing into the mould.

A2.1.3 Casting

Araldite has to be mixed in a mass ratio of 5 parts resin to 1 part hardener. The cured density of Araldite is 1.2 g/cm^3. The volume of the sheet to be cast was determined and the masses of resin and hardener were calculated. The resin was weighed directly in the mixing bottle described above. The hardener was weighed in paper cups. The mixing bottle was placed in a container with hot water and the resin heated to +/- 45°C. Most air bubbles were eliminated from the resin in this way. The (room temperature) hardener was mixed with the resin and the mixture was left to stand for 2 min to eliminate air bubbles formed in the mixing process. The loose end of the tube was placed at the bottom of the mould and the wooden plug was removed by pulling on the attached string. As the resin mixture flowed into the mould the tube was pulled out of the mould so that the end of the tube was always just below the resin surface in the mould. Casting in progress is picture in figure A2.1.

The mould was placed in a warm place, preferably between 30°C and 40°C to promote curing. After 24 hours the cured plate could be removed from the mould. If the curing takes place below 25°C the plate must be heated for a few hours to achieve full curing. The temperature of the mixture before casting is critical. If the temperature is to low the viscosity is to high causing air bubble retention and bad flow into the mould. If the temperature is to high the exothermic curing reaction tends to heat up the mould and the uncast mixture to such an extent that thermal stresses are formed in the cast sheet and the uncast mixture starts melting the casting bottle and smoking. A tub of cold water into which the hot mixture could be dumped was always kept handy in the laboratory for such emergencies. For smaller casts the cast temperature should be higher than for large casts.

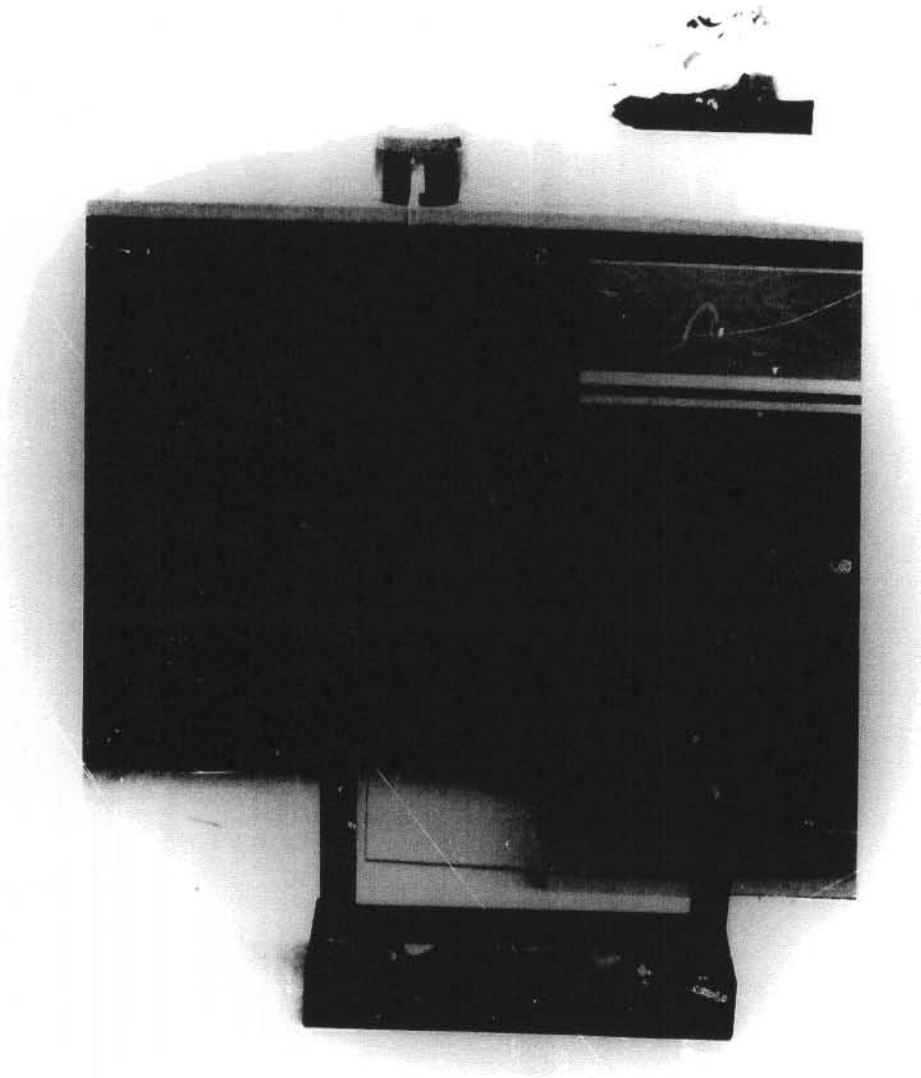

Figure A2.1 Casting in progress

A2.2 Machining

Machining the correct root profiles was done on a numerically controlled milling machine. The control routines were written by two Pascal programs which in turn were written by the student. One program generated the control code to cut blade roots and the other generated code to cut matching rotor sections. The input for the programs could be given from a disk file or from the keyboard. The output could be sent to the

printer, the screen or to a disk file. In addition to the NC program the programs also produced an input file which could be used to rerun the program and an information file which contained all the geometric information in a neat readable form. These three output files (if file output is chosen) were given the same name with different suffixes to prevent confusion and facilitate reference. A complete description of the programs is give in appendix 3.

The programs made provision for different milling cutter sizes to be specified but use was only made of a 6 mm cutter. Cutting speed was kept low to prevent heat buildup and model chipping. Two precuts of +/- 3mm deep were taken with a 5 mm cutter. The remaining 1 mm was then removed with the final cut using a 6 mm cutter. Spray water cooling was also used to keep the model edge temperature down. Model chipping was a major problem initially especially in the fillet area. The problem was eliminated using the precut method, cutting slowly and using sheets that were "young" ie. under one week old.

A2.3 Storing

The cured sheets are best stored in a closed container in a refrigerator. As far as possible these sheets should not be stored for a long time because the material hardens with age. The absorption of moisture, which causes the time edge effect is not critical in uncut sheets because the sensitive edges are not formed yet. Care should be taken to make sure that sheets are fully cured before storing them in a refrigerator as the low temperature practically halts the curing process.

Completed models were stored in airtight containers with silica gel. The silica gel absorbs the moisture in the container and to a certain extent prevents model aging. If the container is then stored in the refrigerator the aging process is further retarded. With all these precautions the useful life of the models is still restricted to about two weeks after which the edge effect becomes so bad that the model becomes practically useless. The sooner sheets and models are used the better.

A2.3 Final finishing

Due to the slightly rough surfaces left by the machining process the contact surfaces of the roots had to smoothed before the roots could be used. The smoothing was done by hand using 1200 grit emery paper. The direction of smoothing was also critical because minimum interference with natural friction was required. This method was found to give the best smoothness without distorting the geometry.

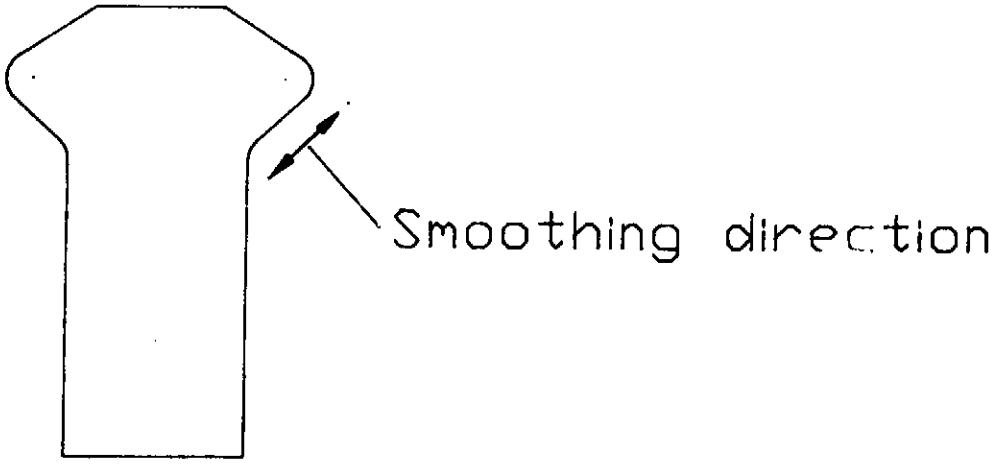

Figure A2.2 Final finishing

A2.5 Material calibration

A material calibration of the Araldite D used in this investigation was done by Buchan [4]. Using a beam loaded with a uniform pure bending moment he found the material fringe order to be f_σ = 14079 Newtons per fringe per meter. This value can be substituted into the photoelastic equation $\sigma_1 - \sigma_2 = N * f_\sigma / t$ to give the difference between the two principal stresses at a given point in a photoelastic model.

APPENDIX A3

A3.1 Fixed friction angle tests

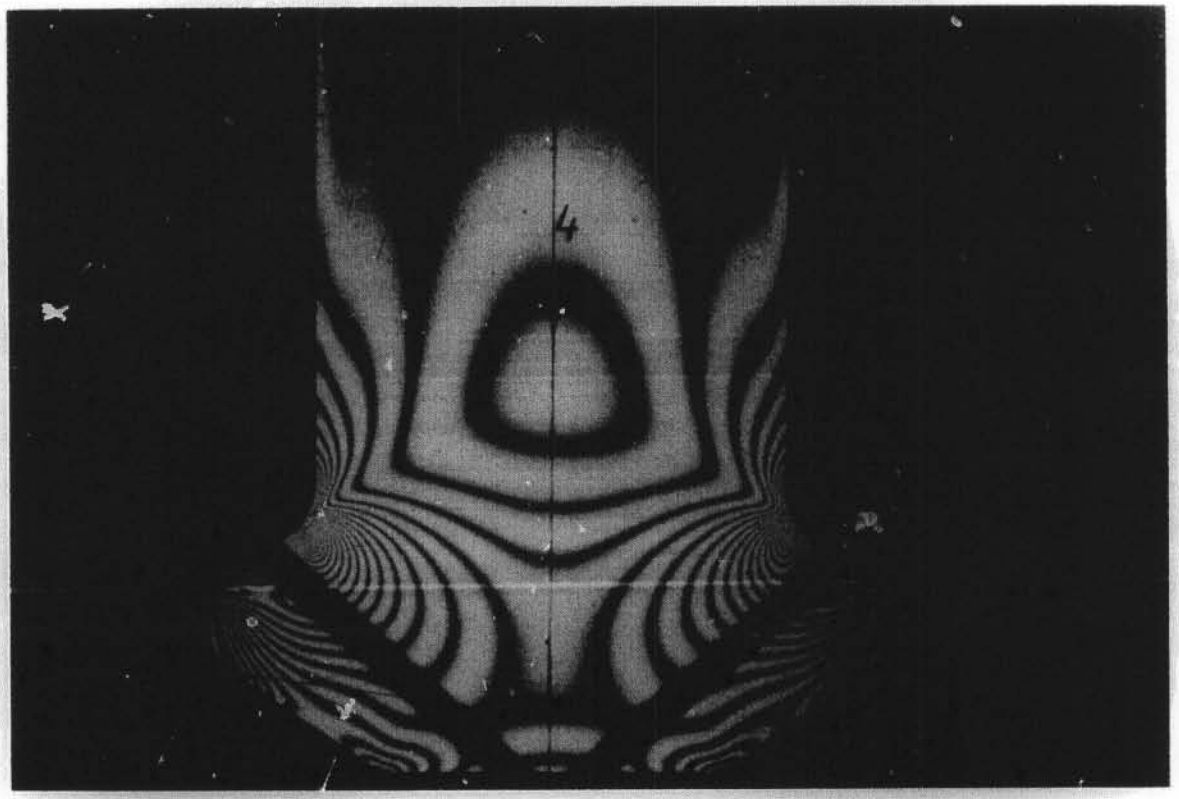

A3.1.1 Root 55 Load angle -10°

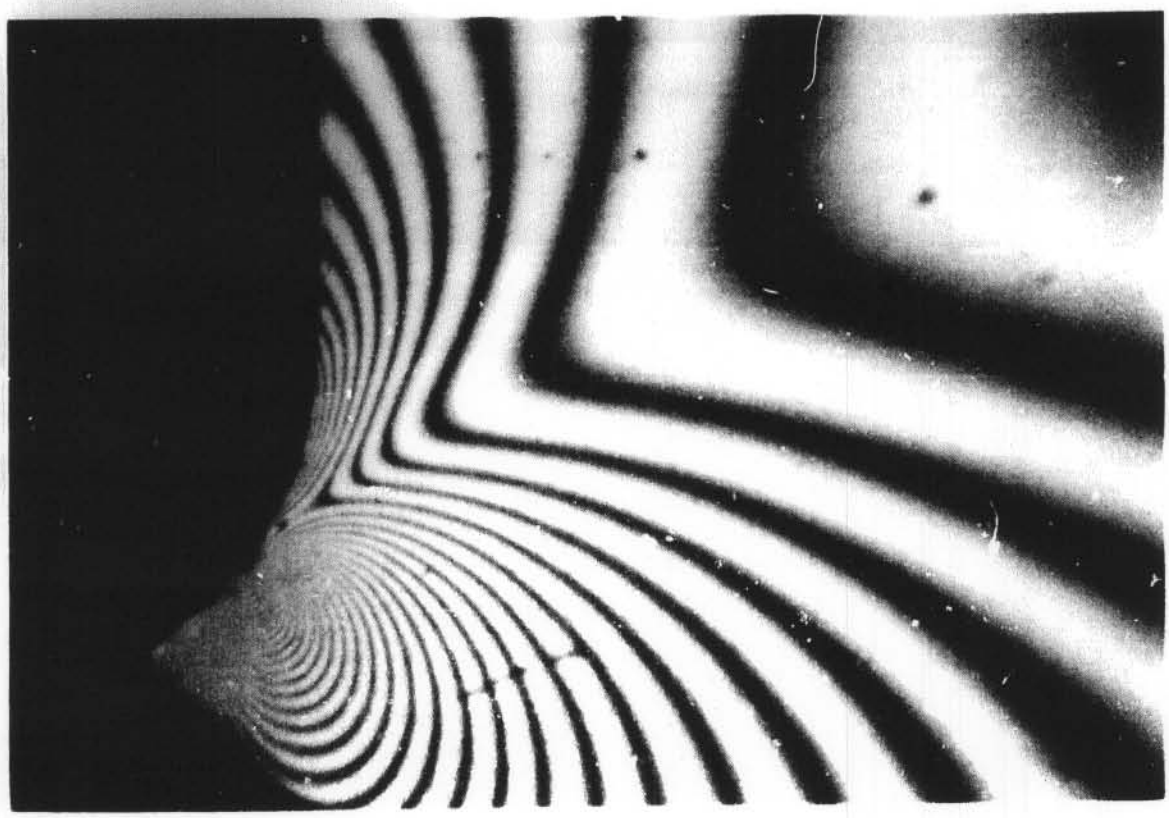

A3.1.2 Root 55 Load angle 10° Fixed friction angle

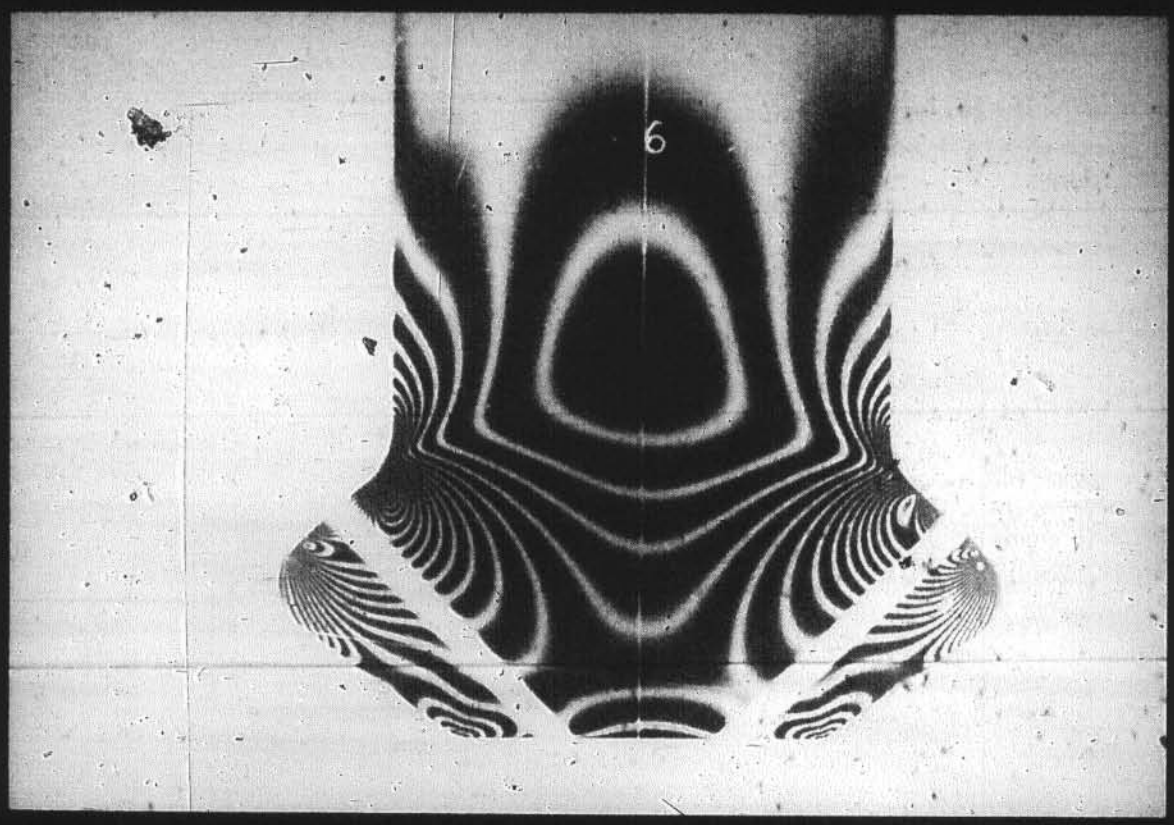
6

7

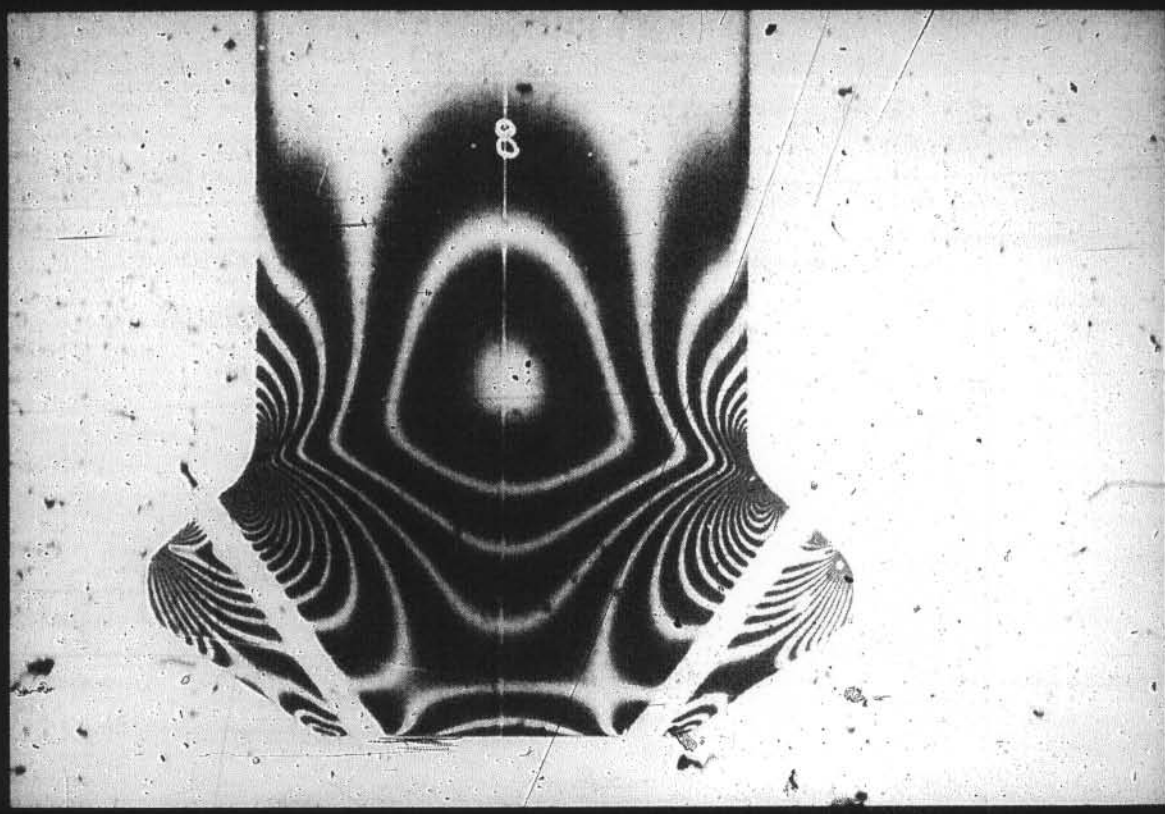
8

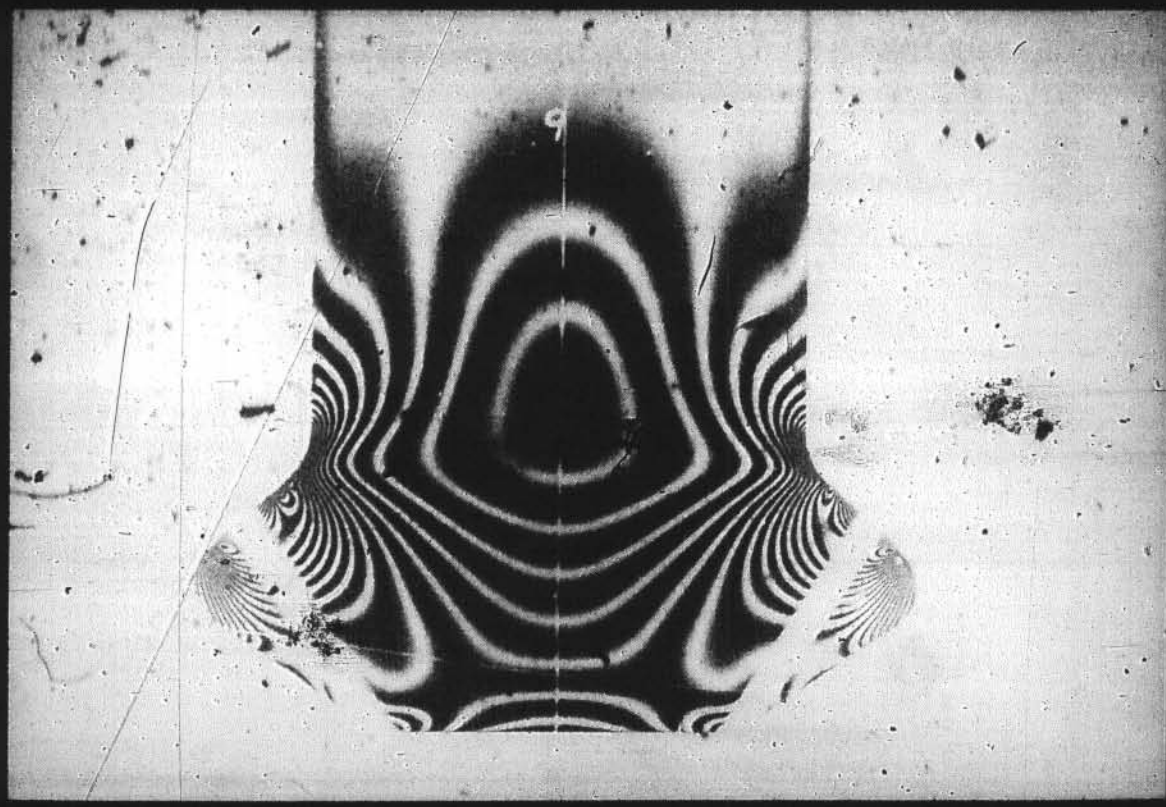
9

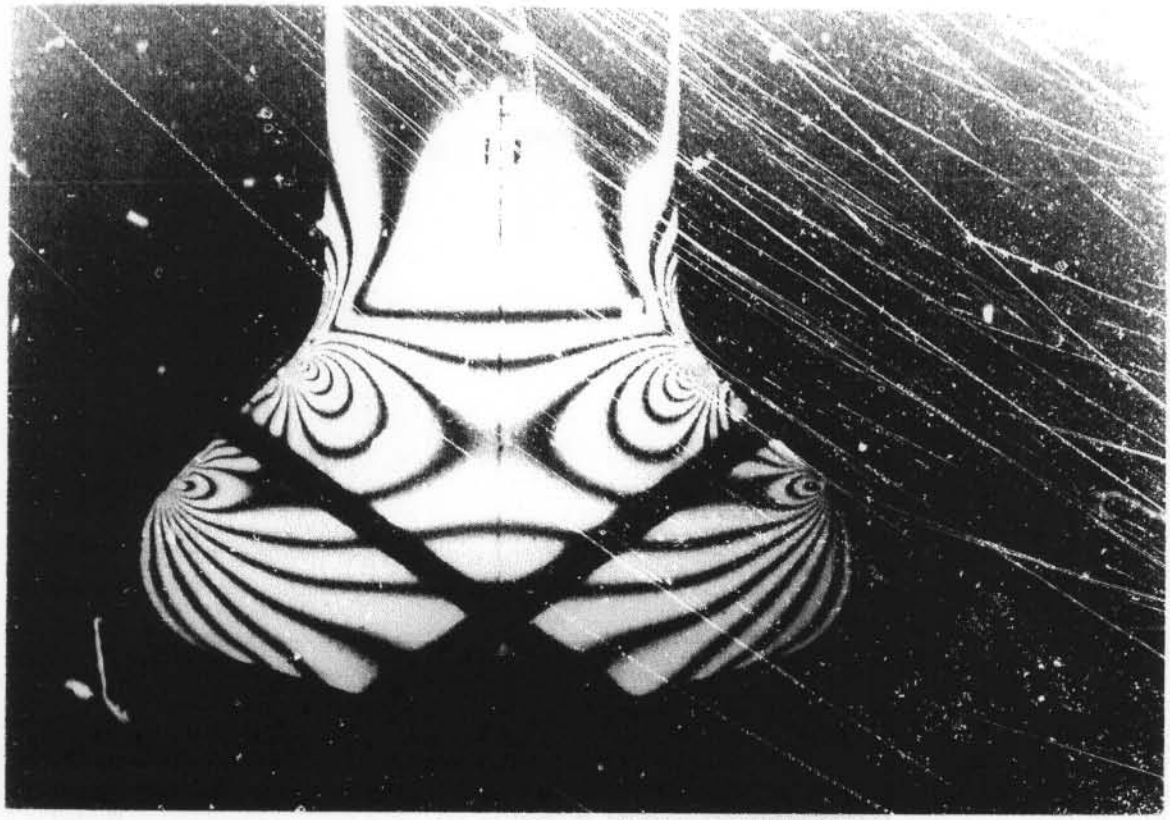

A3.1.7 Root 51 Load angle -10°

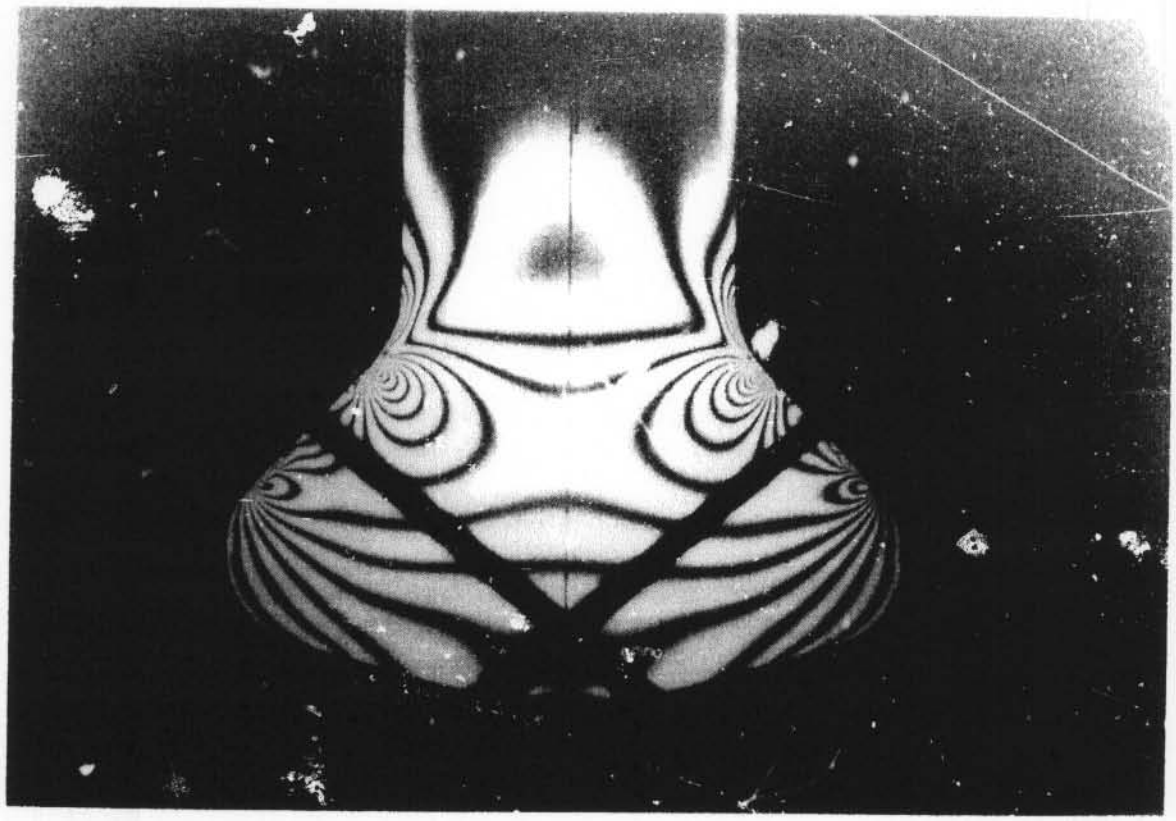

A3.1.8 Root 51 Load angle -5°

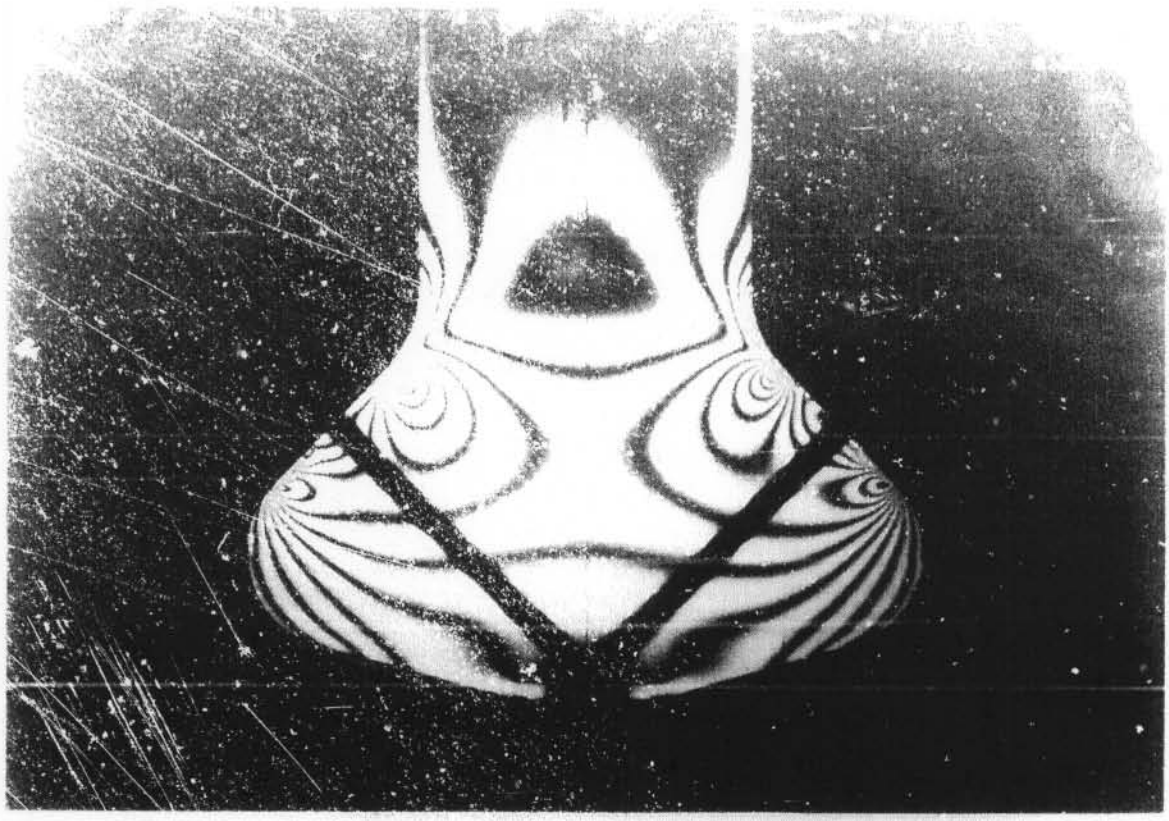

6.1.9 Root 51 Load angle 0°

6.1.10 Root 51 Load angle 5°

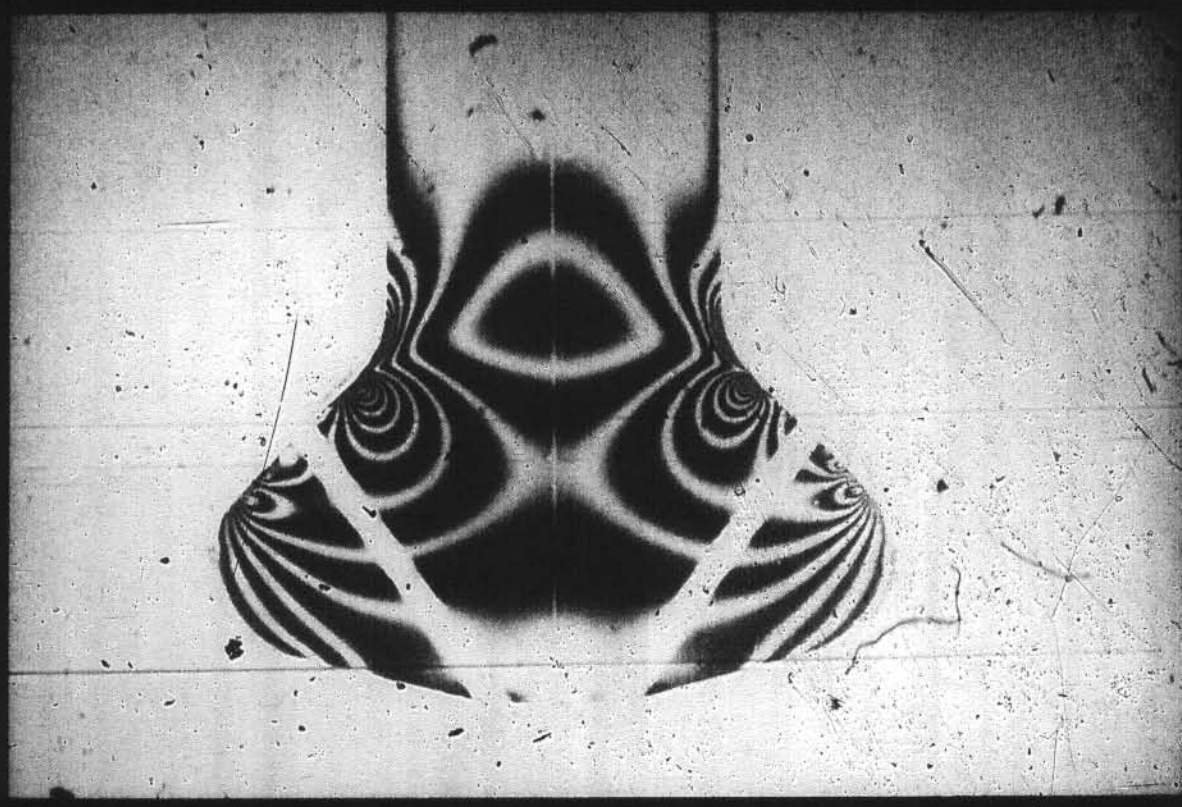

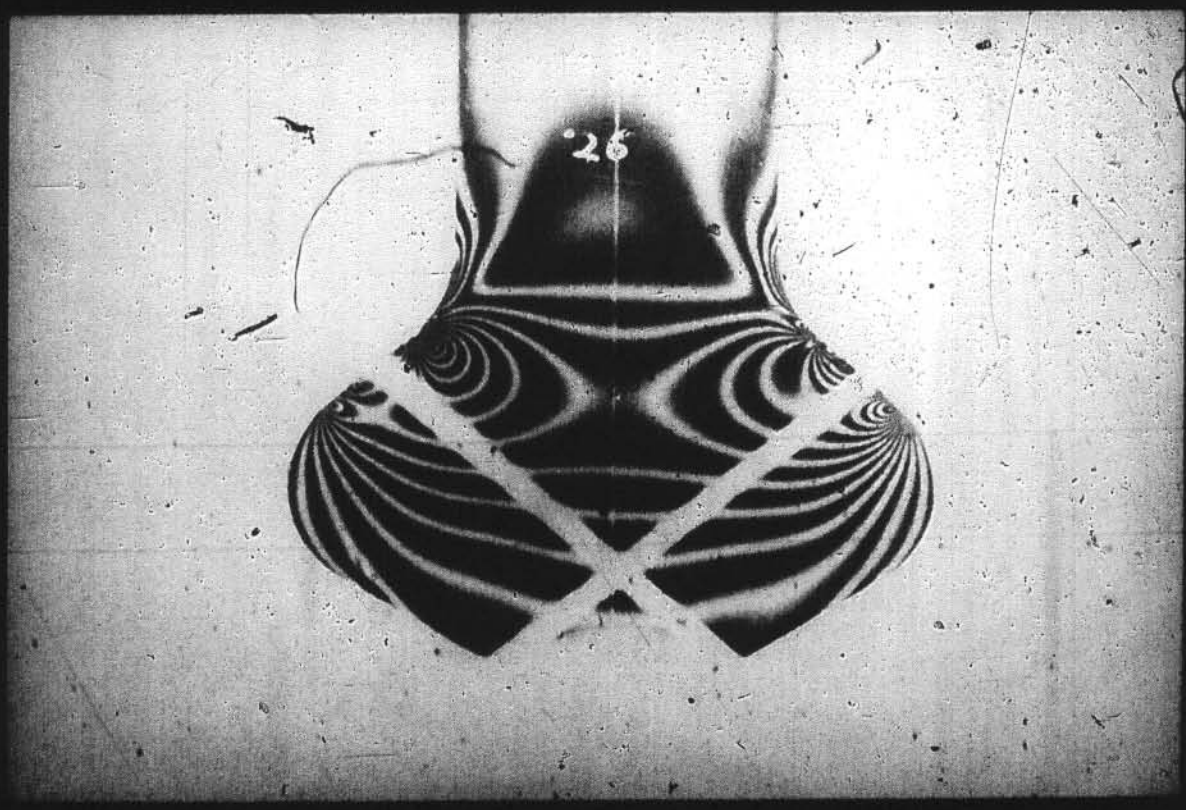
26

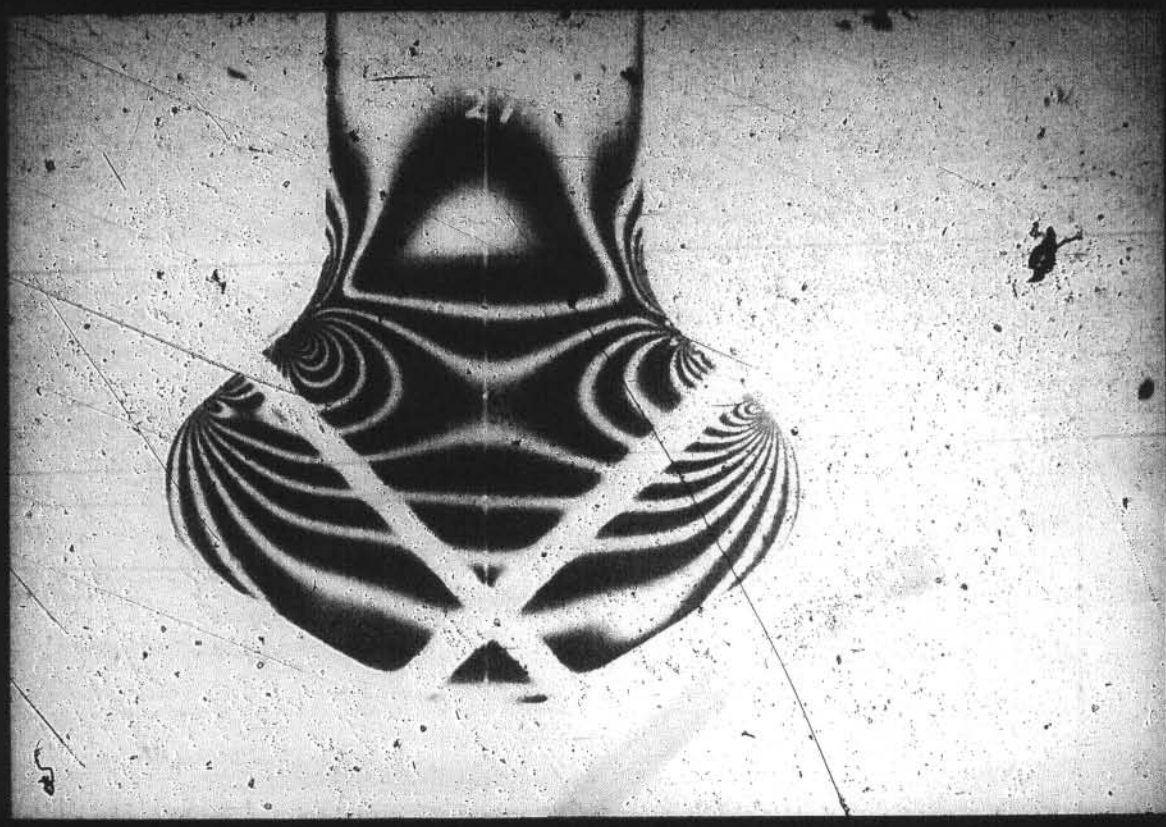

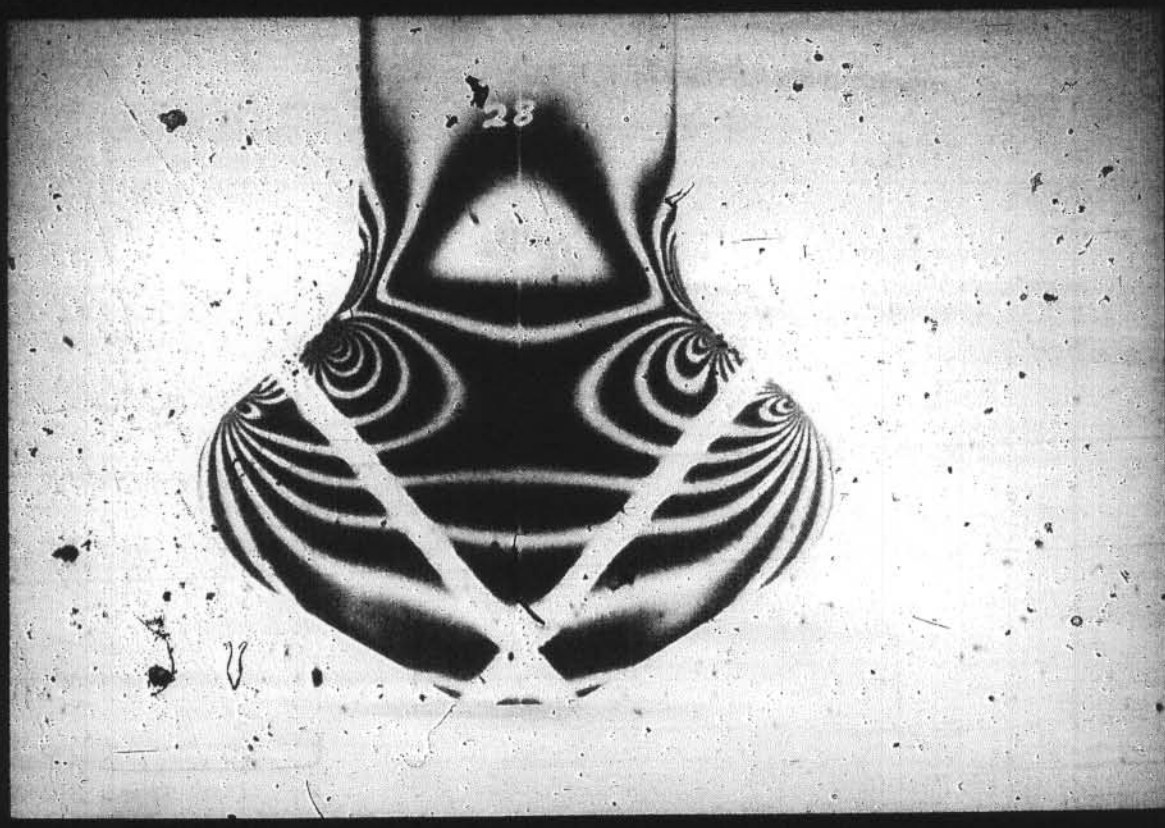
28

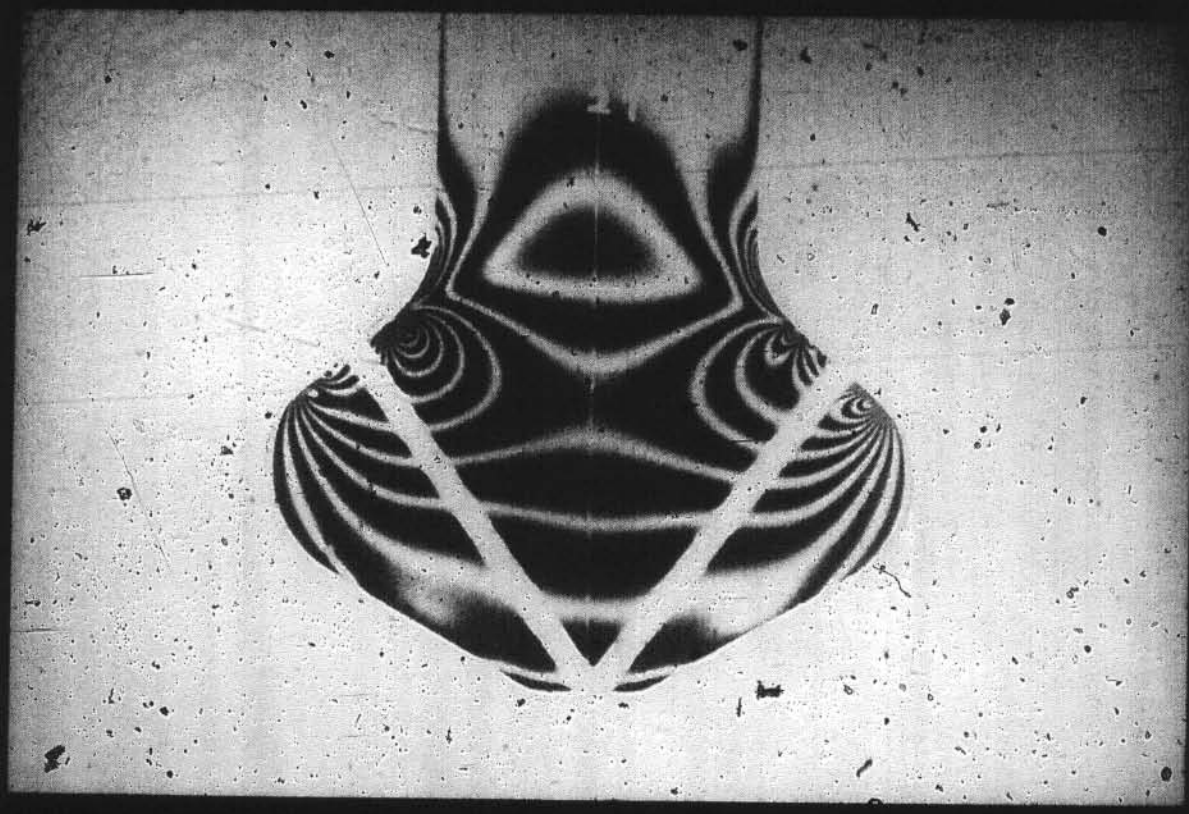

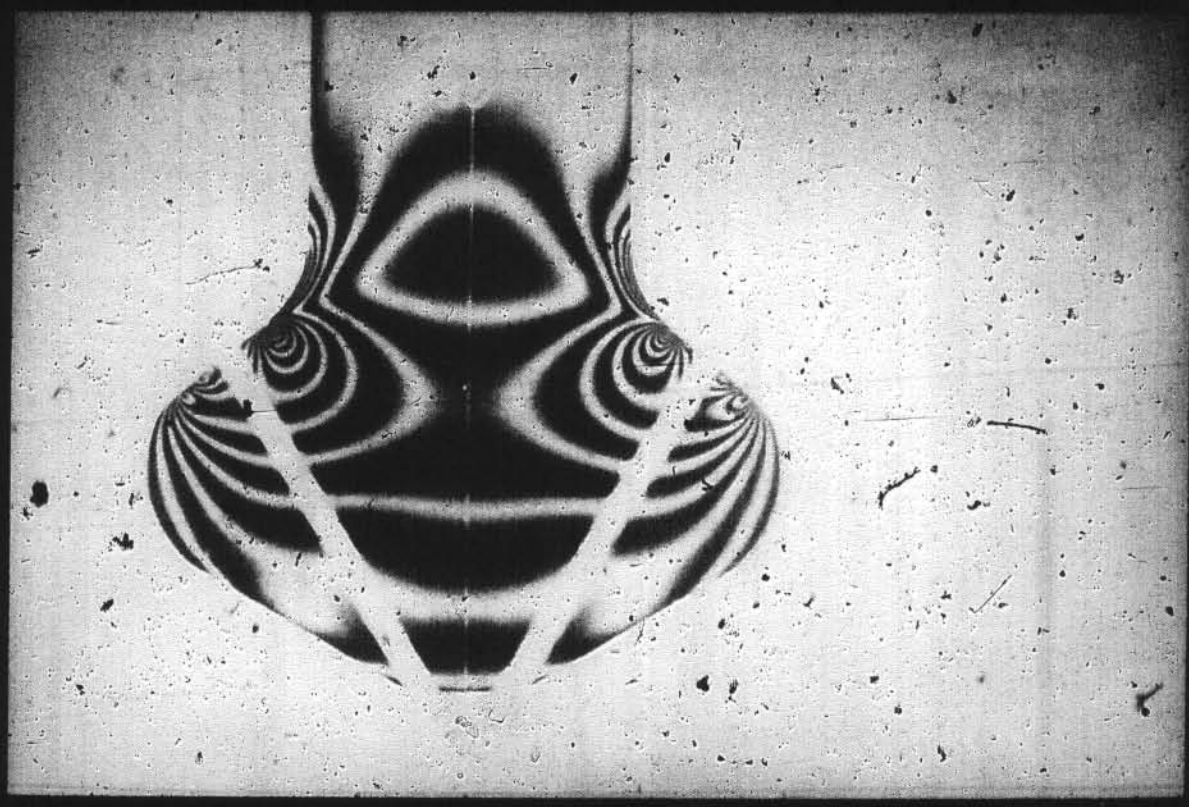

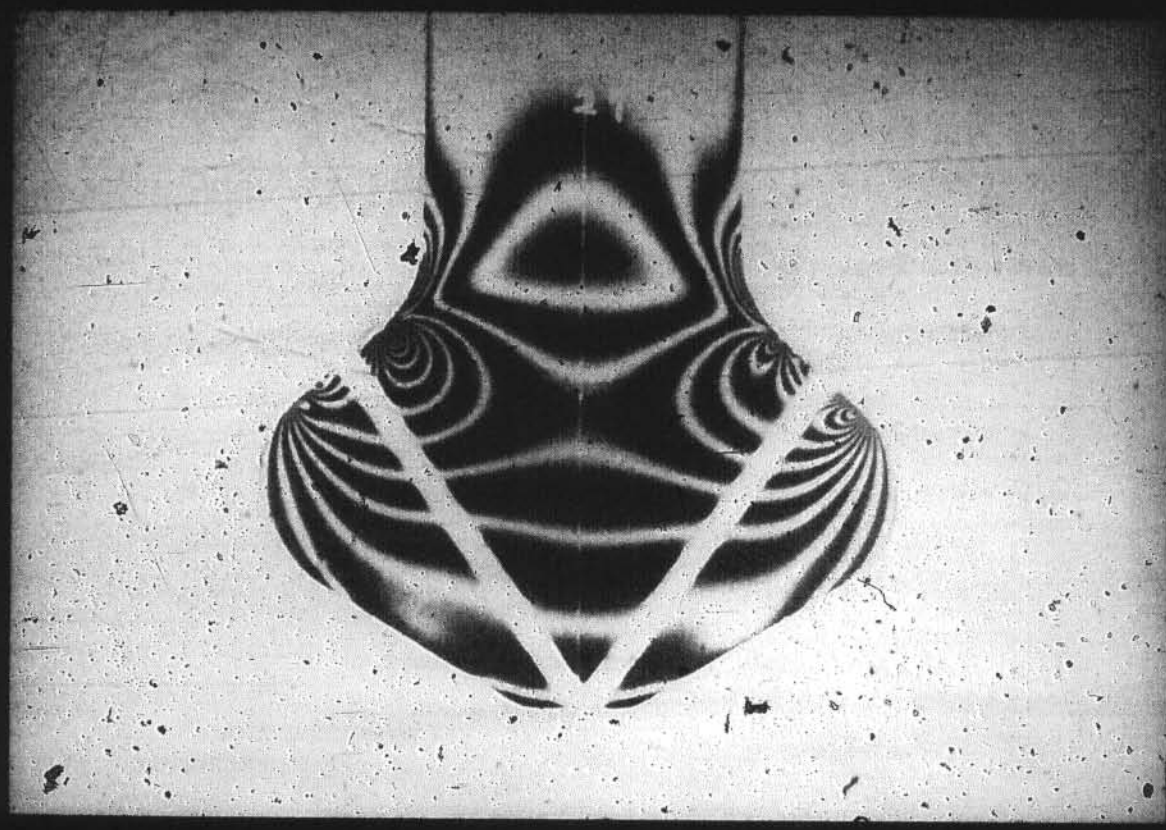

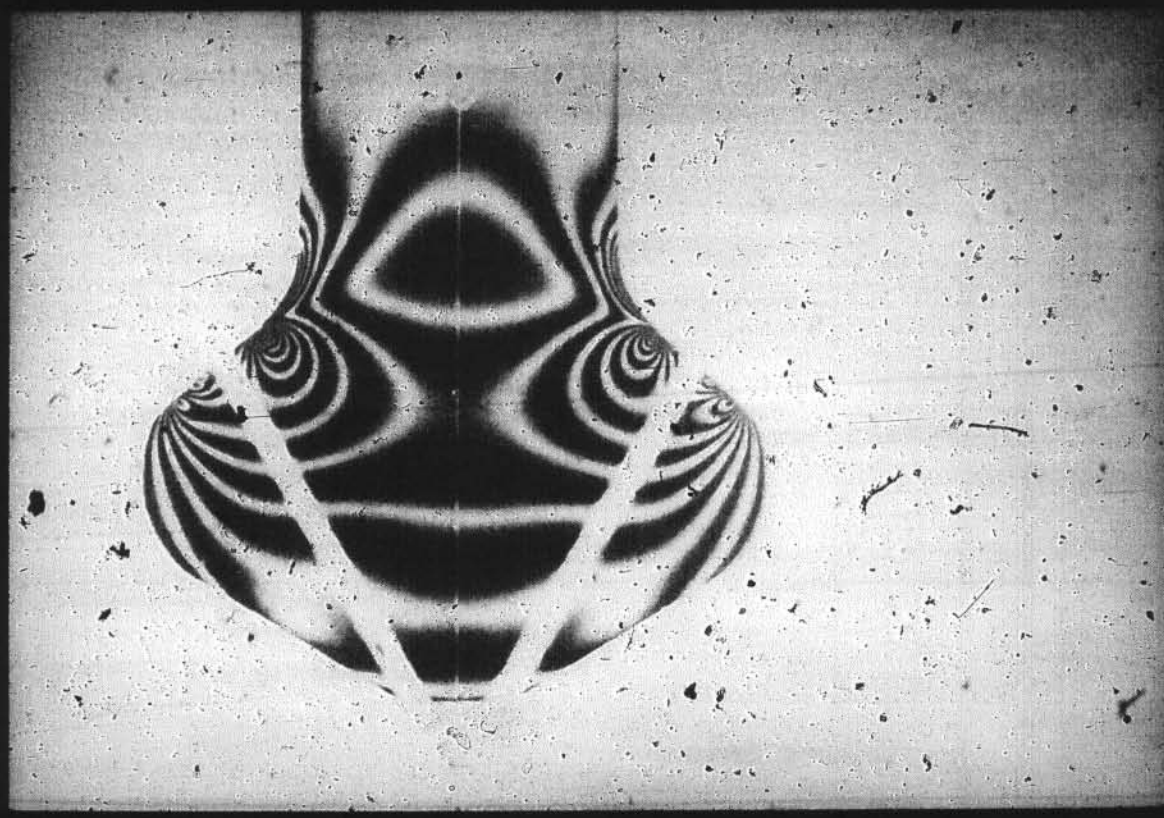

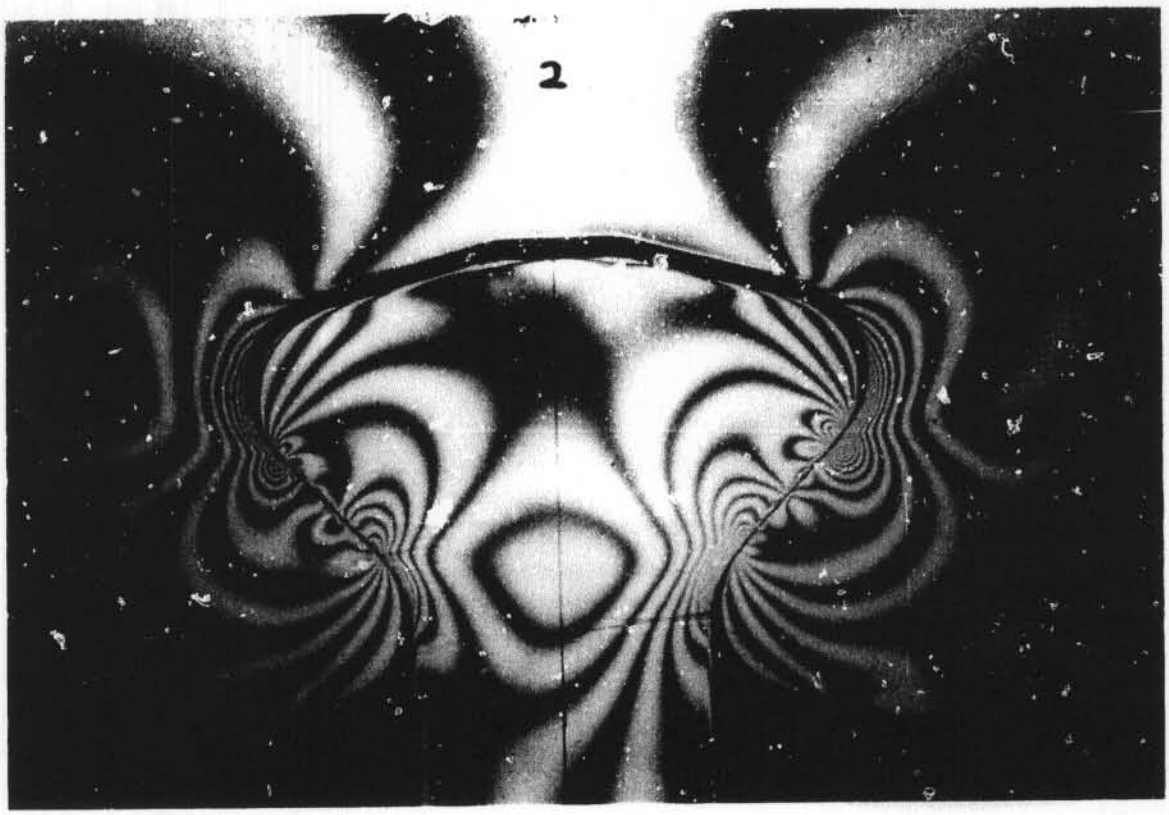
2

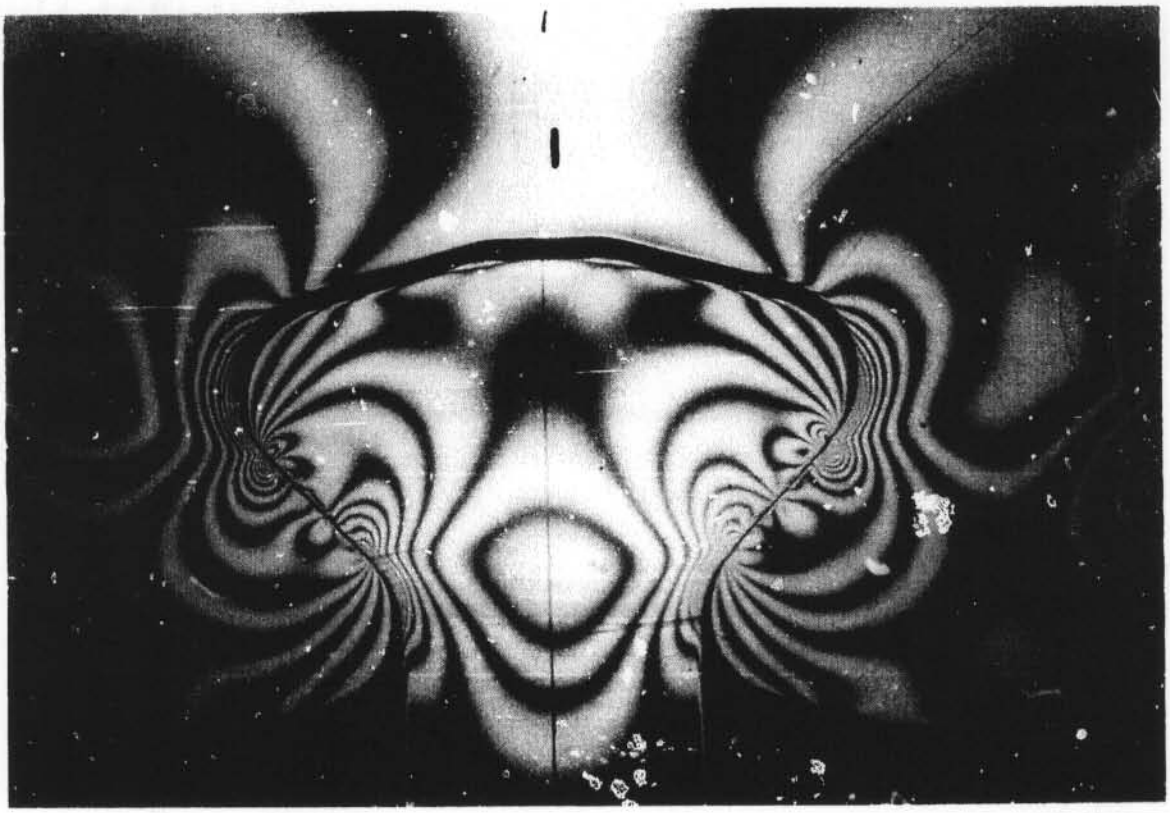
1

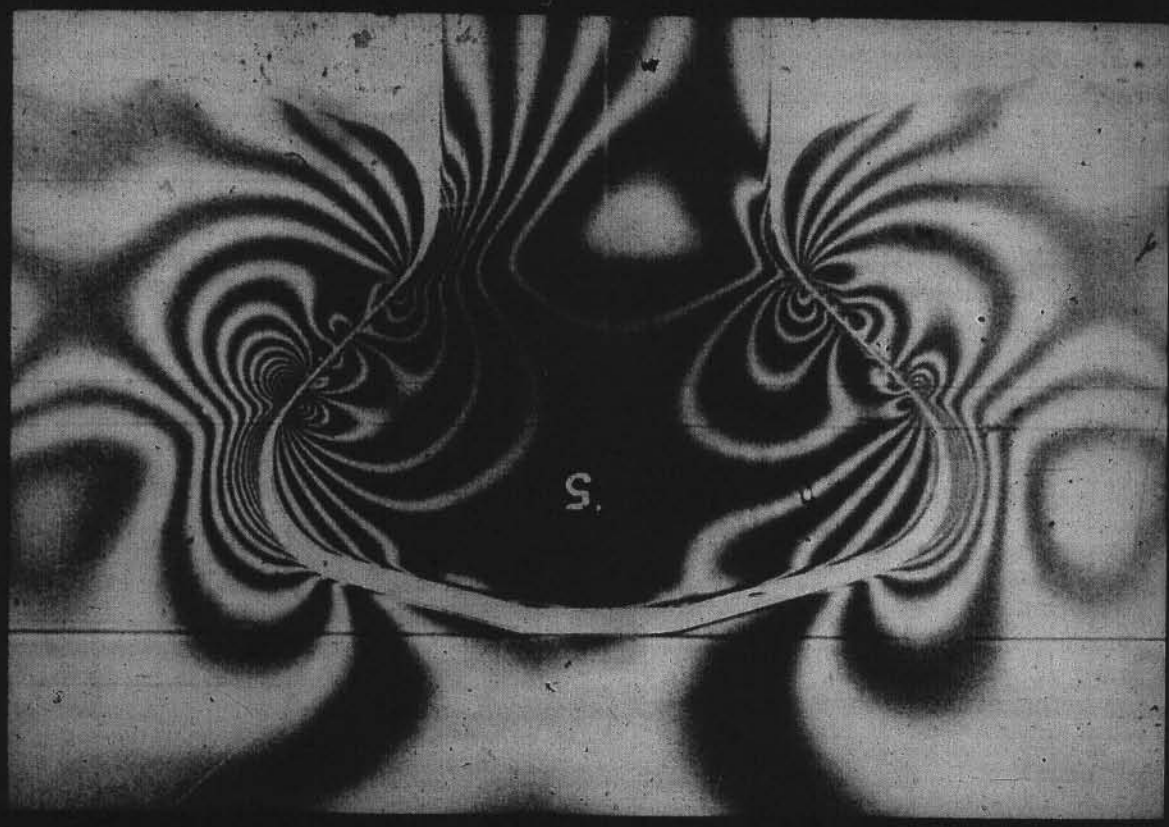
5.

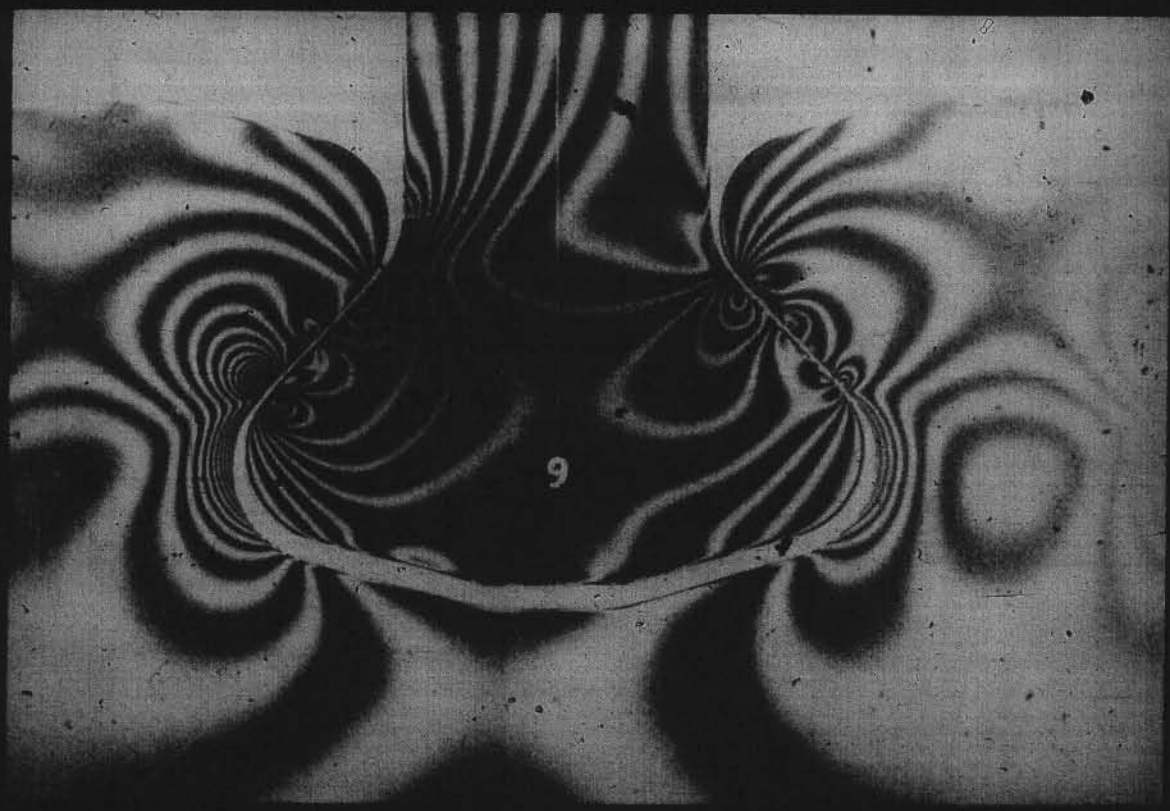
9

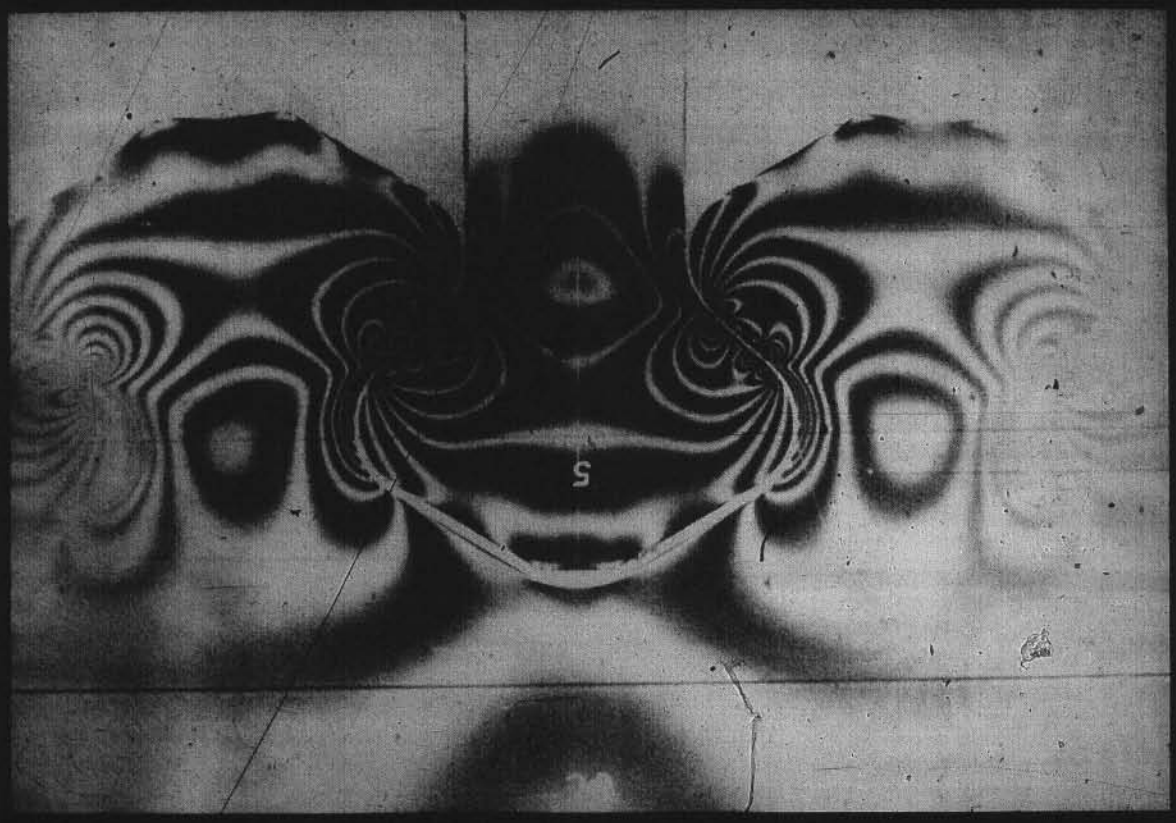
S

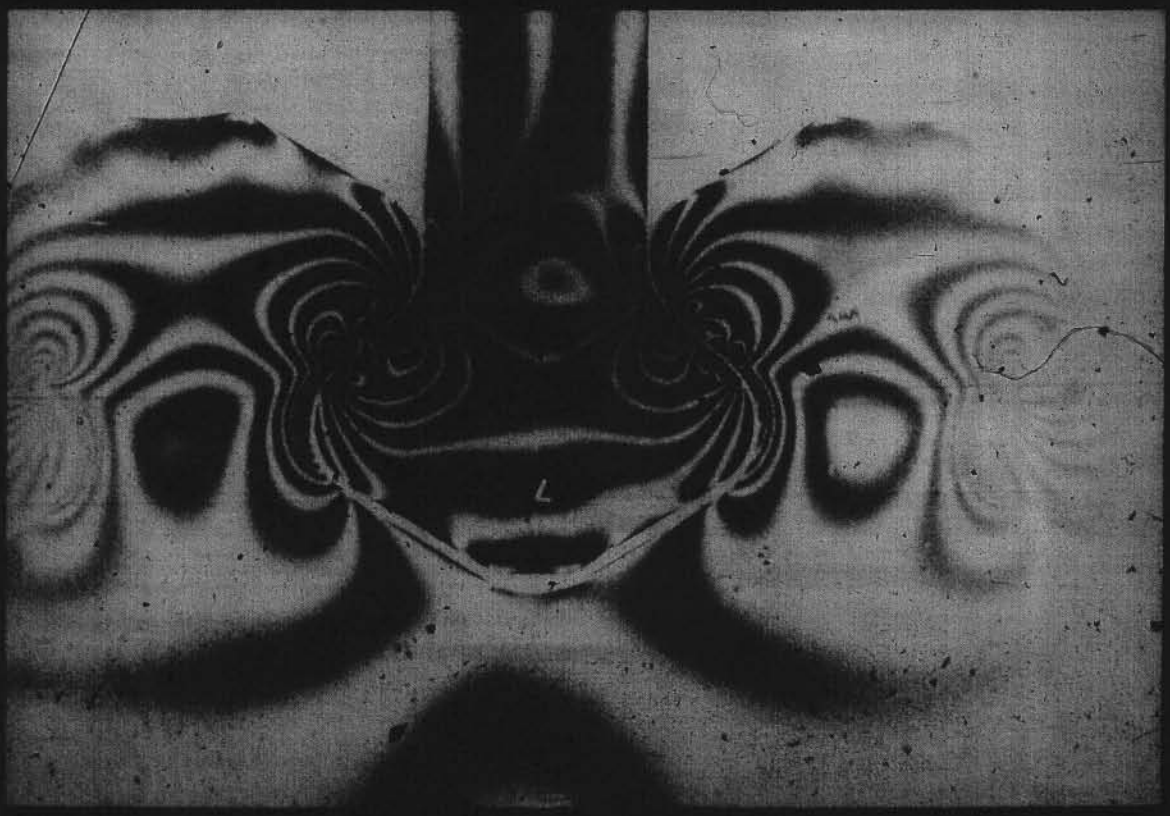
L

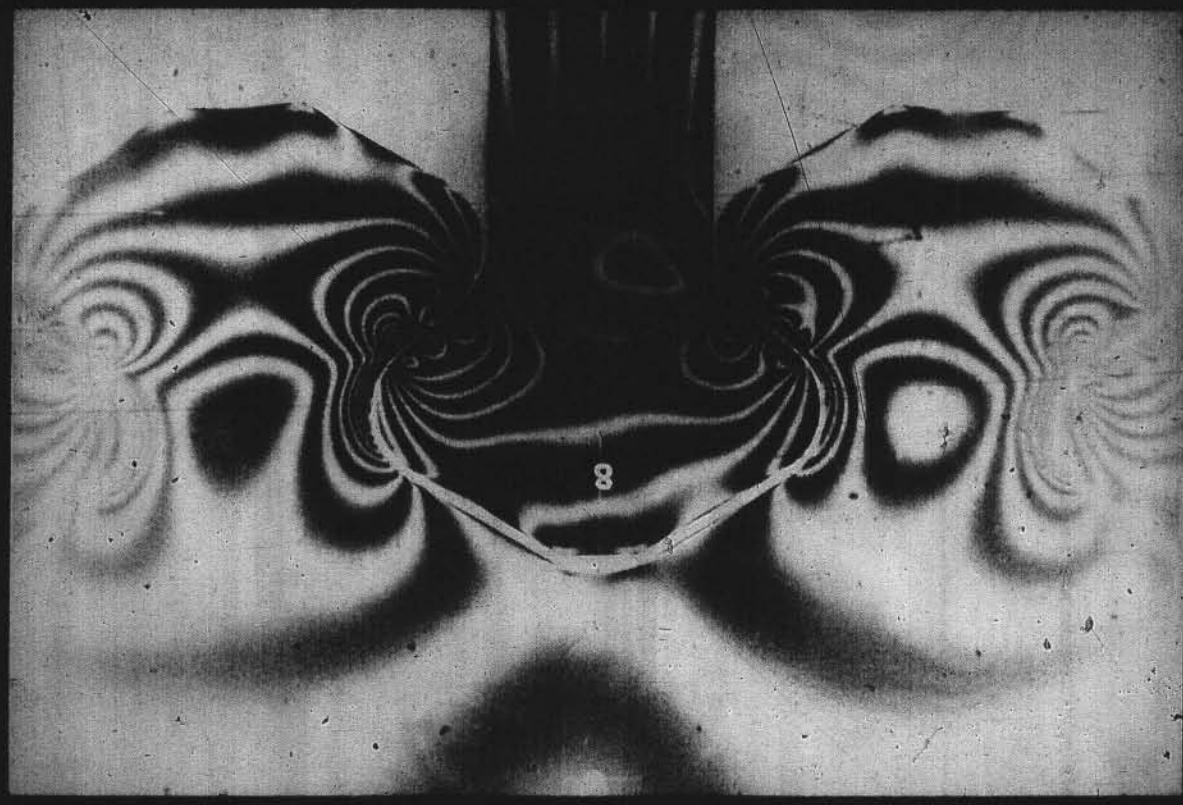
8

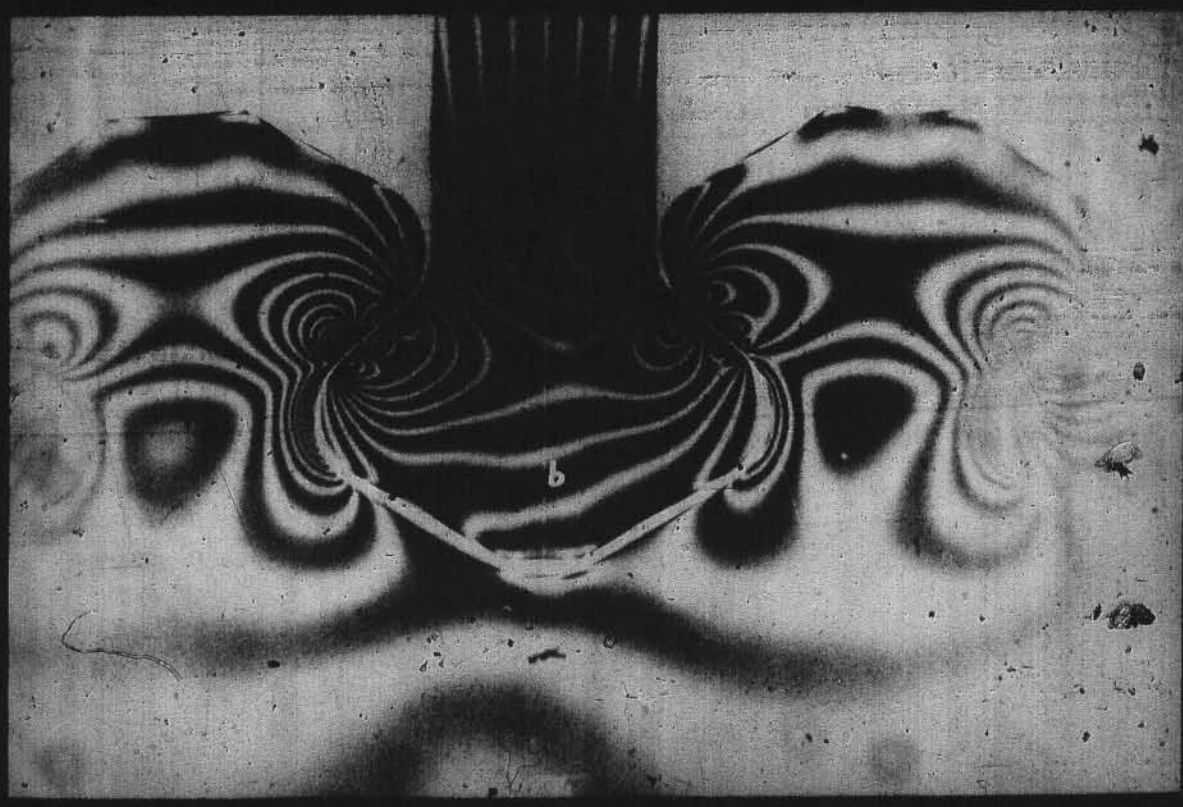
6

17

20

2

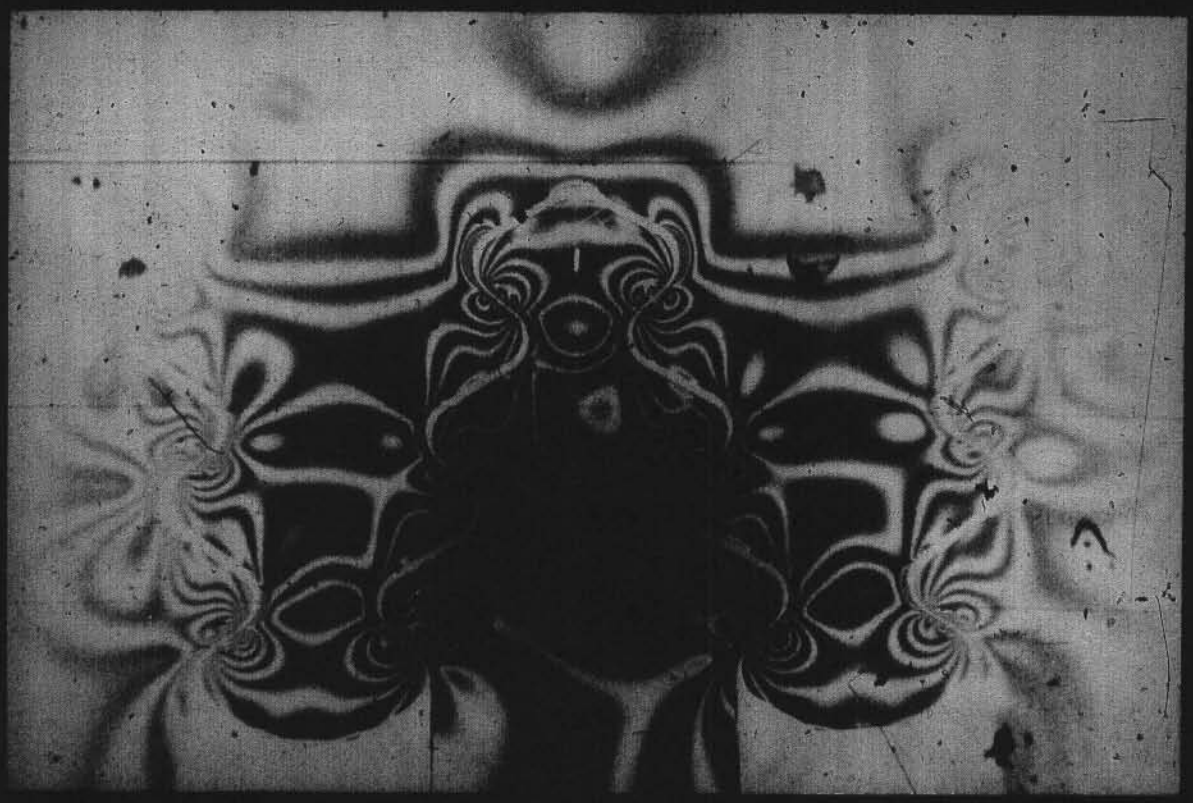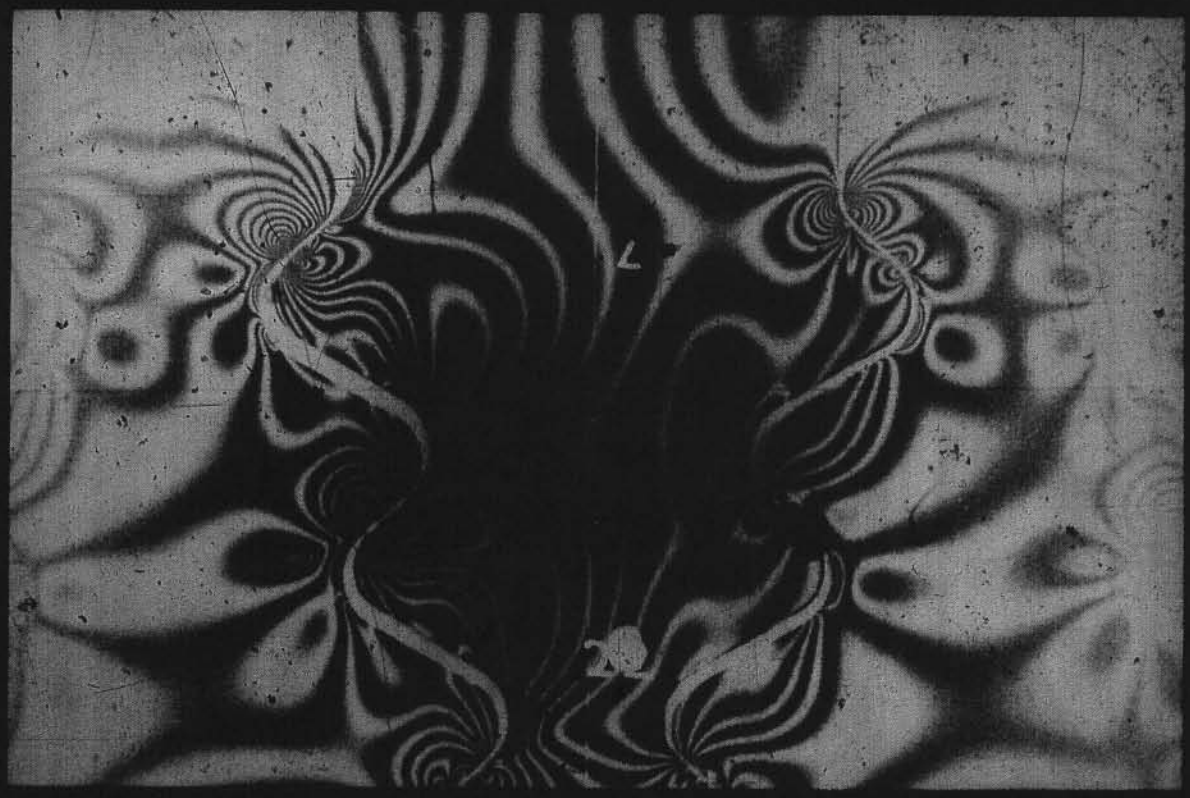
1